論文 / 著書情報
Article / Book Information

題目(和文)	
Title(English)	Near-Field Displacements and Rotations Estimated by Quantitative Analysis in the Frequency Domain using Zero Padded Strong-Motion Accelerograms
著者(和文)	
Author(English)	Emmanuel Javelaud
出典(和文)	学位:博士（工学）, 学位授与機関:東京工業大学, 報告番号:乙第4092号, 授与年月日:2013年9月25日, 学位の種別:論文博士, 審査員:盛川 仁,翠川 三郎,古谷 寛,松岡 昌志,山中 浩明,大町　達夫
Citation(English)	Degree:Doctor (Engineering), Conferring organization: Tokyo Institute of Technology, Report number:乙第4092号, Conferred date:2013/9/25, Degree Type:Thesis doctor, Examiner:Hitoshi Morikawa,Saburoh Midorikawa,Hiroshi Furuya,Masashi Matsuoka,Hiroaki Yamanaka,Tatsuo Ohmachi
学位種別(和文)	博士論文
Type(English)	Doctoral Thesis

Near-Field Displacements and Rotations Estimated by Quantitative Analysis in the Frequency Domain using Zero Padded Strong-Motion Accelerograms

Emmanuel JAVELAUD

Department of Built Environment

Tokyo Institute of Technology

A thesis submitted for the degree of

Doctor of Engineering

2013

Acknowledgements

I am deeply grateful to Professor Tatsuo Ohmachi for welcoming me in his laboratory, and for the continuous guidance, support and encouragements since then.

I would like to express my gratitude to Professor Hitoshi Morikawa for advising and supervising this work over the last years.

I thank Dr. Shusaku Inoue, Mr. Yoichiro Murakami and Mr. Akira Furukawa, former members of Ohmachi Laboratory at Tokyo Institute of Technology, for their help and interest in this work.

This research was partially supported by the Japanese government through the Monbukagakusho scholarship program.

Additionally,
I would like to thank Mrs. Sachiko Kanai and Mr. Yumma Javelaud for their patience, kindness, and continuous support.

Abstract

This dissertation describes an original method that allows to retrieve reliable displacement time histories and permanent rotations from strong-motions, recorded by modern accelerometers, in the near-field of large earthquakes.

Strong-motions recorded by the horizontal components of accelerometers contain records of both the translational accelerations and the instruments tilt. The method leads first to visualize in details the acceleration records' Fourier content by addition of long zero pads to the records, then to separate the permanent residual tilt of instruments from the translational accelerations. When the permanent rotation of instruments is large enough, it dominates the records low frequency content, and permanent rotation angles may therefore be uniquely estimated from strong-motion records. Simultaneously, reliable translation accelerations, and therefore displacements, are obtained.

Analyze of several earthquakes show that the displacements obtained by double integration of the retrieved translational accelerations have good similitude to closely spaced 1-Hz GPS data, over duration of engineering interest, for both the oscillatory and permanent parts of the displacements. The accuracy of the rotation angles is confirmed by comparison with external rotation measurements.

Among the possible practical applications, we focus on the civil engineering ones. We find that the reliable ground motions obtained may be used either to obtain improved displacement response spectra, including at long period, or as direct input motion for time-domain analysis.

Contents

List of Figures

List of Tables

Chapter 1

Introduction

1.1 General Remarks

During large earthquakes, tectonic movements along faults generate in their near field important deformations including transitory and permanent displacements, as well as tilting of the surface. Over the last decades several earthquakes, that had significant impact on communities, occurred worldwide. Among them are the 1985 Mexico Earthquake (Mexico), the 1989 Loma Pietra Earthquake (U.S.A.), the 1994 Northridge Earthquake (U.S.A.) and the 1995 Hyogoken-nanbu (Kobe) Earthquake (Japan). At the time this work was started, the Niigata region was hit by the 2004 Niigata-ken Chuetsu Earthquake (Japan). Many large earthquakes have occurred since then.

An accurate knowledge of the ground motions that occur in the near-field of large earthquakes is a key issue to mitigate the seismic risk. Reliable ground deformation are required for several important practical purposes, including:

- Tsunami prediction. Most often, tsunami are generated by permanent deformation of the ocean floor resulting from earthquakes (Dotsenko and Soloviev, 1995; Levin and Nosov, 2008). The principle of tsunami generation is described in Figure 1.1. The permanent deformation of the sea floor implies that during the generation of the tsunami, a huge volume of water, up to tens of cubic kilometers (Nosov, 2011) is displaced from its equilibrium position. Then, it spreads out of the vicinity source. Reliable sea floor de-

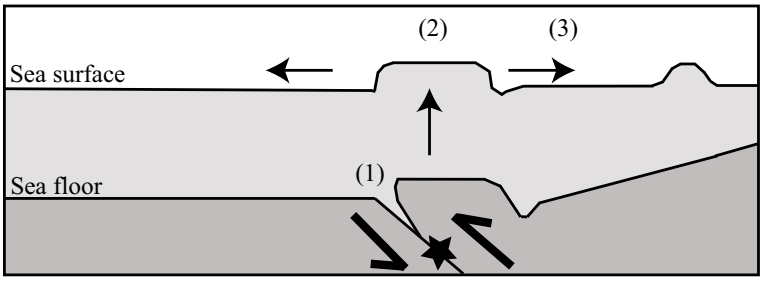

Figure 1.1: Principle of the tsunami generation. Modified from IOC (2013). The permanent deformation of the sea floor (1) lead to the displacement of a huge volume of water (2) that spreads out of the source area (3).

formations, including transitory and permanent deformations (Ohmachi *et al.*, 2001), are needed to accurately simulate and predict tsunami.

- Estimation of ground strain and design of lifelines. The knowledge of reliable ground deformation at different depths is required for several other important practical purposes such as the estimation of ground strain and the design of lifelines. Following the 1995 Hyogoken-nanbu (Kobe) earthquake, Ohtake (2006) observed that damages on water supply pipelines occurred in non-liquefiable ground at places where the safety factor, calculated according to the design code, was of approximately 2. He found that the displacement of non-liquefiable ground in the near-field is larger than given by the seismic code because the displacement at the engineering bedrock is bigger than assumed in the code. The Figure 1.2 shows that the displacement on the surface is the sum of the permanent ground displacement at the seismic bedrock and of the dynamic displacement within the superficial soft sedimentary materials.

- Design of structures. Moreover, the designs of structures and deep foundations, especially for structures located close to capable faults, require the use of design ground motions that must consider both permanent and oscillatory displacements (e.g. Park *et al.*, 2004).

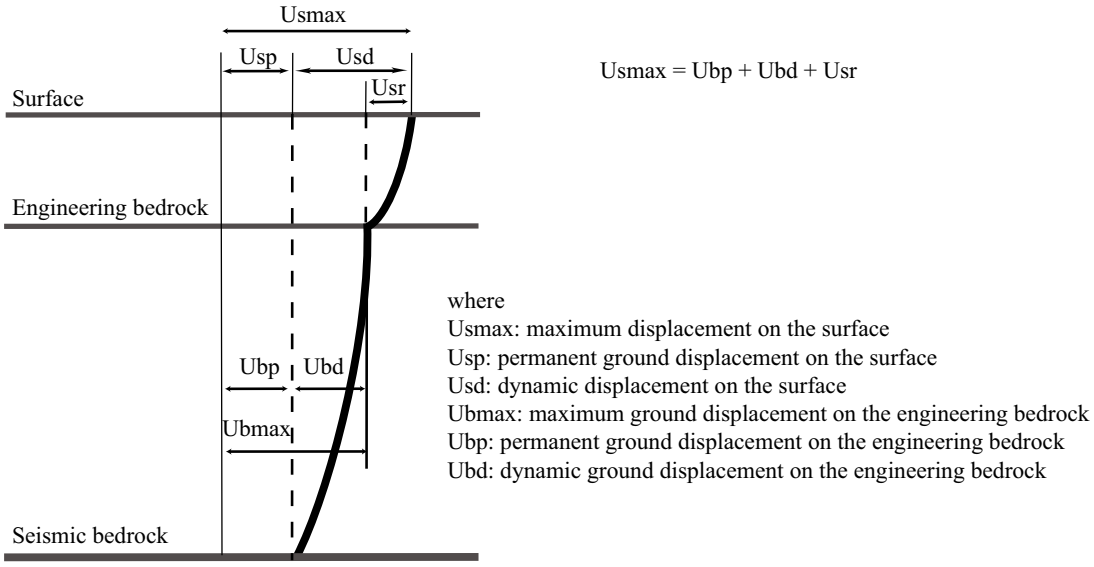

Figure 1.2: Characteristics of the ground deformation in the near-field. The displacement on the surface is the sum of the permanent ground displacement at the seismic bedrock and of the dynamic displacement within the superficial soft sedimentary materials. Redrawn from Ohtake (2006).

This view of the problems indicates that detailed information about the ground deformation, including displacement time histories and permanent rotation, are of importance to improve our knowledge and engineering skills related to these practical applications.

Several methods exist to quantitatively measure the ground deformation generated in the near-field of earthquakes. These include topographic surveys, geodetic techniques with, or without, a network installed on the surface before earthquakes occur, strong-motion velocimeters and strong-motion accelerometers. The Table 1.1 summarizes for each technique the best sampling frequency that one can nowadays expect, together with possible localization of the measurements:

- Ground survey may provide the coseismic residual displacement when pre-event data are available, at places where the surveyors may access.
- Interferometric Synthetic Aperture Radar (InSAR) may be used to evaluate the permanent topographic changes over large areas without advance knowledge of the earthquakes location when satellite images are available

before and after the earthquakes (Massonnet *et al.*, 1993).

Basically, InSAR consists of extracting the phase change between two images of a same area taken before and after an earthquake occurs. The ground resolution of InSAR images in distance (perpendicular to the satellite displacement) and azimuth (along the satellite displacement) depends respectively of the pulse duration and the incidence angle, and of the wavelength and the distance to the measured area. Practically, the ground resolution usually varies from 10 m (Kobayashi et al., 2012) to 100 m per pixel (Massonnet *et al.*, 1993), depending on the recording conditions.

The ability of the method to provide the variation of the displacements during the earthquake depends on the altitude of ambiguity for the pair of satellite orbits (Cavalie, 2007; Hernandez et al., 1997), which is function of the wavelength, distance to the investigated area, angle of incidence, and distance separating the baseline of the two satellites orbits. In practice, the precision is of about 3 cm (Massonnet *et al.*, 1993) for the horizontal displacement. The vertical deformation is more difficult to obtain accurately.

Usually, the variation of the displacement is assumed to be zero at the edge of the InSAR image, which can be an inaccurate assumption. The main limitations of the method are (1) areas of very quickly varying field of deformation when the variation of deformation on a pixel is larger than a wavelength and it is therefore impossible to define continuous line of equal phase (Hernandez et al., 1997), (2) the weather condition that may causes disturbances (Cavalie, 2007), and (3) steep slopes in mountainous areas.

The method relies on the availability of satellite images of the investigated areas taken at appropriate times. These images are usually not freely available from their provider.

- Global Positioning System (G.P.S.; Bock *et al.*, 1993) may be used to obtain up to 1-Hz coseismic displacement time histories at specific positions where GPS stations are installed.

  It requires ground-based receivers. Several GPS networks exist worldwide. In Japan, the GEONET network (Geographical Survey Institute) consists

of 1200 GPS stations covering Japan with an average spacing of 25 km. It performs high frequency measurements (30 s, 1 s).

Different to most geophysical applications for which the position is estimated once a day, for seismic applications, the position is estimated at every data epoch, i.e. every second for 1-Hz GPS. Basically, the position of a GPS receiver is calculated from the estimation of its distance to four or more satellites of known position. This can be done instantaneously but provides imprecise positions of the instruments. Larson (2009) describes the procedure to retrieve accurate displacement time histories from GPS records, which includes the following steps: (1) the spacecraft positions, carrier phase and ambiguities are estimated, and receiver/satellite clock must also be estimated by using a reference; (2) the ionosphere delays are removed with the dual-frequency combination; (3) then, position of the GPS station is computed at each epoch. Processing GPS data to obtain displacement time histories is far more complex than other methods, and cannot be done immediately following an event. It indeed requires data recorded over a very long period of about 1 day to analyze a 100 s displacement time history and to obtain positions with an horizontal precision ranging from a few millimeters (Larson, 2003) to 1 to 2 cm (Miyazaki *et al.*, 2004).

Usually, one of the stations of a specific area is used as reference for the differential calculations. One of the limitation of this method is that it is therefore difficult to obtain accurate displacement time histories in the near-field of large earthquake due to the difficulty to have a reference point that does not experience displacements.

An alternative method to estimate the displacement time histories is to analyze the GPS data of each site separately. To date, there is no established methodology to process single site GPS data, although some methods have been proposed. In this thesis, we use 1-Hz GPS displacement time histories of the 2007 Niigata-ken Chuetsu-Oki earthquake (Japan). They were processed by Murakami (2007) who used a single site data.

Usually, these high rate GPS data are not freely available from the data providers.

- Strong-motion velocimeter may be used to obtain the displacement time histories by simple integration of their record. F-Net VSE-355G/G2 (Okada *et al.*, 2004) strong-motion velocimeters are currently installed within vaults at 70 F-Net stations in Japan. These instruments are sensitive to tilt, and may exhibit low clip levels during the earthquakes. Clinton (2004) observed that when the velocity reaches 16 cm/s, spikes associated with non-physical ground displacements sometimes occur.

- Strong-motion accelerometers record the ground accelerations. Similar to the velocity strong-motion sensors, they are sensitive to tilt. Among all the methods, the use of strong-motion accelerometers is interesting because of the large number of instruments deployed (several thousands) at a very wide range of places.

Table 1.1: Comparison of the different methods available to capture the ground displacement, in terms of their best sampling frequency as well as possible localization of the measurements.

Method	Sampling frequency	Location
Ground survey	before/after the earthquake	where the surveyor can access
InSAR	before/after the earthquake	on the surface
GPS	1 Hz	on the surface
Velocimeter	80 Hz	within vault for F-Net stations
Accelerometers	200 Hz	anywhere

This study was originally performed as an effort to better characterize the ground deformation generated by earthquakes. In addition to the topographical survey, geodetic methods and strong-motion velocimeters, the use of strong-motion acceleration records is interesting to recover coseismic displacement time histories for several reasons including:

- the large number of accelerometers deployed throughout the world that generate a large quantity of high quality data recorded in the near-field of earthquakes. For example, Japan decided to significantly improve its seismic observation system following the 1995 Hyogoken-nanbu Earthquake, and constructed the nation-wide seismic observation networks K-Net and

Kik-Net (Fujiwara *et al.*, 2004). For these two networks alone, over 2000 high quality modern strong-motion accelerometers were installed. These networks were designed to systematically record the near-field motions of all the large earthquakes that occur in Japan, and have performed well, since then.

- the variety of places where they are and may be installed, which include rock sites (for example the Kik-Net bottom instruments), free field sites (for example the K-Net instruments), within structures, boreholes and on the sea floor.

- the high sampling frequency of their records, up to 200 Hz, which implies that the oscillatory part of the displacement is also recorded, together with the permanent one.

- the development and installation of modern high quality digital strong-motion seismometers with low internal noise, such as the K-Net95 instruments installed within the K-Net and Kik-Net networks (Fujiwara *et al.*, 2004).

- following an event, the often immediate and free release of the data by networks.

Displacement time histories can theoretically be obtained by double integration of accelerations recorded by strong-motion seismometers but they usually show larger drift than expected for the true ground displacements (Figure 1.3). This is due to unwanted baseline offsets that contaminate the acceleration records. Removing these unwanted baseline offsets from the acceleration records is necessary to recover reliable translational acceleration time histories and subsequently reliable displacement time histories.

The many advantages of using strong-motion accelerograms to recover reliable displacements time histories in the near-field of large earthquakes, and the current technological turning point brought by the installation of modern high quality instruments, stimulated this research. This work investigates how to retrieve

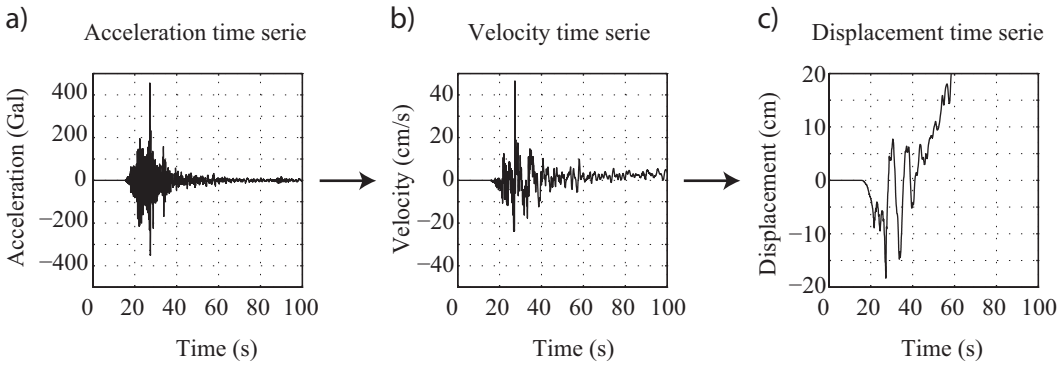

Figure 1.3: (a) Acceleration time history recorded during the 2007 Niigata-ken Chuetsu-Oki earthquake (Japan) at K-Net NIG019 station (EW component). (b, c) Velocity and displacement time series obtained by simple and double integration of the acceleration record, after removal of the pre-event mean from the whole record.

displacement time histories from strong-motion acceleration records, and therefore how to remove the unwanted baseline offsets from records of those modern instruments.

This thesis aims at (1) contributing to the understanding of the baseline offsets that contaminate acceleration records of modern strong-motion seismometers, (2) suggesting methods to remove these baseline offsets from acceleration records, (3) retrieving, in the near-field of large earthquakes, reliable information including translational acceleration time series that may lead to realistic displacement time histories by double integration, as well as permanent rotation of the instruments, and (4) investigating, for the particular case of civil engineering applications, the potential beneficial effects of using reliable translational acceleration and displacement time histories for the design of structures.

1.2 Review of previous studies

Specialized instruments were first developed in the 1930s (Anderson, 2003) to record the strong ground shaking that occur in the near-field of large earthquakes. Since then, there has been constant technological improvements in strong-motion accelerograph technologies, including the main evolution from analog to digital

strong-motion accelerographs.

Several studies have investigated the origin of the baseline offsets that contaminate the acceleration time histories released by strong-motion seismometers. Detailed studies of specific components of the strong-motion seismometers have been performed. The baseline offsets have been attributed to imperfections in the transducer design (Trifunac *et al.*, 1973; Boore and Bommer, 2005), transducer distortions of amplitude and phase (Trifunac *et al.*, 1973), mechanical or electrical hysteresis in the sensor (Iwan *et al.*, 1985; Shakal and Petersen, 2001), cross axis effects due to sensitivity and misalignment of nominally orthogonal sensors (Trifunac *et al.*, 1973; Wong and Trifunac, 1977; Todorovska *et al.*, 1995; Todorovska, 1998), or ground tilt and rotation (Graizer, 1991; Trifunac and Todorovska, 2001; Boore, 2001; Graizer, 2005; Graizer, 2006b; Kalkan and Graizer, 2007; Graizer and Kalkan, 2008; Graizer, 2010). Specific to analog instruments, baseline offsets may also appear during the process of producing the accelerations on film or paper (Trifunac *et al.*, 1973; Todorovska *et al.*, 1995; Trifunac *et al.*, 1999; Boore and Bommer, 2005), or during their subsequent digitizing (Trifunac *et al.*, 1973; Trifunac *et al.*, 1999; Boore and Bommer, 2005). Digital instruments baseline offsets may also be due to analog-to-digital converter error (Boore, 2003), or electronic 1/f noise (Kinoshita *et al.*, 1997; Kinoshita, 1998). By definition, the 1/f noise has a Fourier amplitude inversely proportional to the frequency, with a -1 slope in a log-log plot.

Despite these instrumental limitations, coseismic oscillatory and residual displacements are needed, and various processing methods have been developed to remove the baseline offsets. They include correcting the response of the instrument (Trifunac, 1972; Boore and Bommer, 2005), making baseline adjustments such as parabola (McComb, Ruge and Neuman, 1943), simple step function, pulse followed by a step function (Iwan *et al.*, 1985; Boore, 2001; Boore *et al.*, 2002; Wang *et al.*, 2003; Paolucci *et al.*, 2008) or other functions removed from accelerograms (Graizer, 1979; Boore and Bommer, 2005), filtering (Trifunac, 1971; Trifunac *et al.*, 1973; Graizer, 1979; Boore *et al.*, 2002; Wang *et al.*, 2007; Boore and Bommer, 2005), or a combination of functions removed from accelerograms and filtering (Trifunac, 1971; Boore *et al.*, 2002; Boore and Bommer, 2005).

The Figure 1.4 shows (a) an acceleration time history recorded in the near-

field of the 1999 Chi-Chi earthquake at station TCU129, and (b) the velocity time history obtained by simple integration of a strong-motion accelerogram, after removing the pre-event mean from the whole record. The Figure 1.4b and c shows various processing schemes proposed by Boore (2001) to correct the observed trends, based on the observation of the velocity time history: double steps functions, according to Iwan (1985)'s method, or a quadratic fit to the velocity time history. Details about the corrections schemes proposed by Boore are given in the Figure 1.4's caption.

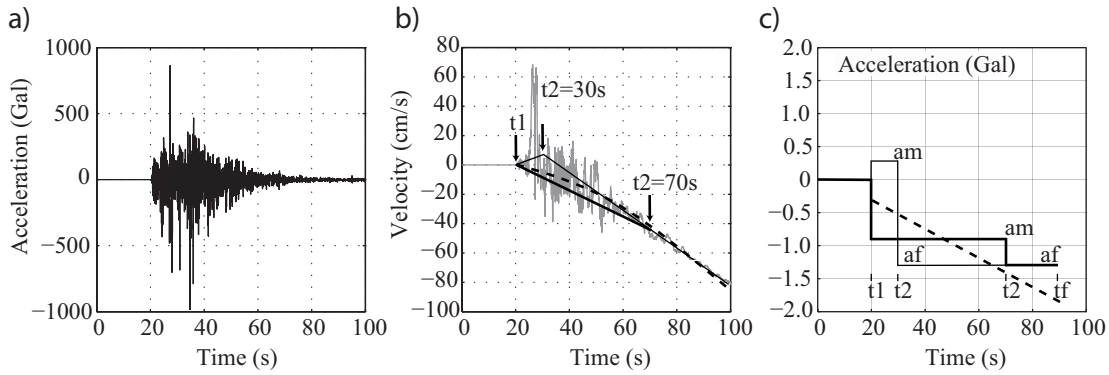

Figure 1.4: (a) Acceleration time history recorded during the 1999 Chi-Chi earthquake (Taiwan) at station TCU129 (EW component). The instrument was situated 1.9 km from the surface trace of the fault. (b) Velocity time history obtained from integration of the acceleration record, after removal of the pre-event mean from the whole record. Boore (2001) proposed several processing schemes: a least-squares line was fit to the velocity from 65 s to the end of the record. Various baseline corrections using the Iwan *et al.* (1985) scheme were obtained by connecting the assumed time of zero velocity t_1 to the fitted velocity line at time t_2. Two values of t_2 are shown: 30 s and 70 s. The dashed line is the quadratic fit to the velocities, with the constraint that it is 0.0 at t=20 s. (c) The derivatives of the lines fit to the velocity are the baseline corrections applied to the acceleration trace. (b and c) are reproduced from Boore (2001) and Boore and Bommer (2005).

The quality of the strong-motion accelerograms increased over the years with the development and deployment of instruments with higher performances. The TCU129 station was equipped in 1999 by Teledyne Geotech Model A900 digital recorders, a force-balance transducer with a natural frequency exceeding 50 Hz, 16-bit resolution, a maximum measurable acceleration of 2 g gain (where g is

the gravitational acceleration), and recording at 200 samples per second (Boore, 2001).

In this dissertation, we used accelerograms released by newer strong-motion seismometers of much higher characteristics, including a high dynamic range (analog-to-digital converter of 24-bit), such as the K-Net95 instrument detailed in chapter 2. The traditional methods described above were very interesting to obtain displacement time histories as realistic as possible when the translational acceleration delivered were contaminated by a sum of various instrumental noises that could not possibly be identified, then corrected, individually.

Recently, so as to have more criteria to select the appropriate processing methods, Emore *et al.* (2007) proposed to include the combined utilization of nearby 1-Hz GPS data together with an inversion technique to constrain the correction scheme. Also, Chanerley and Alexander (2010) and Chanerley *et al.* (2013) proposed purely signal processing approaches aiming at recovering a low frequency flying step in acceleration records. In this work, we focus on a modern high dynamic range strong-motion seismometers with low internal noise, which makes it possible to perform a detailed study of the instrument, our aim being to identify the different sources of noise which collectively contribute to the noise in the final acceleration data.

1.3 Data used

The data used in this dissertation were mainly recorded during the 2004 Niigata-ken Chuetsu earthquake, Japan (M_w 6.6, 23 October 2004, epicenter at 37.29°N, 138.87°E) and the 2007 Niigata-ken Chuetsu-Oki earthquake, Japan (M_w 6.8, 16 July 2007, epicenter at 37.56°N, 136.61°E), which produced large sets of strong-motion records, including near-field ground motions. Both were shallow crustal earthquakes with reverse faulting. The two Japanese nationwide networks K-Net and Kik-Net (NIED) released, for each main shock, nearly 900 digital, three components, strong-motion records. General information about these two earthquakes, that generate crustal movements in the land area around the source region, can be found in Asano and Iwata (2009), Tabuchi *et al.* (2008) and Miyake *et al.* (2010). Unless specified otherwise, the strong-motion data come

from the two networks K-Net and Kik-Net. We also used a few records from the Japanese Meteorological Agency recorded during the 2007 Niigata-ken Chuetsu-Oki earthquake.

Additionally, records of the M_J7.3 2000 Western Tottori earthquake (Japan) by the two GTA-53 (Meisei Electric Co. Ltd) strong-motion seismometers installed at Kasho dam are also used in section 4.3.

1.4 Outline of this dissertation

In view of the numerous possible reasons stated above that may generate baseline offsets in the acceleration time histories released by strong-motion seismometers, we first focus in **Chapter 2** on one modern strong-motion accelerometer. We selected the K-Net 95, installed within the Japanese K-Net and Kik-Net networks, and discussed its response from theoretical and experimental studies. The nature of the different sources of noise, which collectively contribute to the noise in the final digital data, is estimated and modeled. Residual rotation of the instrument (residual tilt) and 1/f digital semiconductor noise are the two main sources of long-period noise that contaminate the acceleration records delivered by the instrument and distributed on the K-Net and Kik-Net networks web pages.

Original in this work, the baseline offsets that contaminate the acceleration records are investigated, not in the time domain, but in the frequency domain. In **Chapter 3**, this thesis therefore presents a method to visualize in details the records' Fourier content. Long zero pads are added to the acceleration records to force computers to calculate the records' Discrete Fourier Spectra at frequencies so close that very detailed visualizations of the records' Fourier Spectra are obtained, including at low frequencies. Long period baseline offsets that contaminate the acceleration records, if any, may at this point be visualized in details.

Based on the preceding analysis and observations, we noticed that simple steps functions are often dominating the low frequency content of records. Their characteristic (starting time, amplitude) can be uniquely retrieved in the Fourier domain. Removing the step functions from the acceleration records lead to stable permanent displacements and reliable translational acceleration time histories.

In **Chapter 4**, we apply the method to strong-motion accelerations recorded in the near-field of large earthquakes.

First, we compare the displacement time histories obtained using strong-motion records of the 2007 Niigata-ken Chuetsu-Oki Earthquake (Japan) with those of 1-Hz GPS, as a check of the method.

Then, the origin of the simple step functions removed from the acceleration time series is confirmed. These simple steps functions are records of the instruments coseismic residual tilt. The accuracy of the permanent rotations angles estimated from acceleration time histories is validated by comparison with external rotation information. The data used come from Kasho Dam, a very well instrumented site, that experienced a very strong shaking including permanent rotation during the 2000 Western Tottori earthquake (Japan).

Finally, we investigate the possible implications of the proposed method to civil engineering applications, and especially focus on the design of structures. The reliable translational acceleration time histories and permanent rotations now available may contribute to better design structures. Improved displacement response spectra, especially at long periods, may indeed be obtained when the residual tilt is removed from the acceleration records. Also, the translational acceleration and the permanent rotation may abe used as input motion for time domain analysis either for numerical simulations or experimental modelisations.

Chapter 2

Performance of modern high dynamic range strong-motion accelerometers

2.1 General Remarks

The translational accelerations recorded by strong-motion seismometers are often contaminated by baseline offsets that prevent recovering the ground displacements by double integration. In order to understand the origin of the baseline offsets and to determine what the output of the seismometer consists of, we perform a detailed analysis of a modern strong-motion seismometer.

Among the modern strong-motion seismometers, we select the K-Net95 that was initially installed within the Japanese K-Net and Kik-Net networks (Fujiwara *et al.*, 2004). The choice of the K-Net95 is motivated by the release of its characteristics (full details in Kinoshita *et al.*, 1997; summary in Kinoshita, 1998) which enable a detailed study of the instrument, and by the very large number of instruments deployed, over 2000, uniformly covering all of Japan. K-Net (Kyoshin network) consists of 1 000+ strong-motion sensors settled on the ground surface and Kik-Net (Kiban kyoshin network) of 675 sets of borehole and surface strong-motion seismometers. K-Net seismometer and Kik-Net seismometer (named SMAC-MDK) are basically the same. The main difference is

that the data released by the Kik-Net network have a sampling frequency of 200 Hz while the K-Net records have a sampling frequency of 100 Hz (Fujiwara *et al.*, 2004).

The K-Net95 was in operation when the 2004 Niigata-ken Chuetsu earthquake (Japan) occurred. It recorded a set of high quality strong-motion records that were first used when we started this work. After years of operations, the K-Net95 instrument had progressively been replaced within the K-Net network by newer instruments. The Table 2.1 summarizes some key characteristics of all the strong-motion accelerometers whose data are used in this dissertation. In the Niigata area, the K-Net95 was replaced in 2005 for all K-Net stations by the K-Net02, an instrument of higher performances, including larger measurable range, lower internal noise (Figure 12.6 in Aoi *et al.*, 2011) and higher effective dynamic range (Aoi *et al.*, 2011). The 2007 Niigata-ken Chuetsu-Oki earthquake (Japan) was therefore recorded by the K-Net02 in operation at that time at the K-Net stations of the area, and still by the SMAC-MDK for the Kik-Net network. Since 2007, the instrumental evolution led to the progressive installation of K-Net02A strong-motion sensors for the K-Net network. Also, the surface instruments of the Kik-Net network (NIED) were partially replaced by Kik-Net06 and Kik-Net11 strong-motion sensors.

Since the installation of the K-Net95 strong-motion seismometer, the newer instruments installed within the K-Net and Kik-Net networks have similar or

Table 2.1: Synthetic characteristics of the instruments used in this dissertation.

	K-Net95	SMAC-MDK	K-Net02	K2 Altus	GTA-53
Maximum measurable acceleration (Gal)	2,000	2,000	4,000	1,000*	2,048
Accelerometer type	V403[a]	V404[a]	FBA-ES[b]	FBA-ES[b]	(FBA)[c]
Analog-to-digital converter	24-bit	24-bit	23.6-bit	24-bit	24-bit
Effective dynamic range**	114 dB (19-bit)	114 dB (19-bit)	132 dB (22-bit)	114 dB (19-bit)	129 dB (21.5-bit)

[a] Akashi Corporation.
[b] Kinemetrics Inc.
[c] Meisei Electric Co. Ltd.
*as set during the laboratory experiment in subsection 2.3.5.
**RMS noise / full scale.

higher characteristics. The results of the K-Net95's analysis performed in this chapter are therefore valid for these instruments, and also for other instruments of similar and higher characteristics such as the Kinemetrics Altus K2 used for laboratory experiments (subsections 2.3.1 and 2.3.5) and the GTA-53 strong-motion accelerometer (Meisei Electric Co. Ltd) that recorded the M_J7.3 2000 Western Tottori earthquake (Japan) at Kasho dam (section 4.3).

In outline, this chapter begins with a practical study of the shape and geographical distribution of the baseline offsets that contaminate the acceleration records (section 2.2). The example of the 2004 Niigata-ken Chuetsu earthquake, Japan, is detailed, and the shape of the baseline offsets estimated from the velocity trends derived from acceleration record.

The following section 2.3 discusses the response of the K-Net95 accelerometer from theoretical and experimental studies, and the origin of the observed baseline offsets. Original, and made possible by the detailed description of the K-Net95 strong-motion seismometer given by Kinoshita *et al.* (1997), we analyze each building part of the strong-motion seismometer with an aim at evaluating and modeling the different sources of noise, which collectively contribute to the noise in the final digital data. We find that the 1/f semiconductor noise and the tilting of the instrument are the two main sources of noise that significantly contaminate the translational acceleration. In his original paper, Kinoshita (1998) indicates that strong-motion records are contaminated by 1/f instrumental noise at low frequencies and stresses that the integration to displacement must suppress this 1/f noise. In this work, we verify the theoretical behavior of each part of the instrument. We especially use the complete equation of motion of a horizontal strong-motion transducer given by Trifunac & Todorovska (2001) and by Graizer (e.g., 2006b), which shows that the sensors record not only the translational acceleration (what they are made for) but also the tilting of the instrument. We carry out laboratory tests to confirm the effect of tilt, and to qualitatively and quantitatively evaluate the 1/f noise level in records.

In this chapter, we do not consider any malfunction of the instrument and consider its response to be its normal response in operation.

2.2 Shapes and spatial distribution of baseline offsets evaluated from acceleration records of the 2004 Niigata-ken Chuetsu earthquake, Japan

The Figures 2.1 and 2.2 show the spatial distribution of acceleration time histories recorded in the near-field of the 2004 Niigata-ken Chuetsu earthquake.

Accelerations of over 1000 Gal (1 g) were recorded by the JMA Kawaguchi station and by the K-Net NIG019 station situated respectively 2.4 km and 7 km from the epicenter.

A general decrease of the maximum recorded accelerations can be observed

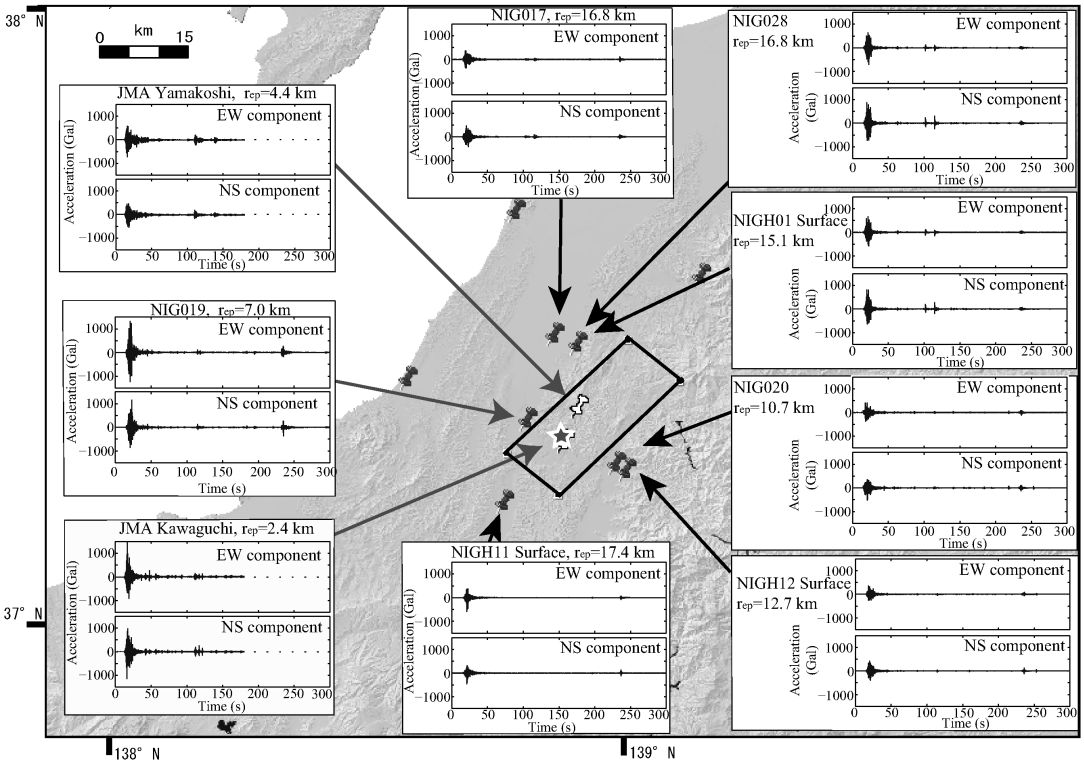

Figure 2.1: Spatial distribution of acceleration time histories recorded during the 2004 Niigata-ken Chuetsu earthquake, after removing their pre-event mean from the whole records (part 1 over 2: near the epicenter).

when the distance from the epicenter increases. The scale used to plot the acceleration records in Figures 2.1 and 2.2 can be used as a first good indicator (± 1500 Gal for the acceleration time histories displayed in Figure 2.1 versus ± 500 Gal for the acceleration time histories displayed in Figure 2.2 where the seismometers are more distant from the epicenter.).

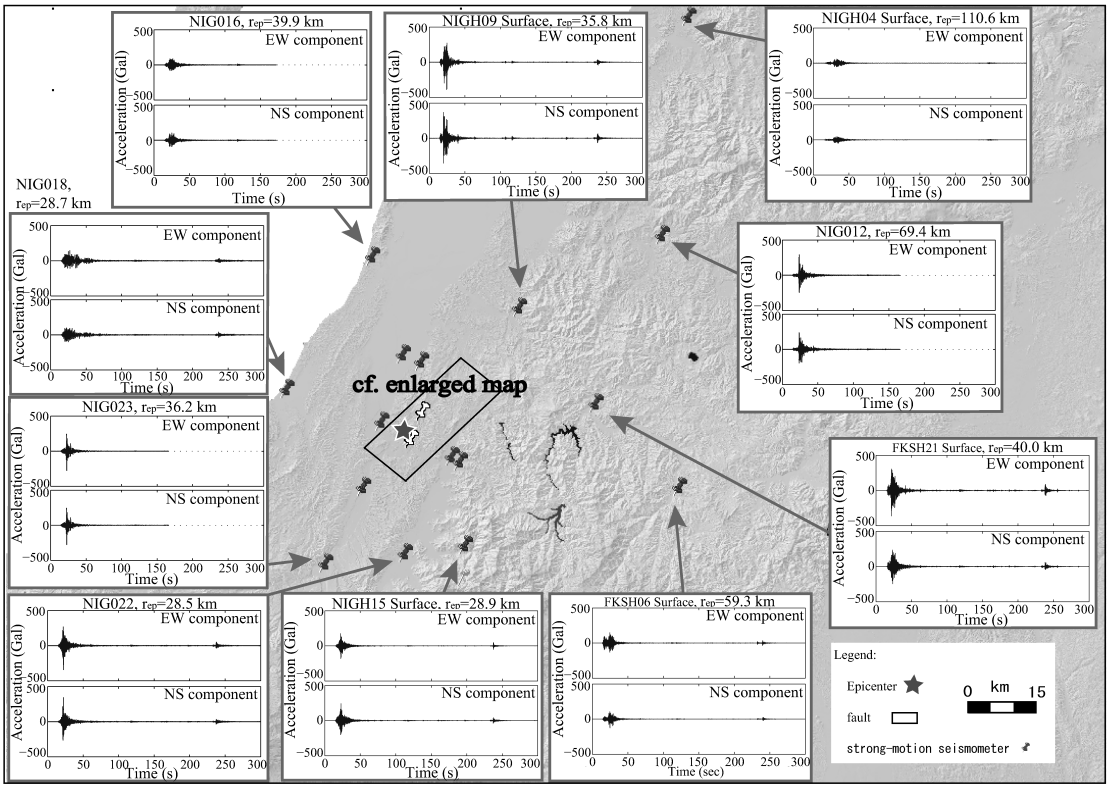

Figure 2.2: Spatial distribution of acceleration time histories recorded during the 2004 Niigata-ken Chuetsu earthquake, after removing their pre-event mean from the whole records (part 2 over 2: the seismometers are more distant from the epicenter).

The shapes of baseline offsets that contaminate the acceleration records are investigated from the trends of the velocity time histories, obtained by simple integration of the acceleration recorded by strong-motion seismometers, after removing the pre-event mean.

The velocity time histories are obtained by simple integration of the acceleration time series, after removing their pre-event mean from the whole records.

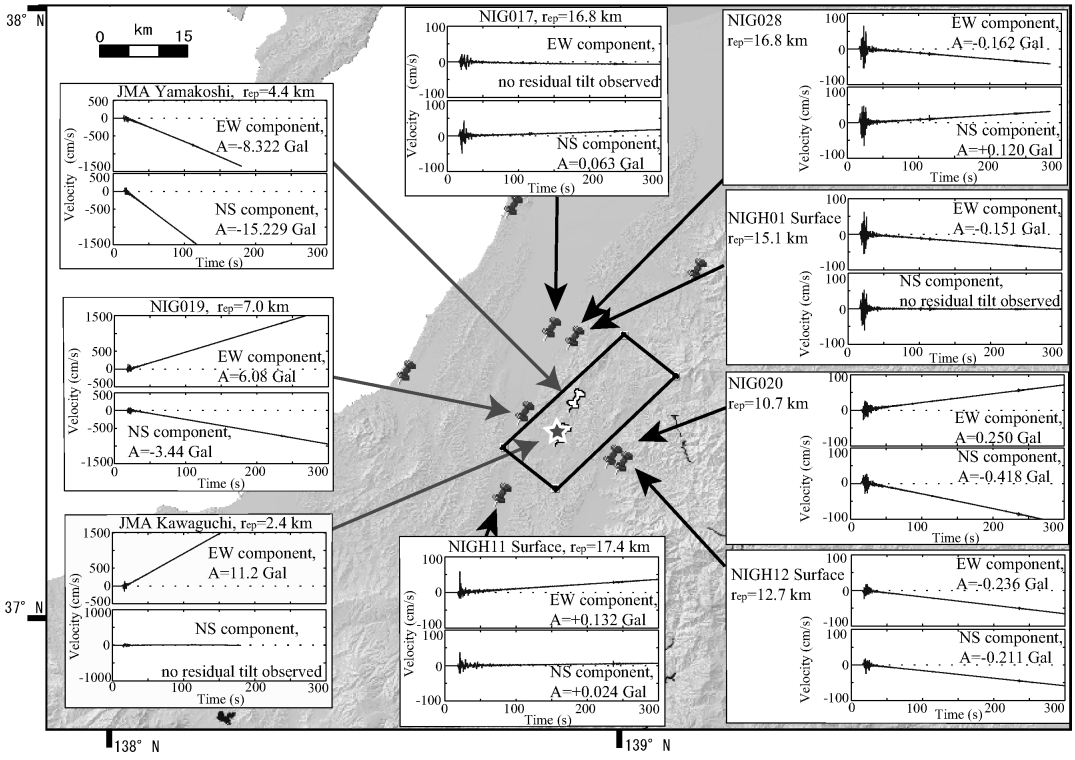

Figure 2.3: Spatial distribution of velocity time histories obtained by simple integration of acceleration recorded during the 2004 Niigata-ken Chuetsu earthquake, and estimated slope A of the velocity trend (part 1 over 2: near the epicenter).

The Figures 2.3 and 2.4 show the spatial distribution of velocity time histories, in the near-field of the 2004 Niigata-ken Chuetsu earthquake.

They reveal three main features. Firstly, the velocity shows linear trend but not everywhere. Secondly, the steeper slopes are observed near the epicenter: the scale variations used to plot the velocity can be used as a good first indicator. Also, the slope A of the linear trends, determined by using the processing scheme detailed later in chapter 3, is given for each record in Figures 2.3 and 2.4. It can be observed that the slope A tends to decrease when the epicentral distance increases (Figures 2.3 & 2.4). This is summarized in Figure 2.5 and shows that the origin of the baseline offsets in the strong-motion records is not a random process. Thirdly, far from the epicenter, there are no more linear trends but shapeless trends. Such shapes can also sometimes be observed near the epicenter of earthquakes and for the vertical components of the acceleration records. These

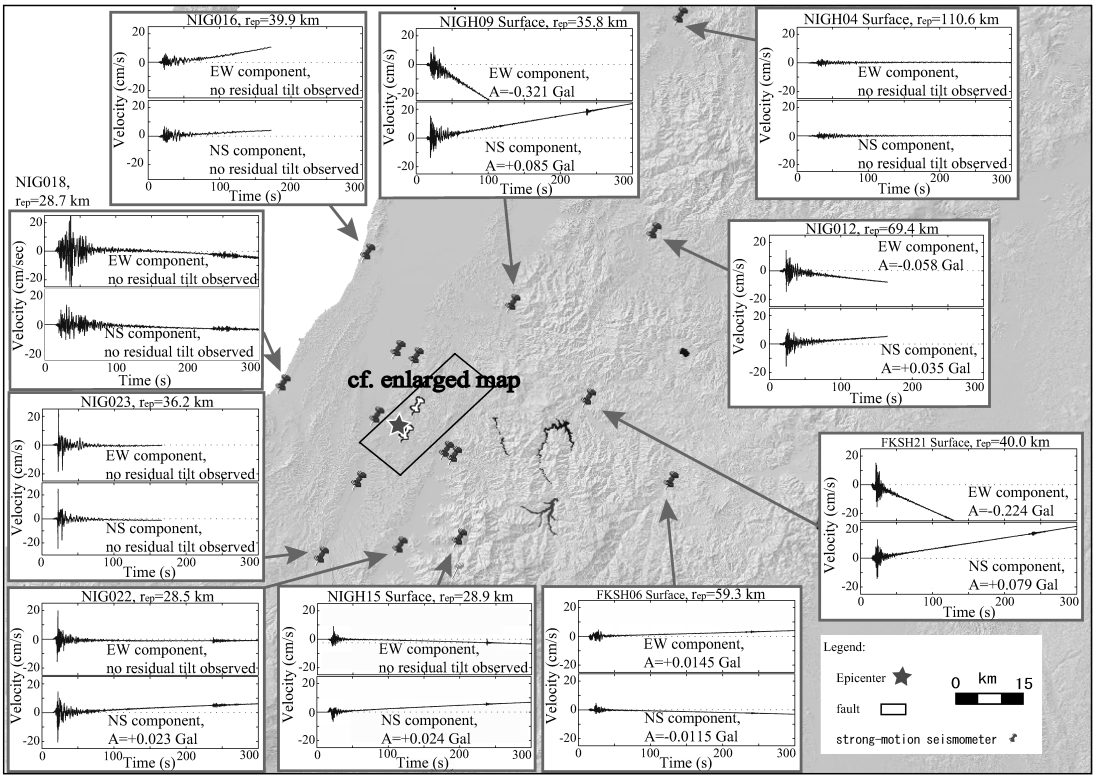

Figure 2.4: Spatial distribution of velocity time histories obtained by simple integration of acceleration recorded during the 2004 Niigata-ken Chuetsu earthquake, and estimated slope A of the velocity trend (part 2 over 2: the seismometers are more distant from the epicenter).

observations show that there are at least two different sources of baseline offsets.

Moreover, to check the possible abnormal behavior of the instruments, the Figure 2.6 shows the slopes of the linear trends observed in the velocity time histories versus the records' Peak Ground Acceleration (P.G.A.). For the two JMA stations (empty circles; four records) located in the very near field of the earthquake, the observed slopes are independent of the P.G.A. As for the K-Net and Kik-Net records (black circles), the largest slopes occur at the largest P.G.A. For a given P.G.A., the slope of the velocity trend varies largely, although the maximum slope tends to decrease when the P.G.A. increases. These observations show that there is no systematic dependence of the P.G.A. and the observed slope in the velocity records. The possible occurrence of accelerometers' abnormal behavior must however be kept in mind when processing the records.

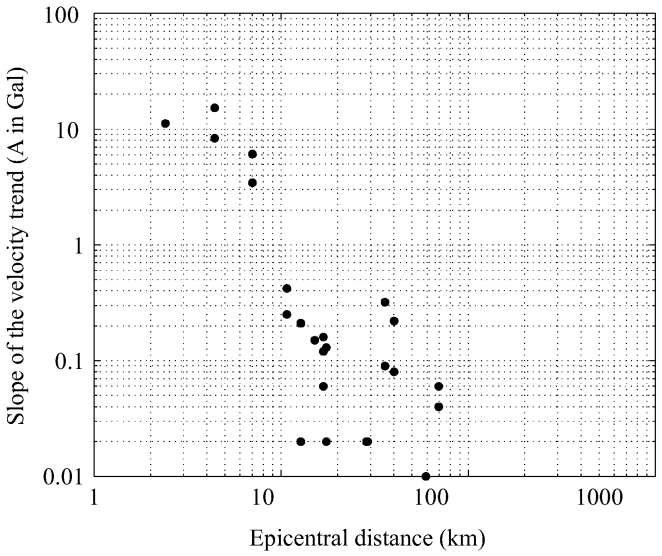

Figure 2.5: Slope of the velocity time histories (A in Gal) versus epicentral distance for the 2004 Niigata-ken Chuetsu earthquake.

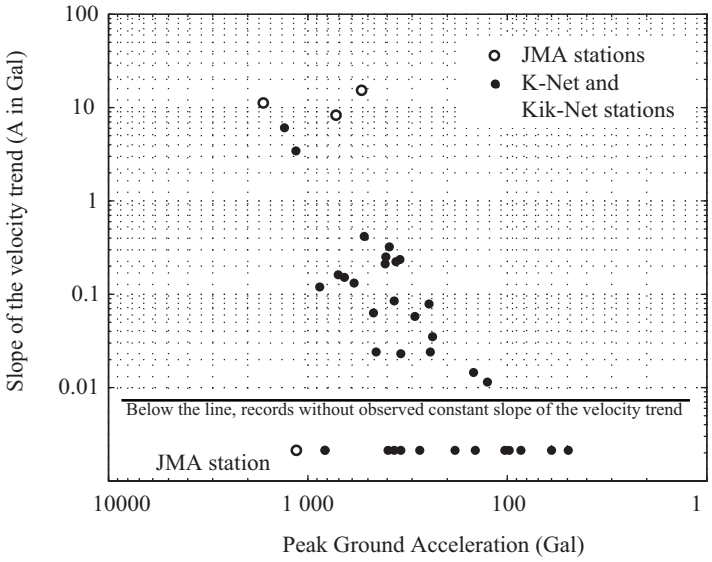

Figure 2.6: Slope of the velocity time histories (A in Gal) versus Peak Ground Acceleration for the 2004 Niigata-ken Chuetsu earthquake.

2.3 Description of K-Net95 and noise model

The K-Net95 strong-motion seismometer consists (Kinoshita *et al.*, 1997; Kinoshita, 1998) of 5 building blocks (Figure 2.7): a seismometer, an amplifier included in the sensor, an analog anti-alias filter for the analog-to-digital converter, an analog-to-digital converter and a digital anti-alias and decimation filter. Brief descriptions of the characteristics of each follow.

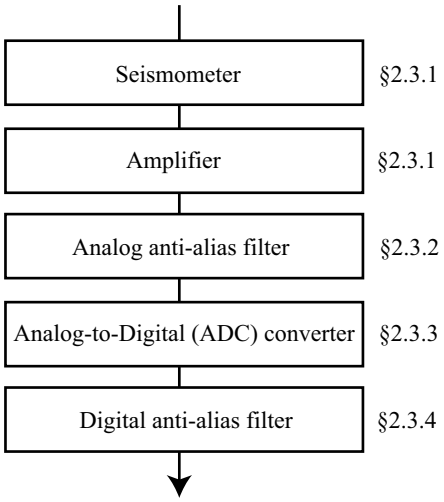

Figure 2.7: Block diagram of the K-Net95 recorded system. The paragraph numbers on the right indicate the subsection in which each elementary block is analyzed in details.

2.3.1 Seismometer

The sensor (Kinoshita *et al.*, 1997), type V403BT, is a tri-axial force-balance accelerometer with a natural frequency of 450 Hz and a damping factor of 0.707 (standard values). Its resolution is better than 0.1 mGal ($10^{-3} cm/s^2$). The seismometer's sensitivity is 3.0014 V/g.

A force-balance accelerometer (FBA) is basically an inertial seismometer that compensates the unknown inertial force acting on its suspended mass with a known force (Aki and Richards, 2002; Wielandt, 2002).

Theoretical response of the sensor. The simplified equation of motion of the accelerometer (NIED, 2000) is given below in equation 2.1.

$$y'' + 2\omega_o\zeta y' + \omega_o^2 y = -x'' \tag{2.1}$$

where x'' is ground acceleration, y the recorded response of the seismometer, $\omega_o = 450$ Hz and $\zeta = 0.707$ the natural frequency and the fraction of critical damping of the transducers.

The response of the seismometer, in the frequency range of interest, is flat to acceleration. Strictly speaking, the response of the accelerometer is frequency dependent (Aki and Richards, 2002; Amini and Trifunac, 1983 and 1985). However, when using a damping ratio $\zeta = 0.707$ $(1/\sqrt{2})$, the amplitude response of V403BT simulated in Figure 2.8 is nearly constant up to 150-200 Hz. K-Net and Kik-Net instruments release data sampled at 100 and 200 Hz respectively. It is thus possible to retrieve information from their records up to 50 and 100 Hz (Nyquist frequency) in the frequency domain. From zero to those frequencies, the amplitude response varies from 1 to 0.9999 and 0.9988 respectively and can be assumed to be constant and equal to one. The phase varies from 0 to $-9.04°$ and $-18.3°$ respectively from 0 to 50 Hz and 100 Hz. In this study, we do not correct the response of the sensor because the amplitude response is flat to acceleration and we neglect the phase shift.

The full equation of motion of a horizontal strong-motion transducer (Trifunac and Todorovska, 2001; Graizer, 2005; Graizer, 2006a and 2006b) can be written as follows. It is derived from the equation of a pendulum-like transducer (Figure 2.9). Compared to equation 2.1, new terms appeared on the right hand side of the equation, related to the instrument rotation ($g \sin \psi_i$ and $g(1-\cos \psi_i)$), the inertial force ($\psi_k'' r_j$) and cross-axis sensitivity ($x_i'' \theta_j$).

$$EW : y_1'' + 2\omega_o\zeta y_1' + \omega_o^2 y_1 = -x_1'' + g \sin \psi_2 - \psi_3'' r_1 + x_2'' \theta_1 \tag{2.2}$$

$$NS : y_2'' + 2\omega_o\zeta y_2' + \omega_o^2 y_2 = -x_2'' + g \sin \psi_1 - \psi_3'' r_2 + x_1'' \theta_2 \tag{2.3}$$

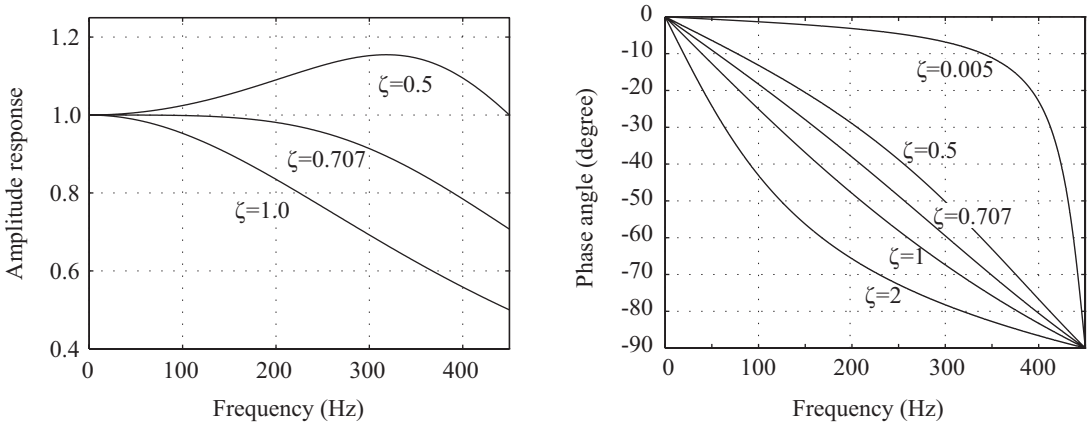

Figure 2.8: Variation of the amplitude response with damping and frequency. V403BT response is the simulation where $\zeta = 0.707$.

For a vertical seismometer

$$UD : y_3^{''} + 2\omega_o \zeta y_3^{'} + \omega_o^2 y_3 = -x_3^{''} + g\,(1 - \cos\psi_1) - \psi_1^{''} r_3 + x_2^{''}\theta_3 \qquad (2.4)$$

where $x_i^{''}$ is ground acceleration in ith direction, y_i the recorded response of the seismometer, $\omega_o = 450$ Hz and $\zeta = 0.707$ the natural frequency and the fraction of critical damping of the transducers.

$g \sin\psi_i$ and $g\,(1 - \cos\psi_1)$ are respectively the horizontal and vertical contribution to the response from tilt, where g is the gravitational acceleration and ψ_i a rotation of the ground surface about x_i axis. When the ground is tilted by an amount of ψ, the response of the system is exactly identical to an horizontal acceleration of magnitude $g \sin\psi$ or a vertical acceleration of magnitude $g\,(1 - \cos\psi)$. The effect of tilt is detailed further below in this subsection.

$\psi_k^{''} r_j$ is the inertial force term due to angular rotation (torsion of the instrument housing), where $\psi_k^{''}$ is the angle of pendulum rotation, and r_j the length of pendulum arm. For strong-motion seismometers, r_j is usually small, and equal to zero in some cases. In the description of the K-Net95 (Kinoshita, 1998), there is no mention that the acceleration records are dependent on this term. It is however possible to estimate an upper bound of the angular rotation's effect from the work of Lee and Trifunac (2009), considering that the length of the pendulum arm is

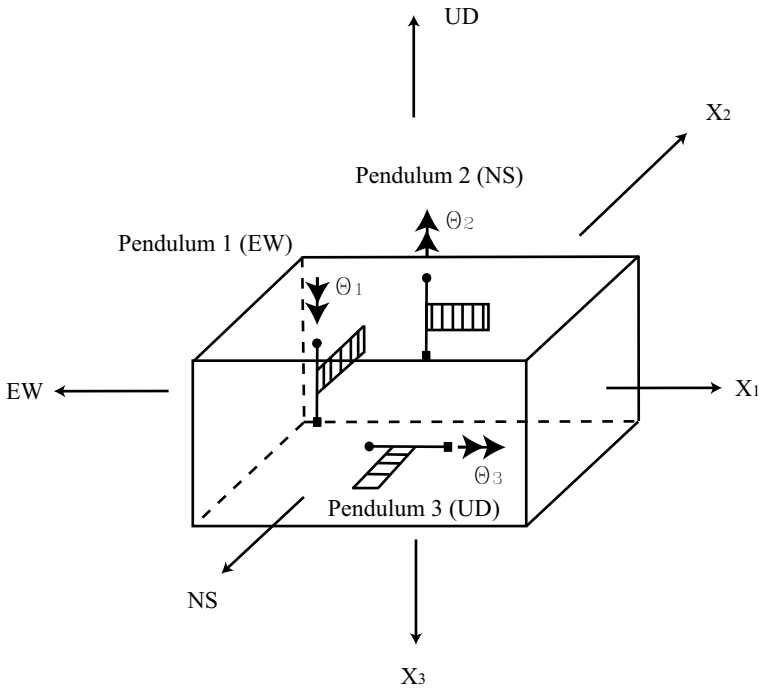

Figure 2.9: Schematic representation of three transducers in an accelerograph. The coordinate axes X_1, X_2, and X_3, serve to describe the motions of the EW, NS and UD transducers (modified from Graizer, 2005).

identical or smaller than the one of older instruments. For example, r ≈ 0,008 m for the SMA-1 strong-motion seismometer (Trifunac and Todorovska, 2001). The estimation of the inertial force due to the angular rotation term shows that it is always much smaller than the translational acceleration at low frequencies. It may however not be neglected for applications requiring detailed information about the very high frequency content of the acceleration records.

$x_i'' \theta_j$ is the contribution to the response from cross-axis sensitivity. Cross-axis sensitivity is the sensitivity of a transducer to motion perpendicular to its principal axis. For the K-Net95, there is no published measurement of its cross-axis sensitivity. However, Kinoshita *et al.* (1997) measured the overall cross-talk of the instrument by using a shaking table. These measured values of cross-talk provide a global quantification (mechanical & electrical) of signal leakage from one channel to another. At frequencies ranging from 1 to 10 Hz, the cross-talk is less than 1%. It is smaller at lower frequencies. In this study, we do not

correct the cross-axis sensitivity, because it is much smaller than the translational acceleration, especially at low frequencies.

Effect of tilting on the seismometer's output. Due to the sensitivity of the strong-motion accelerometer to tilt pointed out above, we further analyze the effect of tilting on the seismometer's output. The response of the seismometer to tilt is first experimentally confirmed. Then, the effect of tilt (transient and residual) on the displacement time histories derived from acceleration is evaluated.

Experimental effect of tilting on the seismometer output. Theoretically, when the ground is tilted by an amount of ψ, the system's response is exactly identical to an horizontal acceleration of magnitude $g \sin \psi$ or to a vertical acceleration of magnitude $g\,(1 - \cos \psi)$.

We used an Altus K2 strong-motion seismometer available for laboratory testing, and experimentally rotated it around its X axis, as shown in Figure 2.10. The

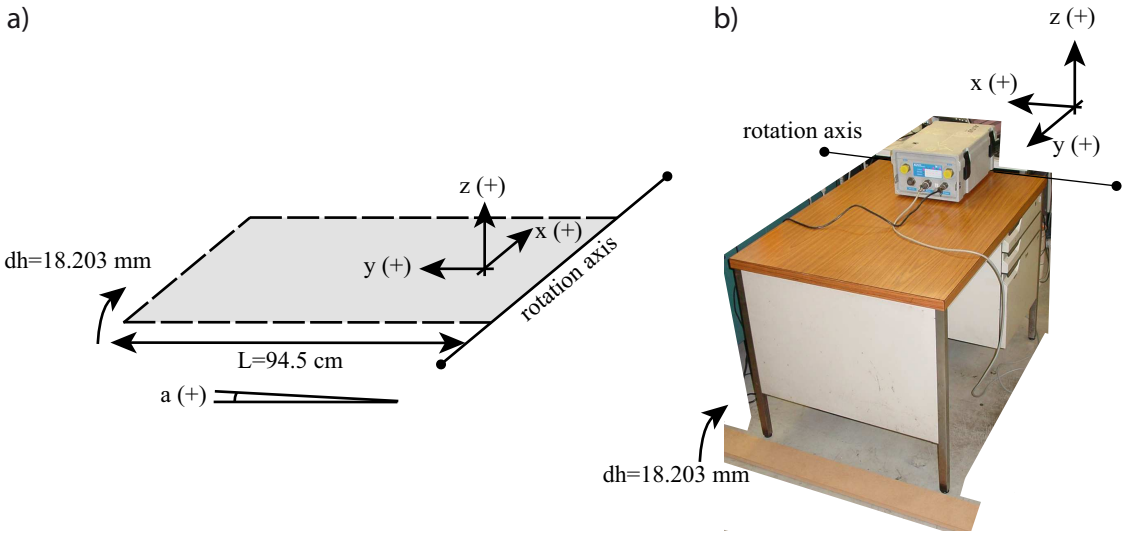

Figure 2.10: Experimental setup for the rotation of a K2 Altus strong-motion seismometer. The axis (X,Y,Z) shows the orientation of the instrument set on a table. It was rotated around its X axis by 1.10° by moving upwards one side of the table. (a) Sketch of the experiment from its side. (b) Picture of the experiment taken from its front.

experiment was carried out on January 20^{th}, 2006, and the angle of rotation was 1.10°. The sampling frequency of the records is 100 Hz. The Figure 2.11 shows the acceleration recorded before and after the tilting of the instrument, the latter lasting from the 16^{th} to the 22^{nd} second of the record. According to equation 2.3, the acceleration offset caused by the rotation and recorded by the Y axis should be $980 \sin(+1.10°) = +18.81$ Gal, which is identical, at the experimental rotation error, to what can be observed in Figure 2.11, Y component. Inversely, an angular rotation of -1.10° would give an output of -18.81 Gal. As expected, the angular rotation is not recorded by the X axis. As for the Z axis, the theoretical acceleration offset caused by the rotation is $980(1 - \cos(+1.10°)) = +0.18$ Gal, which is by far smaller than for the Y axis, and conform to the measured acceleration that shows no significant offset after the rotation. Therefore, any rotation of the strong-motion instrument is recorded simultaneously to the translational ground acceleration. The acceleration time series delivered by the instrument include the record of the instrument's rotation during the transient part of the shaking (transient tilt), but also any residual rotation (residual tilt) as a constant value that lasts until the end of the record.

Effect of transient tilting on the acceleration record. Published comparisons of oscillatory displacements from 1-Hz GPS instruments with those derived from nearby K-Net and Kik-Net accelerograms, after accounting for a baseline offset using the pre-event signal, show very good similitudes (Miyazaki *et al.*, 2004, Figure 2 and Clinton, 2004, chapter 4). The results shown later in chapter 4 (especially at Ojiya stations where the instruments are only 600 m apart from each other) confirm these observations. We therefore assume that the effect of the transient ground tilt on the displacement can be neglected.

Effect of residual tilting on the acceleration record. Any residual tilt is recorded by strong-motion seismometers as a constant value lasting until the end of the record. To get insights of the effect of this addition of low amplitude but long duration information, it is convenient to model the residual tilt. The simplest method to simulate the residual tilt is to consider a step function of amplitude A and duration T, ending at the end of the record. When processing the data, finite length records are used. The step function becomes a box-like function lasting until the end of the record. The Fourier transform of that box-like

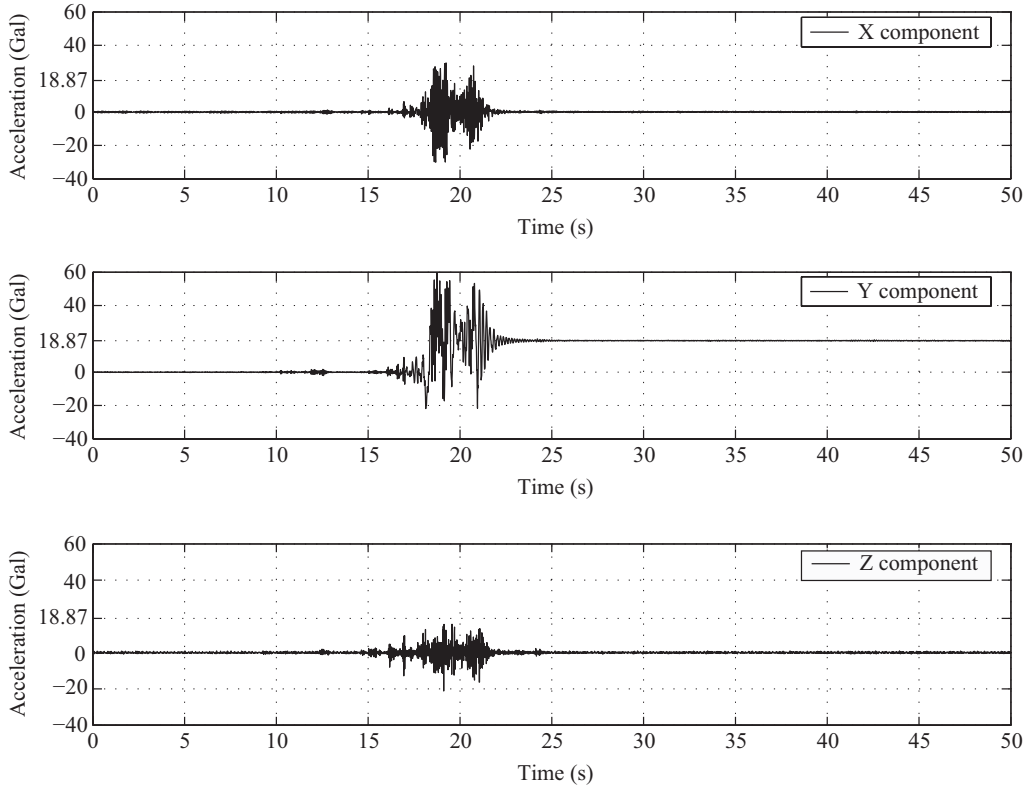

Figure 2.11: Experimental rotation of a K2 Altus strong-motion seismometer around its X axis, and effect on the seismometer output. The acceleration offset caused by a rotation of 1.10° is recorded by the Y axis as an permanent acceleration.

function has an amplitude of $F(f) = AT\frac{\sin(\pi fT)}{\pi fT}$. It shows three main features. First, when the frequency f is equal to, or is a multiple of $\frac{1}{T}$, $F(f) = 0$. Then, $F(f) \to AT$ as $f \to 0$. Furthermore, the envelope of the signal has a slope of 1/f.

2.3.2 Analog anti-alias filter

This analog high-cut filter consists (Kinoshita, 1998) of a two-stage RC filter with time constants of 1/12 600 and 1/62 600 s. We simulated the filter's response. It is flat to 1000 Hz and the phase shift is zero to 100 Hz: from zero to 50 Hz (K-Net) and 100 Hz (Kik-Net), the amplitude response varies from 1 to 0.9997 and 0.9987 respectively and the phase varies from 0 to −1.72° and −3.43° respectively. Therefore, both the amplitude and phase can be assumed to be constant.

2.3.3 Analog-to-Digital converter

The analog-to-digital converter (ADC) consists (Kinoshita *et al.*, 1997; Kinoshita, 1998) of a 1-bit sigma-delta modulator (Mitra and Kaiser, 1993) and a digital decimation filter. It can be approximated to a 24-bit type converter.

Evaluation of the effect of the ADC noise (ie, of its dynamic range) on the final displacement. The effect of the ADC noise on the final displacement is estimated. Basically, the ADC converts the output of the amplifier (3.0014 V/g) into integers. The maximum measurable acceleration of K-Net95 is 2000 Gal. This means that at each sampling time, for each analog input ranging from -6 V to +6 V corresponds an integer value among the $2^{24} = 16\ 777\ 216$ possible ones. The smallest input voltage change that causes the output value of the ADC to increase or decrease by one unit, known as the Least Significant Bit Value or Q, is (Scherbaum, 2001)

$$Q = \frac{\text{Full Scale Voltage}}{2^n}, \tag{2.5}$$

for an n-bit ADC.

Assuming that the conversion induces an uniformly distributed white-noise (Scherbaum, 2001), the standard deviation of the noise is

$$\sigma_a = Q/\sqrt{12}. \tag{2.6}$$

Double integration of this white noise is a random variable with zero mean and non-zero standard deviation. The standard deviation of the final displacement ($\sigma_{d_{end}}$) is (Boore, 2003)

$$\sigma_{d_{end}} = \left(\frac{T^3 \Delta t}{3}\right)^{\frac{1}{2}} \sigma_a, \tag{2.7}$$

where T is the duration of the time series and Δt the sampling interval.
K-Net95 has a Q value of 7.15 10^{-7} V/count, which is 2.34 10^{-4} Gal/count. With this value, equations (2.6) and (2.7) give $\sigma_{d_{end}}$ of 0.004 cm and 0.003 cm for the K-Net and Kik-Net instruments respectively, after integration of 100 s. Thus, this model of the analog-to-digital converter shows that the ADC noise can be

neglected.

Evaluation of the effect of the instrument's noise level (effective dynamic range) on the final displacement. The noise level of the instrument is essentially not due to the analog-to-digital converter of the sensor (of 24-bit) but to the overall acquisition system that has an effective dynamic range of 114 dB (19-bit) (Table 2.1).

Similarly to the preceding paragraph, the standard deviation of the final displacement due to the instrumental noise is of 0.13 cm and 0.09 cm. Therefore, this model shows that the effective dynamic range of the instrument does not affect significantly the displacement obtained by double integration of the acceleration records.

2.3.4 Digital anti-alias filter

In this subsection, we investigate the effect of the digital anti-alias filter on the displacement.

The digital high-cut filter is a three-pole Butterworth filter with a corner frequency of 30 Hz. This filter was designed by applying the bilinear transform to an analog Butterworth filter (Kinoshita, 1998). We used the same procedure to simulate the filter's response, whose amplitude is shown in Figure 2.12.

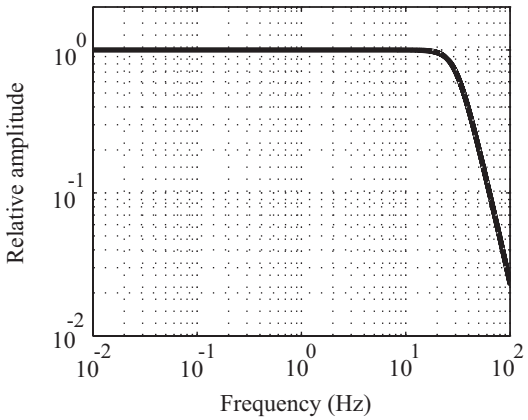

Figure 2.12: Simulation of the amplitude response of the digital anti-alias filter.

A simple model (Figure 2.13) that simulates the amplitude response of a

high-cut filter (Figure 2.13, a) is used. It separates its amplitude response into an all-pass filter (Figure 2.13, b) and a box-like function (Figure 2.13, c). The box-like function has an amplitude of 0 up to 20 Hz, then it linearly increases up to 80 Hz (Kik-Net) where it reaches a value of 1. Above 80 Hz, the amplitude is 1. This function is subtracted from the all-pass filter.

The effect of the box-like function on the velocity is calculated. Let $B(f)$ be the box-like function in the frequency domain and $b(t)$ its inverse Fourier transform in the time domain. Thus,

$$B(f) = \int_{-\infty}^{+\infty} b(t) e^{-j2\pi ft} dt. \tag{2.8}$$

When f=0, $B(0) = \int_{-\infty}^{+\infty} b(t)dt$, where $\int_{-\infty}^{+\infty} b(t)dt \approx \int_{0}^{t_{end}} b(t)dt$ is the residual velocity obtained at the end of the record t_{end} by single integration of b(t). Moreover, $B(0) = 0$ by definition, as can be seen in Figure 2.13. Thus $B(0) = \int_{0}^{t_{end}} b(t)dt = 0$ and adding or subtracting such a box-like function has no effect on the residual velocity and thus on the residual displacement. This simple model shows that the presence of the digital anti-alias filter has no effect when double integrating the acceleration to obtain the displacement.

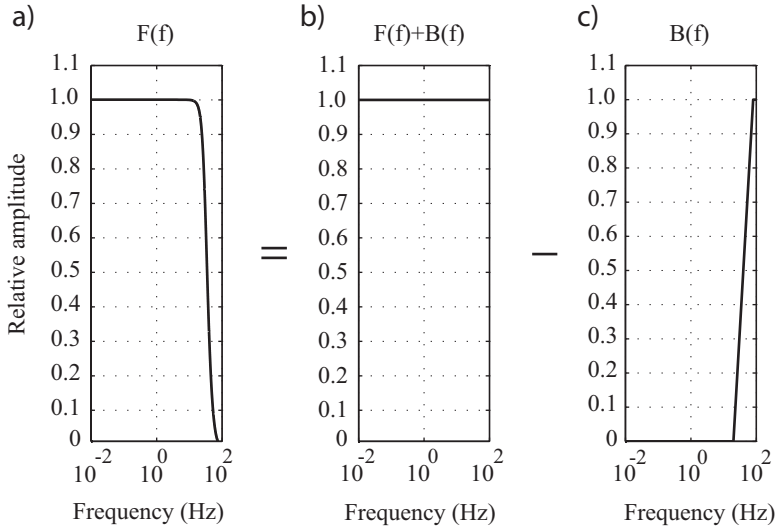

Figure 2.13: Simple model used to investigate the influence of the digital anti-alias filter on displacement.

2.3.5 Presence of 1/f noise at low frequency

As all seismographs using semiconductor circuits, the K-Net95 output acceleration data is contaminated at low frequencies by 1/f noise (Kinoshita *et al.*, 1997; Kinoshita, 1998).

After checking the presence of 1/f noise in records of the Kinemetrics K2 Altus series, an instrument similar in that respect to the K-Net95, and available for laboratory test, we then describe a practical method to determine the 1/f noise level of each accelerometer used in the K-Net and Kik-Net networks. The 1/f noise has by definition a -1 slope in a log-log plot, but its level (Fourier amplitude of the 1/f noise at a given frequency) varies.

Practical evaluation of the 1/f noise level when very long microtremor records are available. The performance of the K2 strong-motion seismometer is evaluated by comparing its theoretical response to the observed one.

Kinemetrics Inc. (Manual) provides the theoretical response of the K2 strong-motion seismometer through an empirical model of the K2 sensor: two pairs of conjugate poles were found to well represent the instrument's transfer function. We simulated the amplitude of the instrument's overall response according to Kinemetrics' model (Figure 2.14).

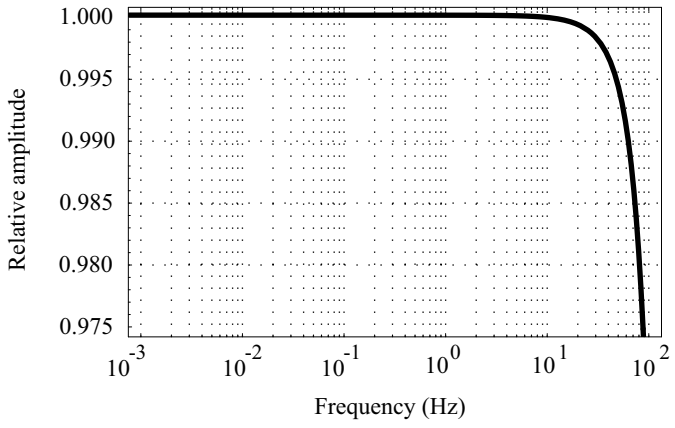

Figure 2.14: Simulation of the Kinemetrics K2 sensor's amplitude response.

Each accelerograph's response can be tested by using ambient vibration noise records. In a first step, we performed simultaneous record of ambient vibration

noise by both a Kinemetrics K2 accelerometer and by a sensitive velocimeter (Figure 2.15). The sensors were installed in the basement of the laboratory building and ambient vibration noise was recorded early morning at 1:30 am so as to have as quiet as possible experimental conditions. The records were made on March 24^{th}, 2006. The Figure 2.16a shows the vertical component of a 775 s acceleration time history recorded by the Kinemetrics K2 accelerometer. Its sampling frequency is 200 Hz. The first 20 s' mean of the acceleration record was first removed from the entire record. The Figure 2.16b shows the Fourier spectrum of the acceleration time history.

The velocity time history recorded by the sensitive velocimeter is given in Figure 2.16c. Its sampling frequency is 200 Hz. Similarly, the first 20 s' mean of the velocity record was first removed from the entire record. The Figure 2.16d shows

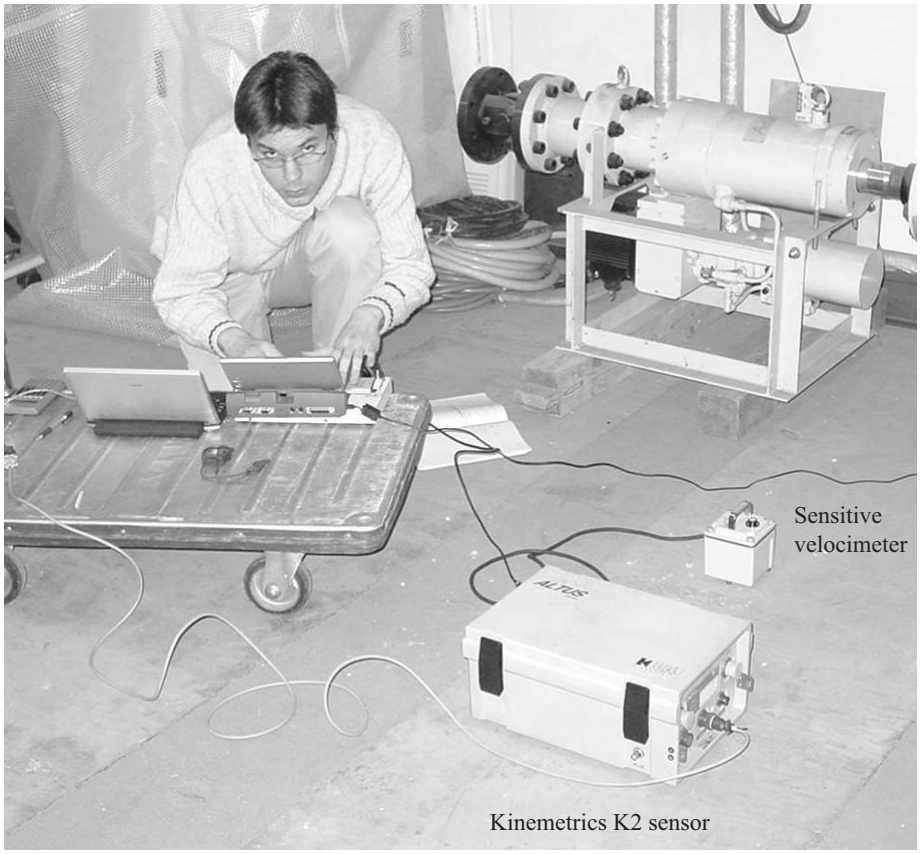

Figure 2.15: Simultaneous record of ambient vibration noise by a Kinemetrics K2 sensor and by a sensitive velocimeter in the laboratory building's basement.

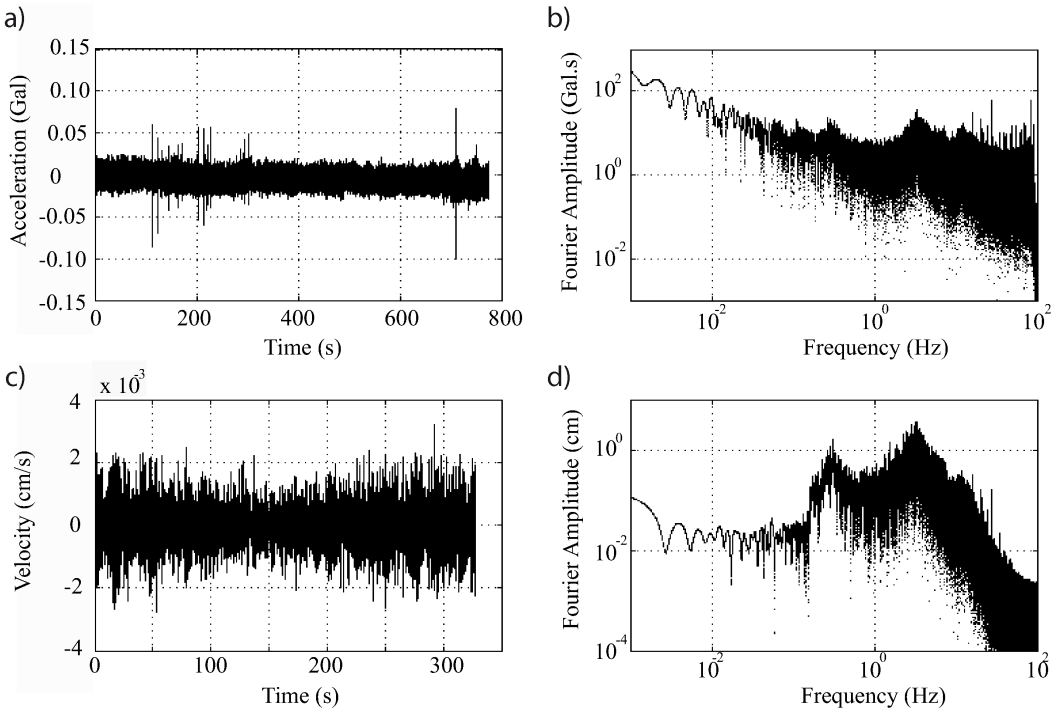

Figure 2.16: (a and c). Simultaneous record of ambient vibration noise by a strong-motion accelerometer (a) and by a sensitive velocimeter (c). The comparison of (a) and (c) in the Fourier domain (b and d) shows that the K2 instrument records the natural response of the building from 0.5 to 20 Hz. b) Above 20 Hz, the noise rapidly decreases in amplitude: the ground acceleration (input of the instrument) is high-cut filtered by the instrument's response (as expected from the theoretical response in Figure 2.14). At low frequencies, up to 0.5 Hz, 1/f digital semiconductor noise predominates.

the Fourier spectrum of the velocity time history.

The comparison of this acceleration record's Fourier amplitude spectrum (Figure 2.16b) with the Fourier amplitude spectrum of the velocity record (Figure 2.16d) shows that the K2 instrument records the natural response of the site from 0.5 to 20 Hz. Above 20 Hz, the noise rapidly decreases in amplitude: the ground acceleration (input of the instrument) is high-cut filtered by the instrument's response (as expected from the theoretical response in Figure 2.14). At low frequencies, up to 0.5 Hz, 1/f digital semiconductor noise predominates.

Similar results were obtained from long ambient vibration noise time histories recorded by the strong-motion accelerometer installed this time in the laboratory

on the ninth floor. The Figure 2.17, left column, shows 240 s acceleration time histories recorded in the laboratory by the three components of a Kinemetrics K2 accelerometer. The records were made during the afternoon on January 18^{th}, 2006. Their sampling frequency is 200 Hz. Figure 2.17, right column, are the Fourier acceleration spectrum of each record. At low frequencies, up to 0.5 Hz, 1/f digital semiconductor noise predominates. The Fourier amplitude of 1/f noise is inversely proportional to the frequency. It has a -1 slope in a log/log plot.

For each component, the real amplitude response of the accelerometer is therefore the sum of its theoretical response and of 1/f noise at low frequency (Figure 2.18).

The amplitude of the 1/f noise depends on the sensor. In Figure 2.17, among the three components, the Y component has the larger 1/f noise and the Z component has the smaller one. This can be easily observed by comparing the Fourier amplitudes in Figure 2.17 (b, d, and f) at the frequency of 10^{-2} Hz for example. Moreover, from our experience, the 1/f noise level varies not only according to each sensor, and but also with time. It must therefore be determined for each accelerometer component before processing the records.

Practical evaluation of the 1/f noise level when long microtremor records (about 100 s) are available. The response of each accelerometer and the 1/f noise level can be evaluated by using ambient vibration noise (microtremor) records. These records are very similar to the pre-event part of the main shocks. They are of same amplitude, but of longer duration. We usually use 100 s long records. Such records can be found among the large number of aftershocks recorded by the K-Net and the Kik-Net networks. Figure 2.19 shows the acceleration power spectrum of the ambient vibration noise recorded at the bottom of an observation borehole at the Kik-Net NIGH04 station. The spectrum shows the characteristics of electrical instruments (Smith, 1999). At low frequencies, up to 0.1 Hz, digital $1/f$ semiconductor (Kinoshita, 1998) noise predominates. Between 0.1 and 20 Hz, the signal consists of white noise. Above 20 Hz, the noise rapidly decreases in amplitude (digital anti-alias filter; subsection 2.3.4). At very high frequencies, the A/D converter noise (subsection 2.3.3) predominates. It is therefore possible to precisely estimate the 1/f noise level.

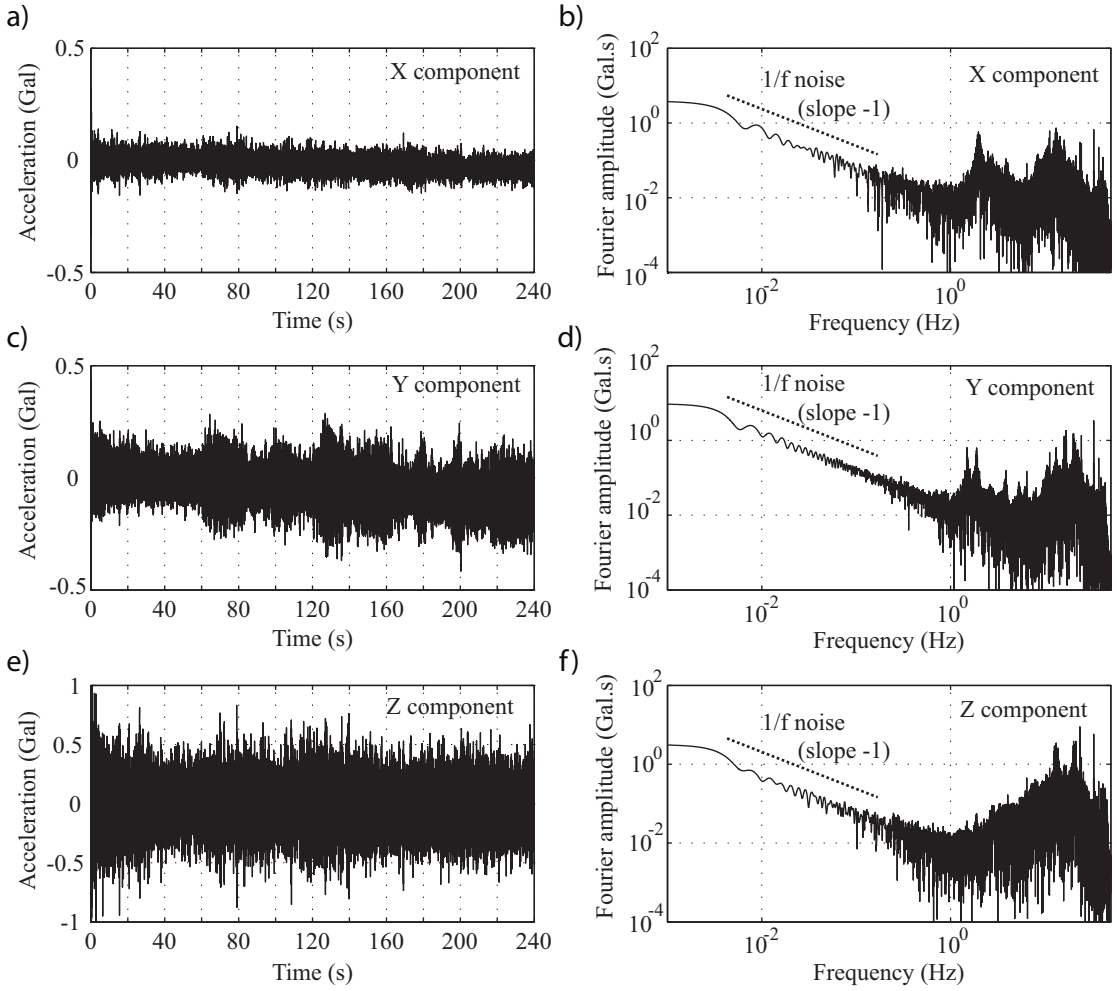

Figure 2.17: (a, c and e) Kinemetrics Inc. K2 accelerometer ambient vibration noise records and (b, d and f) their Fourier transform. At low frequencies, up to 0.5 Hz, 1/f digital semiconductor noise predominates. The Fourier amplitude of 1/f noise is inversely proportional to the frequency. It has a -1 in the log/log plots.

Practical evaluation of the 1/f noise level when long microtremor records (about 100 s) are not available. The example detailed here comes from Kasho dam that is equipped with two modern three components digital strong-motion seismometers type GTA-53 (Meisei Electric Co. Ltd).

The GTA-53 sensor is a triaxial force-balance accelerometer, whose characteristics are as follows: its analog-to-digital converter and digital anti-alias filter

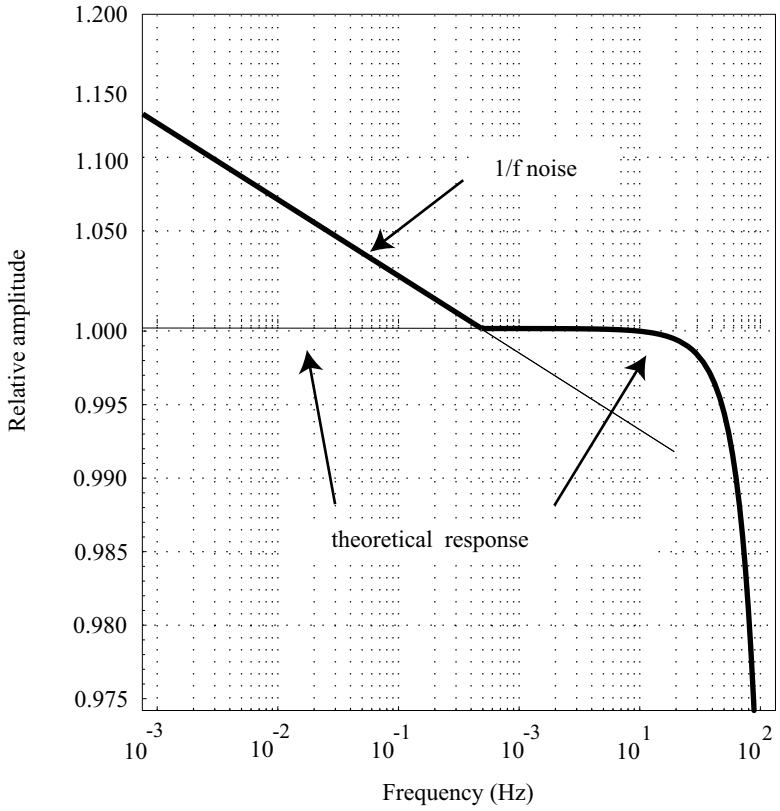

Figure 2.18: The observed response of the accelerometer is the sum of its theoretical response and of 1/f low frequency semiconductor noise.

consist of a sigma-delta modulator and a digital filter that can be approximated to a 24 bit type converter (Meisei Electric Co. Ltd); for this instrument, the least significant bit value, smallest acceleration change that causes the analog-to-digital converter's output to increase or decrease by one unit, is 0.000391 Gal/count; the overall instrument's response is flat from DC to 41 Hz; records are delivered with a sampling frequency of 100 Hz.

Here, long noise records are not available and we therefore performed the testing by using the records of both a very small amplitude aftershock and of the main shock's pre-events. We selected a small aftershock because its low frequency content is controlled by the 1/f instrumental noise (this will be discussed later in chapter 3, processing case 1). Figure 2.20 a and b, shows the acceleration time histories recorded on the 9^{th} of October, 2000, whose amplitudes are less than

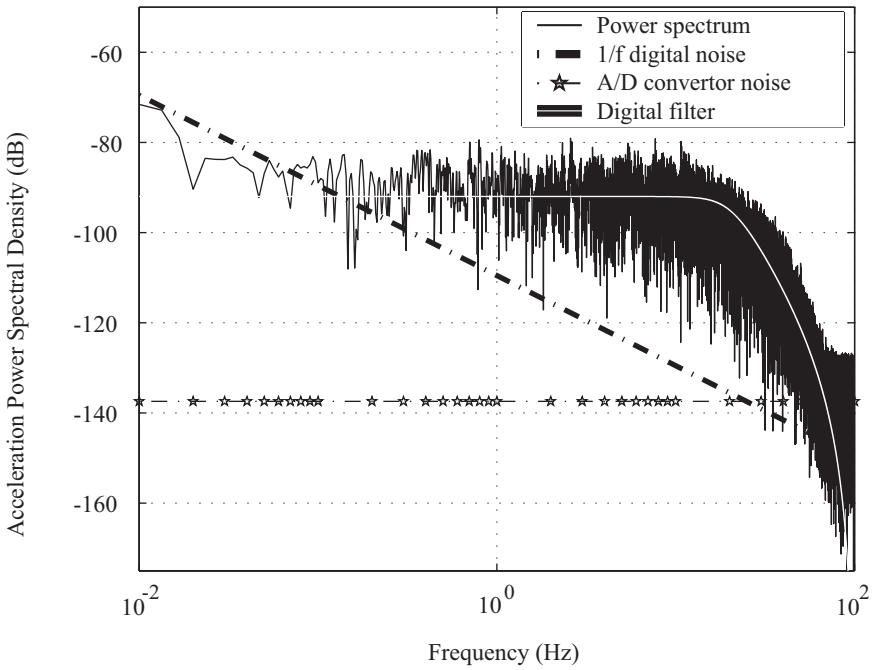

Figure 2.19: Power spectrum calculated from a noise record at Sekikawa NIGH04 station, underground seismometer, recorded soon after the 2004 Niigata-ken Chuetsu earthquake, Japan. The power spectrum representation allows comparison with Kinoshita's original papers.

16 Gal for both the EW and NS components (to be compared with about 530 Gal recorded during the main shock). In Figure 2.20 c and d, this aftershock's Fourier amplitude spectra decrease at low frequencies till about 0.2 Hz, which provides information about the 1/f low frequency noise levels. Figure 2.20 c and d, also shows the main shock pre-events' Fourier amplitude spectra. They can be used to retrieve the instruments' middle to high frequency responses, which, in this case, are consistent with the instruments' theoretical response: for the EW and NS components, between 0.4 and 40 Hz the signals consist of white noise; above 40 Hz they rapidly decrease in amplitude due to the high-cut filter (Figure 2.20 c and d).

At low frequencies, both the overall ambient vibration noise and small aftershock Fourier spectra decrease with increasing frequencies, confirming the presence of 1/f noise, whose level estimated for each component (Figure 2.20 c and d: 1/f noise model, with a -1 slope in the log-log plot) is now available for further

studies investigating the nature of the low frequency content of strong-motion records.

2.4 Conclusions of Chapter 2

In this chapter, we analyzed the performance of a specific modern strong-motion seismometer, the K-Net95, that was widely installed within the K-Net and Kik-Net networks. The different sources of noise, which collectively contribute to the noise in the final digital data, are estimated and modeled. The conclusions drawn from this chapter are as follows:

- The full equation of a strong-motion seismometer indicates that the instrument records not only the translational acceleration but also the instrumental rotation, cross-axis acceleration and angular rotation (subsection 2.3.1). The analysis shows only the instrumental rotation should not be neglected for the horizontal components when computing the displacement. When the ground is tilted by an amount of ψ, the response of the system is exactly identical to an horizontal acceleration of magnitude $g \sin \psi_i$, where g is the gravitational acceleration and ψ_i a rotation of the ground surface about x_i axis.

- The analysis shows that the analog anti-alias filter for the analog-to-digital converter (subsection 2.3.2), the analog-to-digital converter's noise (subsection 2.3.3), as well as the digital anti-alias filter (subsection 2.3.4) have no significant effect when double integrating the acceleration to obtain the displacement.

- Strong-motion acceleration records are contaminated by 1/f semiconductor instrumental noise at low frequencies. In his original paper detailing the characteristics of the K-Net95 instrument, Kinoshita (1998) mentioned the presence of 1/f noise and indicated that it must be suppressed when computing the displacement time histories by double integration. In this chapter, we experimentally confirm the presence of 1/f noise in the acceleration time

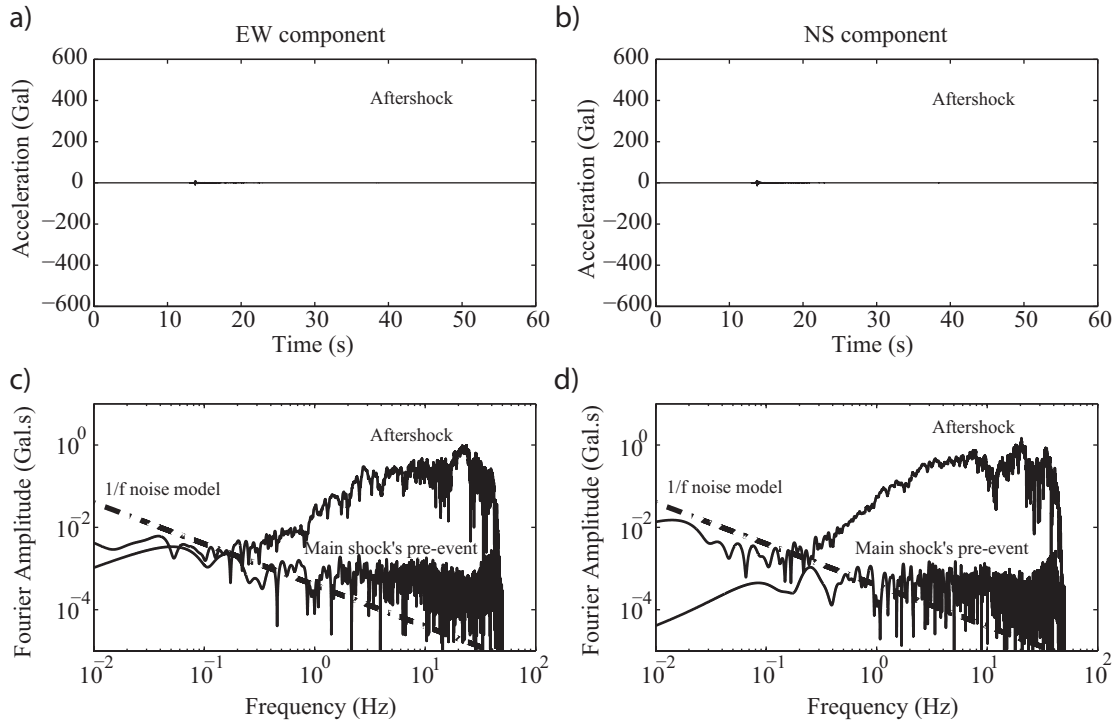

Figure 2.20: (a, b) Small aftershock recorded within the inspection gallery on the 9^{th} of October, 2000, at 15H 14min 30s. The accelerations are less than 16 Gal (we used the same scale as in Figure 4.6 a, b, where the main shock's acceleration records are displayed). (c and d) The Fourier amplitude spectra calculated from the above small aftershock time histories decrease until 0.2 Hz and provide information about the instruments' internal 1/f noise. The Fourier amplitude spectra calculated from the pre-event parts of the main shock recorded at the low inspection gallery are also displayed. They provide information about the instruments' middle to high frequencies and confirm their theoretical response: from 0.4 to 40 Hz, the signals consist of white noise; above, they rapidly decrease in amplitude due to the high cut filter. For each EW and NS component, the overall Fourier spectra determined from both aftershock and pre-event records, decreased at low frequencies, allowing an estimation of the instruments' 1/f noise levels (dashed line).

histories released by the instrument (the 1/f noise has a -1 slope in a log-log plot), and detail how to practically estimate the noise level (its Fourier amplitude at a given frequency) for each instrument.

- The analysis of the K-Net95 performance therefore shows that its output contains four different informations. These are (1) the translational acceleration and (2) the tilt of the ground, both of them being modified during the recording process by the response of the seismometer, namely (3) its theoretical response, and (4) the addition of electronic 1/f noise at low frequencies. The content of the acceleration time series must therefore be discussed in terms of the relative importance of the above four different elements. As for their low frequency content, it will always be dominated by either 1/f semiconductor noise or by residual tilt.

Chapter 3

Proposed method in the frequency domain using zero padded strong-motion accelerograms

3.1 General Remarks

The translational accelerations recorded by strong-motion seismometers are often contaminated by baseline offsets that prevent recovering the ground displacements by double integrations. Following the detailed analysis of the K-Net95 strong-motion seismometer (chapter 2), this chapter describes the proposed processing scheme.

The flow chart of the proposed method is given in Figure 3.1. Original in this dissertation, the baseline offsets that contaminate the acceleration records are analyzed in the frequency domain, and not in the time domain. After a zero-order correction applied in a first step to every strong-motion accelerograms (section 3.2), the visual display of the recorded accelerations' Fourier transform is improved (section 3.3) by addition of long zero pads to the acceleration records. This provides very detailed visualizations of the records' frequency content, including at low frequencies.

The very detailed visualizations of the records' low frequency content make it possible to distinguish the origins of the long period noise that contaminates the translational accelerations recorded in the near-field of large earthquakes. The long period noise is due to the 1/f digital semiconductor noise or the residual rotation of the instrument (residual tilt). The quantification of these two terms allows to discuss the low frequency content of the records, and leads to describe when it is possible to obtain realistic displacement time histories (sections 3.4 and 3.5).

Practically, the low frequency content of records is first compared with the instruments' 1/f noise model (obtained separately from ambient vibration noise measurements) and then with a step function. A detailed method about how to obtain estimations of the 1/f noise is given in section 2.3.5. Three different situations may occur depending on which component is dominating the low frequency content of records:

- Case 1: the record's low frequency content is dominated by the 1/f noise (section 3.4). In this case, it is not possible to obtain reliable translation acceleration time histories;
- Intermedite case: the record's low frequency content is dominated by the translational acceleration or by 1/f noise up to very small frequencies (section 3.4). In this case, it is possible to obtain reliable translation acceleration time histories.
- Case 2: the record's low frequency content is dominated by the permanent rotation (section 3.5). In this case, it is possible to obtain reliable translation acceleration time histories.

Practical selection of records. The method requires a minimum acceleration data length. K-Net and Kik-Net usually release 300 s long signals recorded at a sampling frequency of 100 Hz or 200 Hz, which give good results when processed according to the proposed method. If any, aftershocks must be removed from the acceleration records before processing them if a permanent baseline offset occur during the aftershock.

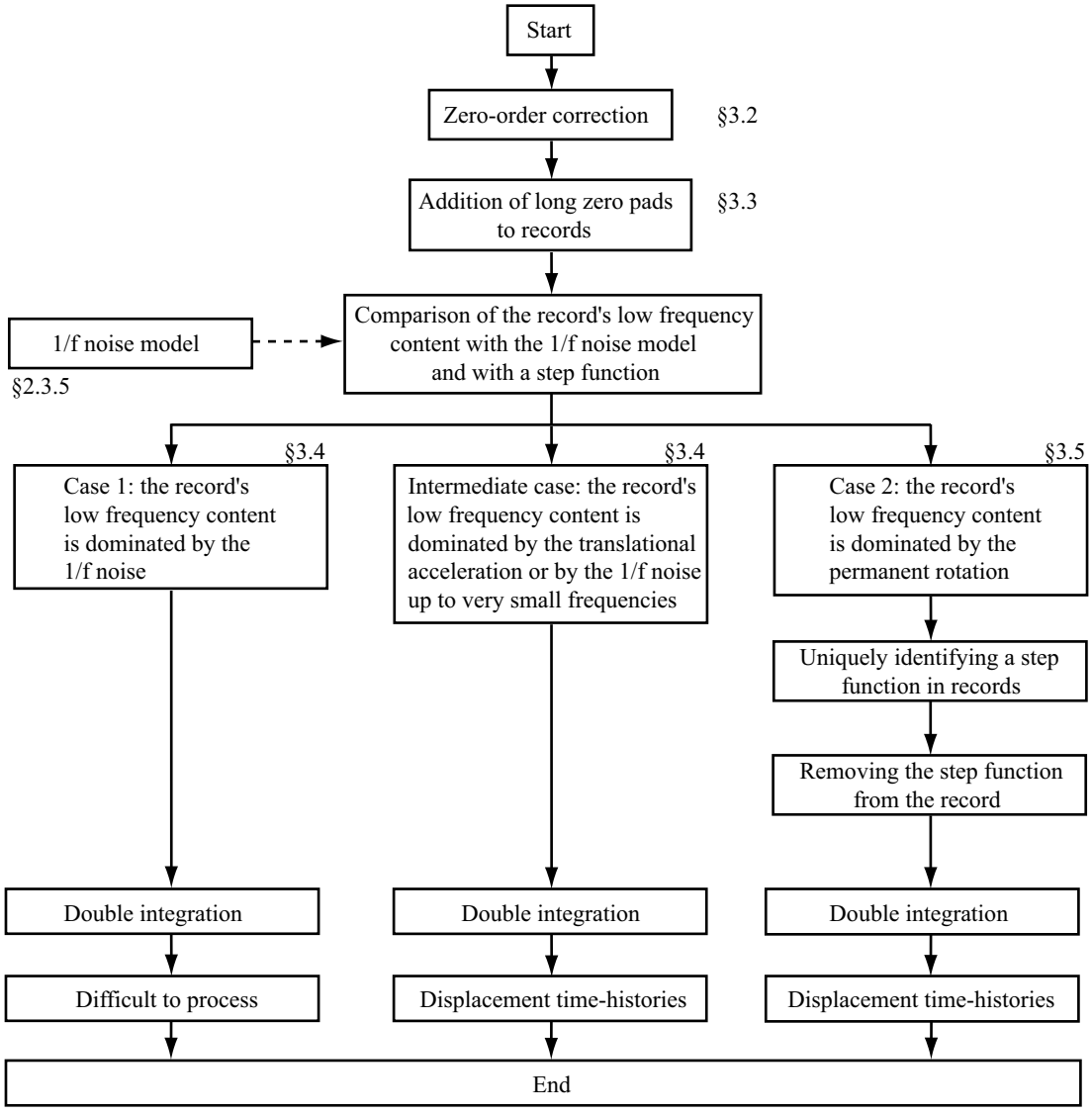

Figure 3.1: Flow chart of the proposed processing scheme. The paragraph numbers on the right indicate the section in which each elementary block is detailed.

3.2 Zero order correction

We apply the usual condition that the acceleration is zero before the earthquake shaking starts: the pre-event mean of the acceleration record is systematically subtracted from the whole record.

Practical application. Baseline shifts of strong-motion accelerometers' output are commonly observed and the acceleration is usually not equal to zero before the earthquake shaking starts. The example of the acceleration time histories recorded at station NIG019 during the 2007 Niigata-ken Chuetsu-Oki earthquake (Japan) is given in Figure 3.2. In practice, the starting time of the earthquake is visually estimated from the acceleration records, and the mean of the pre-event part is removed from the whole records. In a second step, we accurately determine

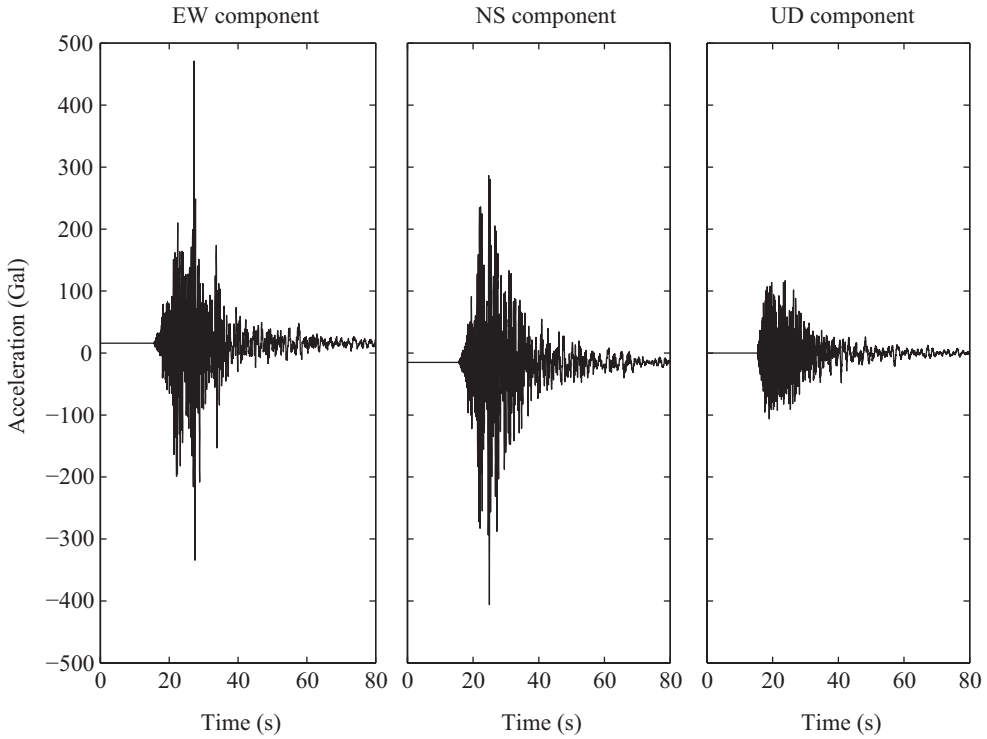

Figure 3.2: Raw acceleration (without any correction) time histories delivered by the K-Net strong-motion accelerometer at station NIG019 during the 2007 Niigata-ken Chuetsu-Oki earthquake. Large offsets can be observed for the EW and NS components and a smaller one for the UD component.

the P-wave arrival time by using Nakamura's V/H technique (Nakamura and Saito, 1983; Nakamura, 1988). It assumes that the incident wave from below is reaching the ground surface vertically, and therefore the UD component is constituted of P-waves mainly whereas the EW and NS components are mainly constituted of S-waves. The V/H ratio is calculated at each time t as follow (Nakamura, 1988)

$$V/Hratio = \sqrt{\frac{H_t}{V_t}} \tag{3.1}$$

whith

$$H_t = x''^{\,2}_{EW,t} + x''^{\,2}_{NS,t} + \alpha.H_{t-1} \tag{3.2}$$

$$V_t = x''^{\,2}_{UD,t} + \alpha.V_{t-1} \tag{3.3}$$

where $x''_{EW,t}$, $x''_{NS,t}$, and $x''_{UD,t}$ are the acceleration time histories released by the strong-motions accelerometers in respectively the EW, NS, and UD components. When the V/H ratio drastically increases for the first time and is above one, the vertical motion is predominant. This indicates the arrival of the P-waves.

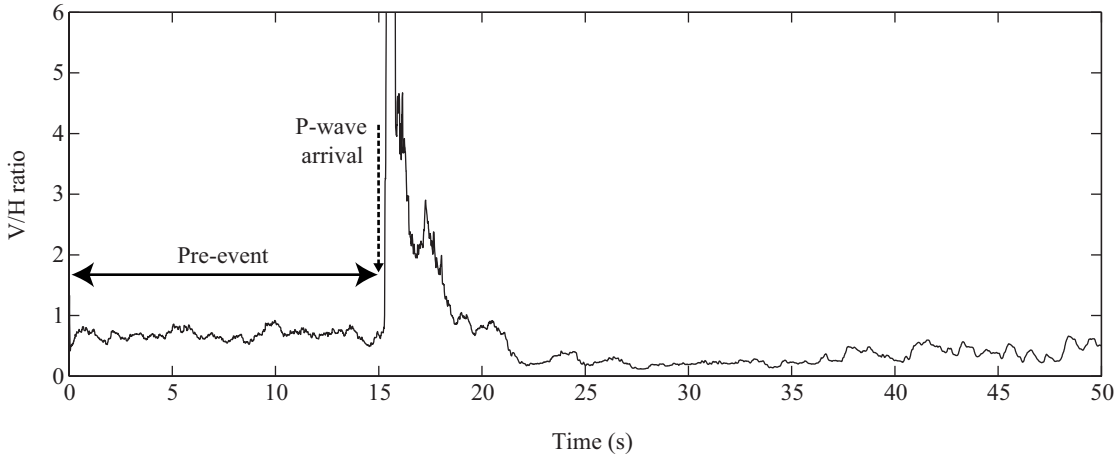

Figure 3.3: Accurate P-wave arrival time determined by using Nakamura's V/H technique (Nakamura and Saito, 1983; Nakamura, 1988) for the accelerations recorded at K-Net station NIG019 during the 2007 Niigata-ken Chuetsu-Oki earthquake (Japan). The P-wave arrival time is determined at the 15^{th} second by the drastic increase of the V/H ratio for the first time.

A standard value of 0.98 is often used for the coefficient α. The V/H ratio obtained at NIG019 station during the 2007 Niigata-ken Chuetsu-Oki earthquake is given in Figure 3.3. The drastic increase for the first time of the V/H ratio at the 15^{th} second indicates that the P-waves arrival. We then calculate again the pre-event mean over a more accurate pre-event duration and remove it from the whole acceleration record.

3.3 Zeros pads for improving the visualization of records' Fourier content

In geosciences, including earthquake engineering and civil engineering, the earth or human made structures' natural behaviour is nowadays very often quantitavely surveyed and monitored by the use of various kinds of instrumentations. Instruments record a very wide range of signals, including acceleration, velocity, displacement or rotation time histories. Following the current trend in technical evolution, digital instruments have become more popular than analog ones, and are now widely used. In this context, digital record quality is continuously increasing, with, for instance, signals recorded at higher frequency sampling, data logger developed with always higher dynamic range and lower internal noise (Araki *et al.* 2011). In some applications, such as strong-motion acceleration records, the absence of low cut filter is making 0 Hz data usable.

Examples in Figure 3.4, left column, show three signals: in (a), a 5.5 s velocity time history recorded at the sampling frequency of 1000 Hz; in (c), a 100 s GPS displacement time history recorded at the sampling frequency of 1 Hz and in (e), a 100 s acceleration time history recorded nearby to the preceding GPS station at a sampling frequency of 100 Hz. Digital instruments provide, at discrete intervals, quantitative information about the continuous input signal. Strictly speaking, recorded signal representations should be sequences of discrete points separated by time gaps corresponding to the sampling spacings (Figure 3.4, left column, a and e). A line is however usually drawn between the recorded values, which gives a false impression of continuity but eases the signals' visualization. Figure 3.4c, the line drawn between the recorded data helps to visually understand

the displacement's dynamic evolution during the earthquake.

Often, information about the frequency content of these recorded time histories is needed, and computer based Fourier transforms are routinely performed on the signals. In Figure 3.4 (b, d and f) are drawn the Fourier amplitudes of these three records, calculated by applying a discrete Fourier transform, the Fast Fourier Transform, on the time histories. It can be noted that the points defining the spectra are quite separated from each other, and it is sometimes difficult to retrieve important frequency information from the records' computed Fourier content, because of difficulties to precisely determine specific frequencies.

In the examples above, the number of frequencies at which the Fourier amplitudes are displayed is not enough to allow either a precise determination of the frequencies of maximum Fourier amplitudes for the velocity record (Figure 3.4, b), or the low frequency amplitudes of the nearby acceleration and displacement records (Figure 3.4, d and f), which makes their comparison impossible. In the usual representation of Fourier spectra, a line is drawn between the points, giving a false impression that the Fourier amplitudes are calculated at every frequency, and that the spectra are continuous. Better visual display of instrument records' Fourier content are needed for finer analysis of their frequency content. This situation motivated this section 3.3, in answer to the following question: Is it possible to obtain more detailed pictures of records' Fourier content, and if so, by which means?

In outline, this section begins with a signal processing based study of the Fourier spectra of any recorded signal (subsection 3.3.1). It details the evolution of the signal's Fourier transform during the recording steps done by any digital instrument, then through the processing steps applied by the users. The three main steps of the signal evolution are schematically given in Figure 3.5: a), the instrument's input signal is continuous in both time and frequency domain, whereas the sequence of numbers it delivers (Figure 3.5, b) is discrete in the time domain but still has a continuous theoretical Fourier transform. However, computer based Fourier transform (Figure 3.5, c) provides the frequency content of output signals at a discrete (not continuous) number of frequencies only, which implies a loss of information. This subsection then explains how the user can best perform the Fourier transform to visualize as much information as possible from

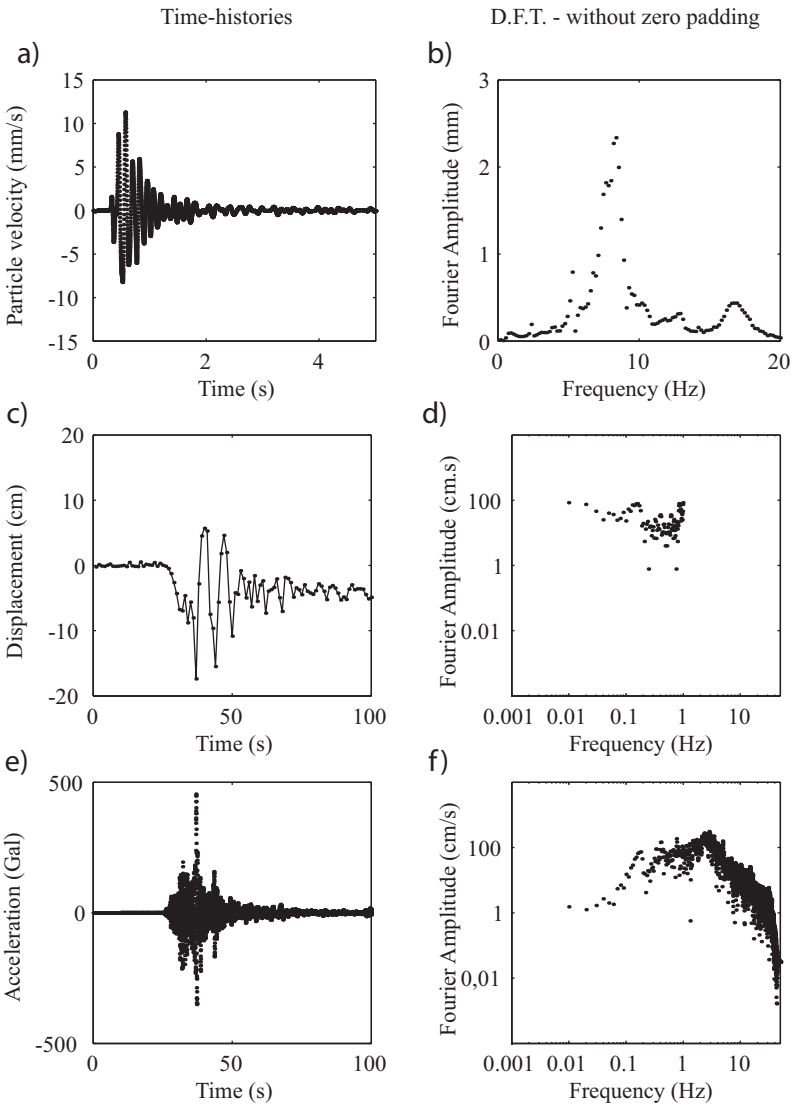

Figure 3.4: The left column shows three signals: (a) a 5.5 seconds velocity time history recorded at the sampling frequency of 1000 Hz; (c) a 100 sec GPS displacement time history recorded at the sampling frequency of 1 Hz and (e) a 100 sec acceleration time history recorded nearby to the preceding GPS station at a sampling frequency of 100 Hz. A line is sometimes drawn between the discrete recorded values to ease their visualization, such as in (c). Second column (b, d and f) are displayed the Fourier amplitudes of these three records, calculated by applying a discrete Fourier transform, the Fast Fourier Transform, on the time histories. The points defining the spectra are quite separated from each other, and it is difficult to retrieve important frequency information from the records' computed Fourier content.

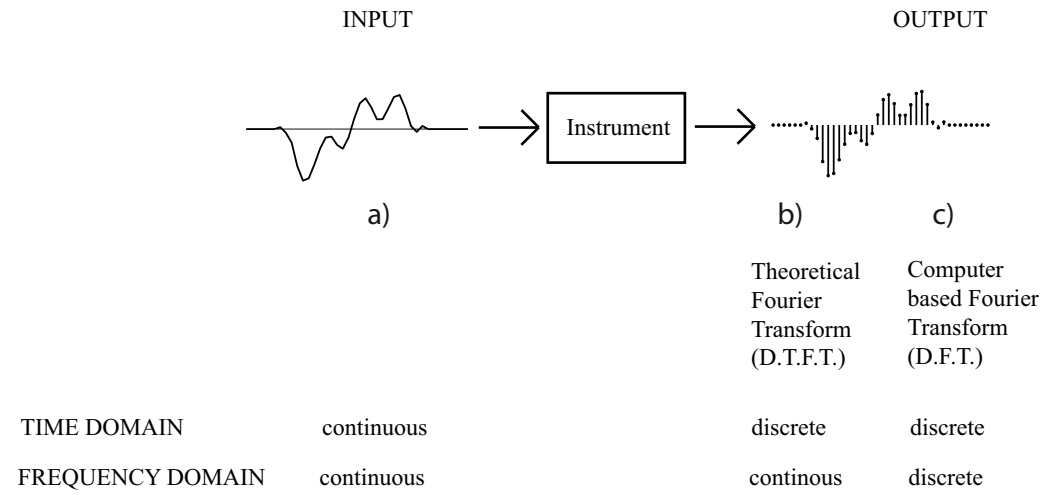

Figure 3.5: Schematic evolution of a signal and its Fourier transform during the recording steps done by any digital instrument, then through the processing steps applied by the users. (a) The input signal is continuous in both time and frequency domain. Its Fourier transform is the Continuous-Time Fourier Transform (C.T.F.T.). (b) The instrument's output signal is discrete in the time domain, but still continuous in the frequency domain where the signal's theoretical Fourier transform is the Discrete-Time Fourier Transform (D.T.F.T.), best Fourier transform that one can expect to obtain from the data. (c) Discrete in the frequency-domain, the computer based Discrete Fourier Transform (D.F.T.) provides a partial view of the output signal's Fourier content.

available records (instruments' output signals). Adding long zero pads before and/or after records can be used to force computers to calculate the frequency amplitudes of records at a much greater number of frequencies, therefore improving their Fourier transform's visualization. The Discrete-Time Fourier Transform (D.T.F.T.; Figure 3.5), best Fourier transform representation that one can expect to obtain from available data, can therefore be visualized. In the second part of this section (subsection 3.3.2), we apply the processing method on a simple signal, a box-like function, which allows the comparison of the Fourier transform obtained by processing the time history data with the theoretical one. The last subsection (subsection 3.3.3) applies the processing scheme to the recorded signals detailed in Figure 3.4 and shows what information is revealed.

3.3.1 Fourier transform and zero padding

This subsection details the evolution of the signal's Fourier transform during the recording steps done by any digital instrument, then through the processing steps applied by the users. It also describes how to best perform the Fourier transform to reveal all the frequency information contained in available time history data.

Recording process effect on the Fourier transform

During the recording process, a digital instrument transforms its input, a continuous-time signal a(t) (Figure 3.6), into a discrete-time signal a[n]=a(nT) where T is the sampling interval. In terms of Fourier spectra, the recording process corresponds to a transformation from a Continuous-Time Fourier Transform (C.T.F.T.) to a Discrete-Time Fourier Transform (D.T.F.T.).

To be stored and released, the recorded signal is truncated and becomes a N data long finite discrete-time signal a[n] (Figure 3.6). For example, a signal recorded during 100 s is stored as N=10,000 data if sampled at the frequency of 100 Hz. In the time-domain, truncating the record corresponds to a convolution of the signal with a rectangular box. In the frequency domain, this has no significant effect on the D.T.F.T. if we can consider that the record has captured all the event, and therefore the signal is zero outside captured range.

The processing steps applied up to this point are all dependent on the definition of the recording system (length of time histories recorded and released; instrument characteristics, including sampling frequency and errors: aliasing effect, quantization error, 1/f electronic noise, etc.) and are therefore dependent on the instrument or network management decisions. The stored and released finite length a[n] is the most complete information available about the event, and the D.T.F.T. of a[n], although not strictly identical to the initial C.T.F.T., the best Fourier transform representation that one can expect to obtain from the available data released.

In the next paragraph, the computed Fourier transform of a[n] is compared with its D.T.F.T. so as to verify that data users classically obtain the best possible visual display of the records' Fourier transform (the D.T.F.T.). The comparison shows that usual computer based Fourier transform provides an incomplete visu-

time domain	frequency domain
Input	
	$A(f) = \int_{-\infty}^{+\infty} a(t)e^{-j2\pi ft}dt$
continuous-time signal a(t)	continuous-time Fourier transform (C.T.F.T.)
Instrument Digital instrument	
Output	
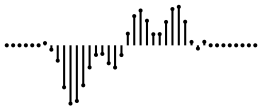	$A(jw) = \sum_{n=-\infty}^{+\infty} a[n]e^{-jwn}$
a[n]=a(nT) discrete-time signal	where $a[n]$ is a discrete-time interval sequence for which the time between individual samples is T and $w = 2\pi f$ the angular frequency discrete-time Fourier transform (D.T.F.T.)
Stored output as finite-length sequence	
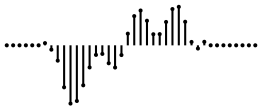	$A(jw) = \sum_{n=0}^{N-1} a[n]e^{-jwn}$
a[n]=a[n] for n=0,1,2...,N-1, a[n]=0 elsewhere finite discrete-time signal	if the record captures all the event and the recorded signal is zero outside the captured range discrete-time Fourier transform (D.T.F.T.)

Figure 3.6: Effect of the recording process on the Fourier transform of a signal. Scherbaum (2001) and Oppenheim and Schafer (2010) notations are used.

alization of the D.T.F.T. The following paragraph then details how to improve the visual display of the records' computed Fourier transform so as to obtain an accurate representation of the D.T.F.T.

Fourier transform applied by the users: gap between the D.T.F.T. and the processed D.F.T.

Subsequent processing steps (Figure 3.7) are applied by the users of the records who perform computer-based analysis of the data. The Fourier transform carried out by computers is the Discrete Fourier Transform (D.F.T.), not the D.T.F.T. It is usually implemented by using the Fast Fourier Transform (F.F.T.).

Different from the D.T.F.T., which is a continuous representation of the Fourier amplitude spectrum, the D.F.T. provides the records' Fourier amplitudes only at a finite number of equally spaced frequencies $f_k = k/(N.T)$, where N is the length of the finite-time sequence a[n], T the sampling interval, and k an integer ranging from 0 to N-1. At these frequencies, the Fourier amplitudes of both the D.F.T. and the D.T.F.T. are identical (Oppenheim and Schafer 2010). The D.F.T. tool provides a visual representation of the D.T.F.T. but only at a finite number of frequencies f_k. In this section, we therefore draw the D.T.F.T. as a continuous thin line, while the D.F.T. amplitudes are represented as points at discrete frequencies.

When using the D.F.T. tool, if the sampling spacing Δf between the frequencies f_k is not small enough, important information of the D.T.F.T. spectrum located between the frequencies f_k do not appear in the computed (D.F.T.) Fourier spectrum's representation. The non-displayed information are contained in the initial record a[n], but not drawn in the computed Fourier spectrum' s representation.

The Figure 3.7, top row, shows a N=32 data long record and its D.T.F.T. Applying the D.F.T. on the 32 data long signal provides equally spaced values of the D.T.F.T.: in Figure 3.7, center row, superimposed on the D.T.F.T. thin line are the Fourier amplitudes calculated at discrete frequencies when performing the D.F.T. (small circles). Because the D.F.T. does not provide a continuous visual display, the peaks of the D.T.F.T., located between the Fourier amplitudes

time domain	frequency domain
Stored output as finite-length sequence (Under network management control)	
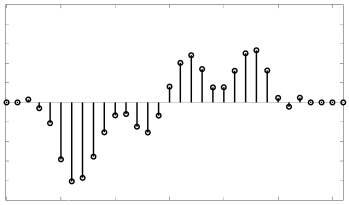	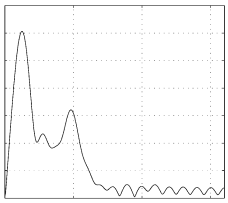
N=32 data long signal	D.T.F.T. $A(jw) = \sum_{n=0}^{N-1} a[n]e^{-jwn}$
Computation of D.F.T. (Under user control)	
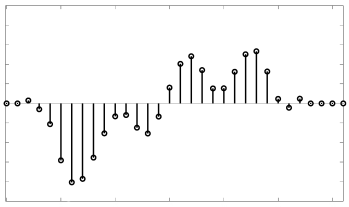	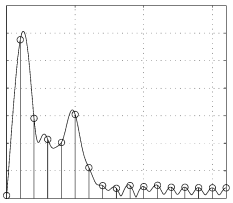
N=32 data long signal	D.F.T. (circles) vs. D.T.F.T. $A[k] = \sum_{n=0}^{N-1} a[n]e^{-j2\pi kn/N}$ *where* $k = 0, 1, 2, ..., N-1$ i.e. $A[k] = A(jw)\|_{w=2\pi k/N}$ *where* $N = 32$ *data*
Addition of zero pads before computing the D.F.T. (Under user control)	
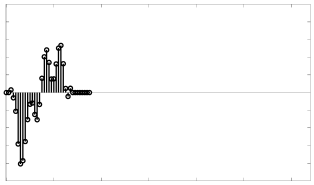	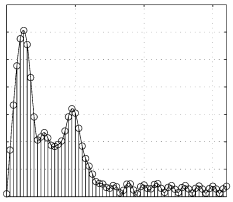
$N = 32$ data long signal + added zero pads to make the record $2^7 = 128$ data long	Zero padding the record lead to a reduction of the frequency interval between calculated Fourier amplitudes (D.F.T.) $A[k] = A(jw)\|_{w=2\pi k/N}$ where N=128 data

Figure 3.7: Zero padding records, before performing the Discrete Fourier Transform, leads to the calculation of their Fourier amplitudes with smaller frequency spacing, and to an improved visual display of their Fourier transform.

calculated by the D.F.T., are missed: as it is, the D.F.T. does not provide a detailed enough representation of the D.T.F.T.

This analysis shows the presence of a gap between the Fourier transform's representation that the users performed (D.F.T.) and the Fourier transform's representation that can be expected to be obtained from the data (D.T.F.T.). Both have significant differences due to the different number of Fourier amplitudes displayed. It should therefore be possible to visualize much more information about the frequency content of digital records than done when simply applying a D.F.T. on records.

The next paragraph details how to improve the computed Fourier transform's visual display so that to obtain an accurate representation of the D.T.F.T.

Reduction of the gap between the D.F.T. and the D.T.F.T. by addition of zero pads

The D.F.T. calculates the Fourier amplitudes of a record at discrete frequencies f_k. To obtain a visual display of the record's Fourier amplitudes at frequencies sufficiently close so that the D.F.T. becomes indistinguishable from the D.T.F.T itself, it is necessary to reduce the frequency spacing between the frequencies f_k as much as possible, when performing the D.F.T.

In signal processing, the frequency spacing of the Discrete Fourier Transform is $\Delta f = 1/N.T$ where T is the sampling interval and N the number of data. When N increases, Δf decreases, and it is possible to obtain the Fourier amplitudes of a record at closer frequencies by addition of zero pads before taking the D.F.T. (Oppenheim and Schafer 2010). The addition of a high degree of time domain zeros is an usual step in classical signal processing (Oppenheim and Schafer 2010) and is commonly used to obtain a continuous representation of the D.T.F.T.

In the example (Figure 3.7), we zero padded the 32 data long record to make it $2^7 = 128$ long (Figure 3.7, bottom row, time domain). The D.F.T. of the padded record is shown in Figure 3.7, right column, bottow row. With the Fourier amplitudes calculated at closer frequencies, the dots denoting the D.F.T. provide a much better picture of the record's frequency content. Increasing the number

of zero pads beyond 128 would lead to an quasi continuity between the dots, and an extremely detailed D.T.F.T. representation.

Without increasing the duration of records, adding zeros before and/or after the records results in Fourier amplitudes calculated with a smaller frequency spacing, and a better display of the records' Fourier amplitude spectra. The added zeros do not add information, nor improve the ability to resolve close frequencies (which depend for example on the sampling frequency). They however allow the user to recover the D.T.F.T. and thus enable him to make the best use of data at hand. Interestingly, they also makes it possible to obtain a very detailed visualization of the low frequency content of the digital time histories.

In the next subsection, we compare the theoretical Fourier transform of a simple function, a box-like function, with the D.F.T. obtained by processing the time domain data. To illustrate the method, two applications are then given as examples of practical situations where the method has been successfully applied.

3.3.2 Comparison of theoretical Fourier Transform vs. D.F.T. of a box-like function

This subsection details the example of a simple box-like function a(t), represented in Figure 3.8, and defined in equation 3.4, where A is a real number and $\tau = t_2 - t_1$. The choice of a box-like function is motivated by the possible comparison of the Fourier transform obtained by processing the record with its theoretical one.

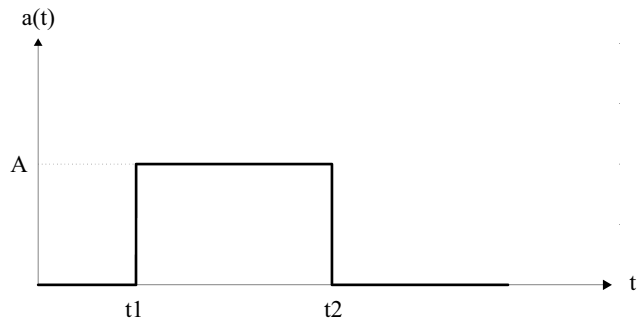

Figure 3.8: Time domain representation of a simple box-like function.

$$a(t) = \begin{cases} 0 & : 0 \leq t < t_1, \\ A & : t_1 \leq t \leq t_2, \\ 0 & : t_2 < t. \end{cases} \tag{3.4}$$

The Fourier amplitude of this box-like function is

$$|A(f)| = A\tau \frac{|\sin \pi f \tau|}{\pi f \tau}. \tag{3.5}$$

Let A(f) be the Fourier transform of $a(t)$,

$$\begin{aligned} A(f) &= \int_{-\infty}^{+\infty} a(t) e^{-j2\pi ft} dt, \\ &= \int_{-\infty}^{t_1} 0 \, e^{-j2\pi ft} dt + \int_{t_1}^{t_2} A e^{-j2\pi ft} dt + \int_{t_2}^{+\infty} 0 \, e^{-j2\pi ft} dt, \\ &= \int_{t_1}^{t_2} A e^{-j2\pi ft} dt. \end{aligned} \tag{3.6}$$

As an application, we consider the following values: $t_1 = 25$ sec, $t_2 = 75$ sec, $\tau = t_2 - t_1 = 50$ sec, and A the amplitude of the box-like function equal to 1 cm/s^2. The numerical representation of this function is done with a sampling frequency of 100 Hz.

The theoretical Fourier transform of the step function is compared with its D.F.T. In Figure 3.9, the thin continuous line represents the theoretical shape of the function's Fourier amplitude. Superimposed are the D.F.T. amplitude's dots calculated at discrete frequencies. The Figure 3.9, bottom, shows enlarged parts, from 0 to 0.1 Hz (Figure 3.9, b) and from 1.0 to 1.1 Hz (Figure 3.9, c). The D.F.T. dots alone do not provide a complete visual display of the signal's Fourier transform.

Adding zero pads to the time history results in smaller spacing of the D.F.T. (Figures 3.10 and 3.11). Increasing the number of D.F.T. amplitude dots provides a better picture of the Fourier amplitude spectra (Figures 3.10), until the dots are so dense that they completely merge and form a line superimposed on the

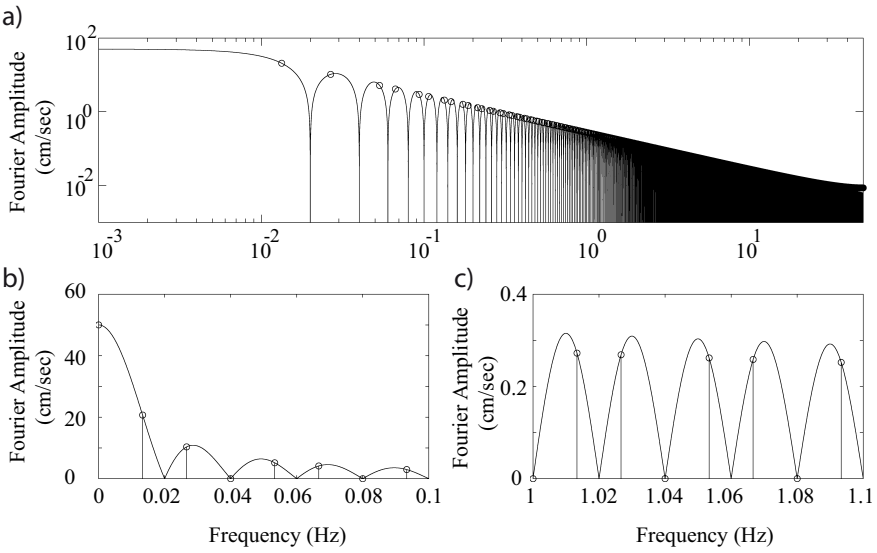

Figure 3.9: Superposition of a simple box-like function's (defined in the text) theoretical Fourier transform (continuous line) with the D.F.T. amplitudes (dots) calculated at discrete frequencies. Here, zero pads were not added to the time history data.

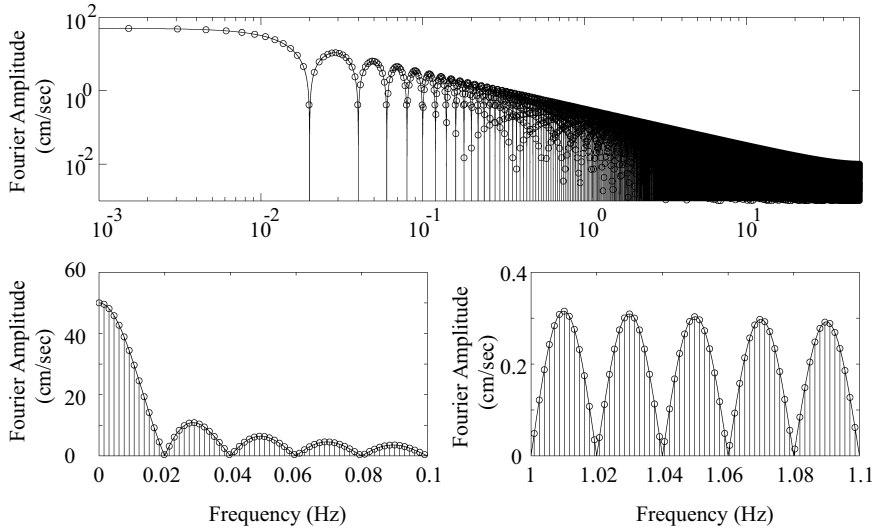

Figure 3.10: Superposition of a simple box-like function's (defined in the text) theoretical Fourier transform (continuous line) with the D.F.T. amplitudes (dots) calculated at discrete frequencies. The time history data were zero padded to make the record 2^{16} data long, before computing the D.F.T.

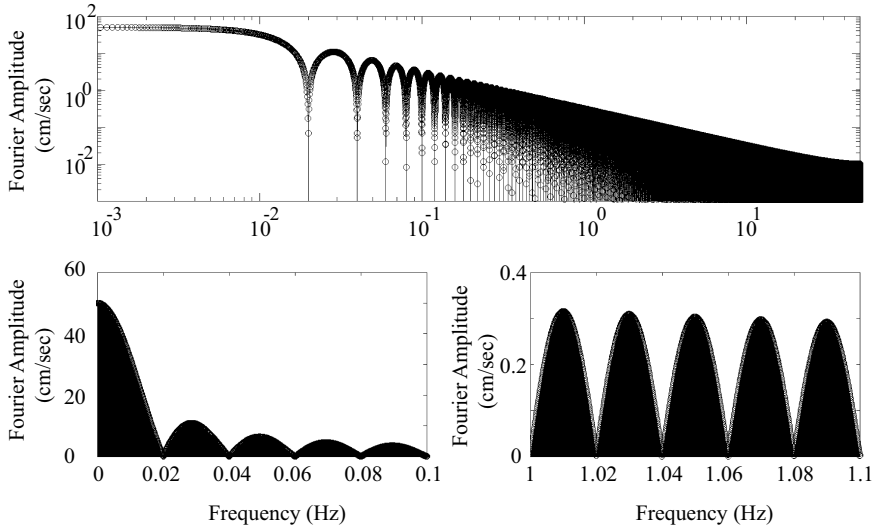

Figure 3.11: Superposition of a simple box-like function's (defined in the text) theoretical Fourier transform (continuous line) with the D.F.T. amplitudes (dots) calculated at discrete frequencies. The time history data were zero padded to make the record 2^{20} data long, before computing the D.F.T.

theoretical Fourier transform (Figure 3.11). It also provides a better view of the record's low frequency content. This example confirms the usefulness of the addition of zero pads to records in order to improve the visual display of their computed Fourier transform, and to recover the D.T.F.T.

3.3.3 Examples of information revealed by adding zero pads to records

We outline the usefulness of the proposed method with the two examples initially shown in Figure 3.4.

The first example (Figure 3.12, a) shows a particle velocity time history recorded during the monitoring of a structure during nearby construction work. The time domain response of the structure is given in Figure 3.12a, together with its D.F.T. (Figure 3.12, b). The frequency spacing of the D.F.T. is $\Delta f = 0.18$ Hz (for this record, N=5501 data and T = 0.001 sec). Here, it is therefore impossible to determine with precision specific frequencies of the record, such as the peak

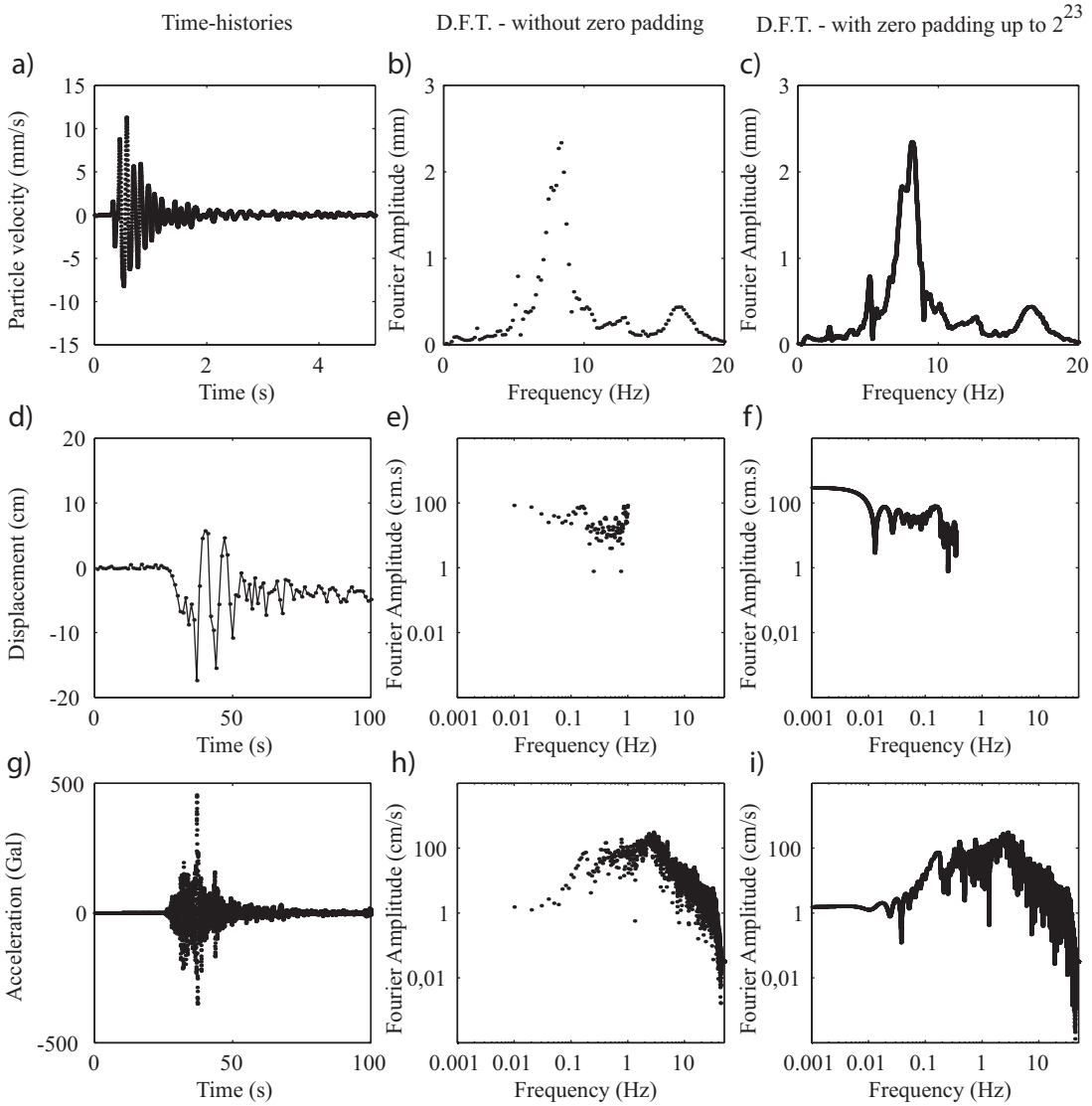

Figure 3.12: The left column shows three signals: (a) a 5.5 seconds velocity time history recorded at the sampling frequency of 1000 Hz; (d) a 100 sec GPS displacement time history recorded at the sampling frequency of 1 Hz and (g) a 100 sec acceleration time history recorded nearby the preceding GPS station at a sampling frequency of 100 Hz. A line is sometimes drawn between the discrete recorded values to ease their visualization, such as in (d). Second column (b, e and h) the Fourier amplitudes of these three records are displayed. They were calculated by applying a discrete Fourier transform, the Fast Fourier Transform, on the time histories. The points defining the spectra are quite separated from each other, and it is difficult to retrieve important frequency information from the records' computed Fourier content. Right column (c, f and i), long zero pads were added before and after the signals before computing the D.F.T., which forced the computer to calculate the Fourier amplitudes at closer frequencies. This reveals every details of the records' D.T.F.T., best Fourier transform representation that one can expect to obtain from the available data.

amplitudes (Figure 3.12, b), because the number of points describing the Fourier amplitudes are quite sparse. Adding zero pads to the record so as to make it up to 2^{23} data long, makes the Fourier amplitudes determined at discrete frequencies so close ($\Delta f \approx 0.0001$ Hz) that they become indistinguishable one from another (Figure 3.12, c), and the Fourier amplitude of any specific frequency of the signal can be determined precisely. The visual display of the record's computed Fourier transform had been so much improved that it became similar to the D.T.F.T, which is the best Fourier transform representation that one can expect to obtain from the velocity record.

The second example shows collocated acceleration and 1-Hz GPS displacement time histories (Figure 3.12, d and g), recorded by the Japanese K-Net network NIG019 station (EW component) and by the Japanese Geographical Survey Institute during a large earthquake that occurred in Japan, the 2007 Niigata-ken Chuetsu-Oki earthquake. Both records D.F.T. were computed before (Figure 3.12, e and h) and after (Figure 3.12, f and i) adding zeros to make them a power of two data long. Adding zero pads to the records makes the Fourier amplitudes determined at discrete frequencies so close that they reveal every detail of the records' D.T.F.T., including a very detailed picture of their low frequency content now available for comparison and further studies investigating their shape and origin.

3.3.4 Fourier transform and zero padding

Acceleration time histories are first padded with zeros to improve the visualization of their Fourier content.

Practical application. In practice, we add long zero pads to records to make them up to 2^{23} or 2^{24} data long. Such large numbers of zero pads force computers to calculate the Fourier amplitude of acceleration records with a frequency spacing Δf of respectively 1.19 x 10^{-5} Hz and 5.96 x 10^{-6} Hz for records sampled at 100 Hz.

Zero pads may be added either before or after the acceleration records, or both before and after the records. For convenience, we usually prefer the latter

situation.

The number of zero pads added to records is governed by the processing scheme's case 2 detailed later in subsection 3.5. For a typical 300 s long strong-motion acceleration record with a pre-event part of 15 s, the maximum duration T of the step function (defined later in subsection 3.5) is 285 s, which correspond to a frequency 1/T of 3.508 x 10^{-3} Hz. As the Fourier amplitude are computed at discrete frequencies of interval Δf, the frequency 1/T can be practically estimated with a maximum error of $\Delta f/2$. This corresponds to estimating T with a maximum error ΔT of 0.5 s and 0.25 s when zero pads are added to make records respectively of 2^{23} or 2^{24} data long.

If we assume a step function of amplitude A equal to 1 Gal, the error in the estimation of T leads to an under or over estimation of the duration of the step function, which by double integration leads to a maximum error in the displacement of respectively 0.13 and 0.03 cm (=0.5 A ΔT^2, where A=1 Gal and ΔT = 0.5 s or 0.25 s). For standard processing, it is therefore recommended to add zero pads so as to make the records up to at least 2^{23} data long.

As for a step function of amplitude A equal to 10 Gal, the error in the estimation of T leads to an error in the displacement of respectively 1.25 and 0.31 cm. When the amplitude of the step function is very large, it is therefore recommended to add zero pads so as to make the records up to 2^{24} data long, so that the effect of the estimation of T on the permanent displacement can be neglected. In some cases, adding longer zero pads to records may be required.

3.4 Case 1: At low frequencies, the 1/f semiconductor noise overshadows the translational acceleration and the residual tilt

During the 2004 Niigata-ken Chuetsu earthquake, NIGH04 station was 111 km distant from the epicenter of the main shock. The acceleration power spectrum of the main shock recorded at station NIGH04 is shown in Figure 3.14 together with the $1/f$ noise model determined from the noise record (Figure 2.19).

At low frequencies, the $1/f$ digital noise predominates. Let $A_{acc}(f)$ be the

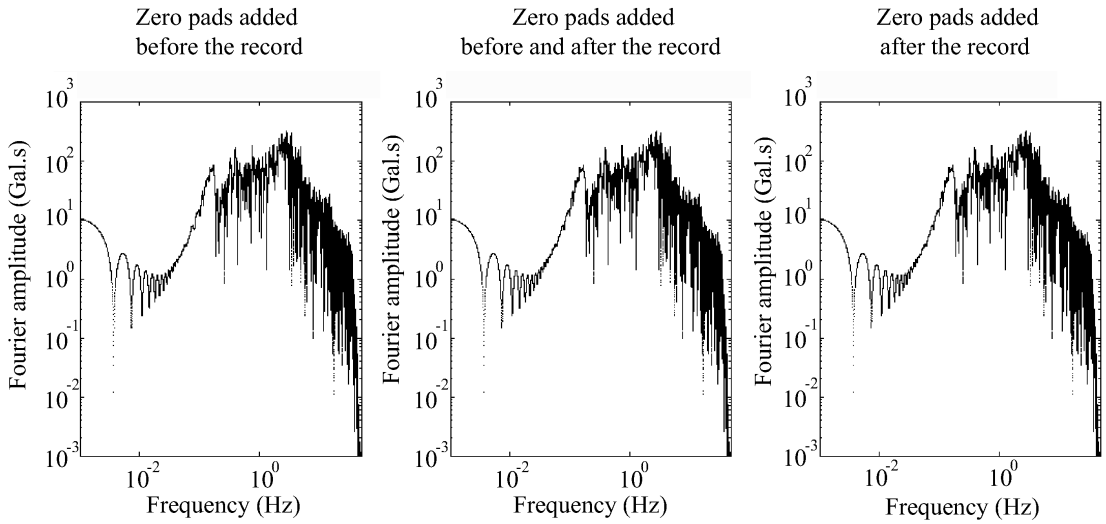

Figure 3.13: Comparison of the Fourier amplitude obtained after adding zero pads before, after, or both before and after the records, so as to make them up to 2^{23} data long. The Fourier spectra does no depend on the position of the zero pads.

sum, in the frequency domain, of $A_g(f)$ and $A_{noise}(f)$ where $A_g(f)$ is the true ground translational acceleration and $A_{noise}(f)$ the sum of the digital $1/f$ and white noises. The same relation holds for the velocity V(f). Therefore, the velocity $V(f) = V_g(f) + V_{noise}(f)$, where $V_g(f)$ is the true ground velocity and $V_{noise}(f)$ the sum of a digital $1/f^2$ and $1/f$ noise.

By definition of the Fourier transform, for a 300 seconds record,

$$v(t) \Leftrightarrow V(f) = \int_{-\infty}^{+\infty} v(t)e^{-j2\pi ft}dt = \int_{0}^{T=300s} v(t)e^{-j2\pi ft}dt. \tag{3.7}$$

When $f = 0$,

$$V(0) = \int_{0}^{T=300s} v(t)e^{-j2\pi 0t}dt = \int_{0}^{T=300s} x'(t)dt$$

$$= [x(t)]_0^{T=300s} = displacement(t = 300s).$$

Thus the residual displacement is equal to the Fourier amplitude of the velocity at zero frequency. Because $V(0) = V_g(0) + V_{noise}(0)$ where $V_g(f) \ll V_{noise}(f)$, instrumental noise completely overshadows the Fourier amplitude of the ground acceleration at low frequencies. It is therefore not possible to recover the exact residual ground displacement in such cases.

However, if the frequency at which the 1/f noise stops to dominate the record is small (i.e. $V_g(f) \ll V_{noise}(f)$ being true only at very low frequencies), it is possible to obtain stable displacement time histories over duration of engineering interest. As an example shown in Figure 3.15, the double integration of the acceleration recorded by the underground Kik-Net NIGH12 station during the 2004 Niigata-ken Chuetsu earthquake leads to a stable residual displacement of 14 cm. The frequency at which the 1/f noise stops to dominate the record (0.004Hz determined from the Fourier acceleration spectra) is so small that the 1/f noise does not affect much the displacement time histories.

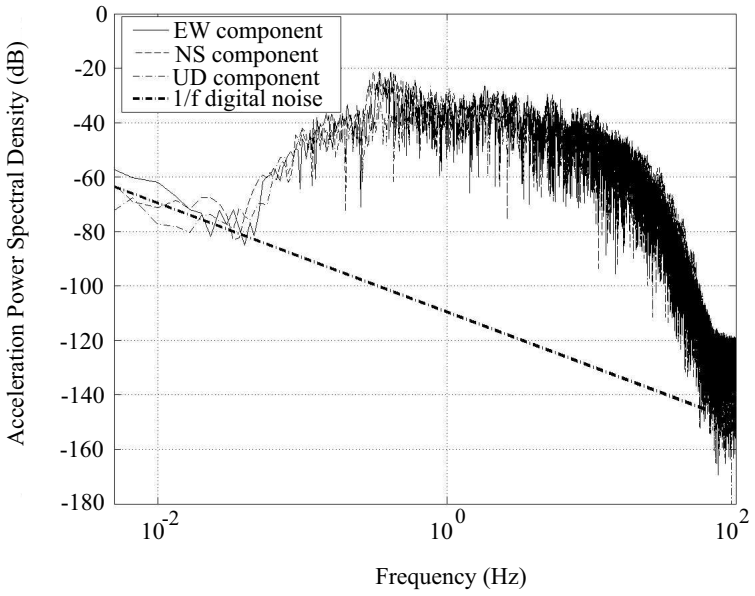

Figure 3.14: Power spectrum calculated from a record at Sekikawa NIGH04 site, underground seismometer, during the 2004 Niigata-ken Chuetsu earthquake. The 1/f digital noise model was determined in Figure 2.19. The power spectrum representation allows comparison with Kinoshita's original papers.

3.5 Case 2: At low frequencies, the residual tilt overshadows the translational acceleration and the 1/f semiconductor noise

During the 2007 Niigata-ken Chuestsu-Oki earthquake, the K-Net NIG019 station was in the near-field of the earthquake. After adding zero pads to the record of its EW component, we find that in this case the low frequency content of the acceleration time history (Figure 3.16, d) is similar to the Fourier spectra of a box-like function (Figure 3.16, b).

The amplitude A and duration T used to define a box-like function in the time domain (Figure 3.16, a) can be extracted in the frequency domain from the Fourier transform of the box-like function (Figure 3.16, b): by definition, the Fourier amplitude at zero frequency is A.T, and the frequency when the Fourier amplitude is zero for the first time is 1/T. Therefore, A and T of a box-like function can uniquely be derived from its Fourier transform. It is important to

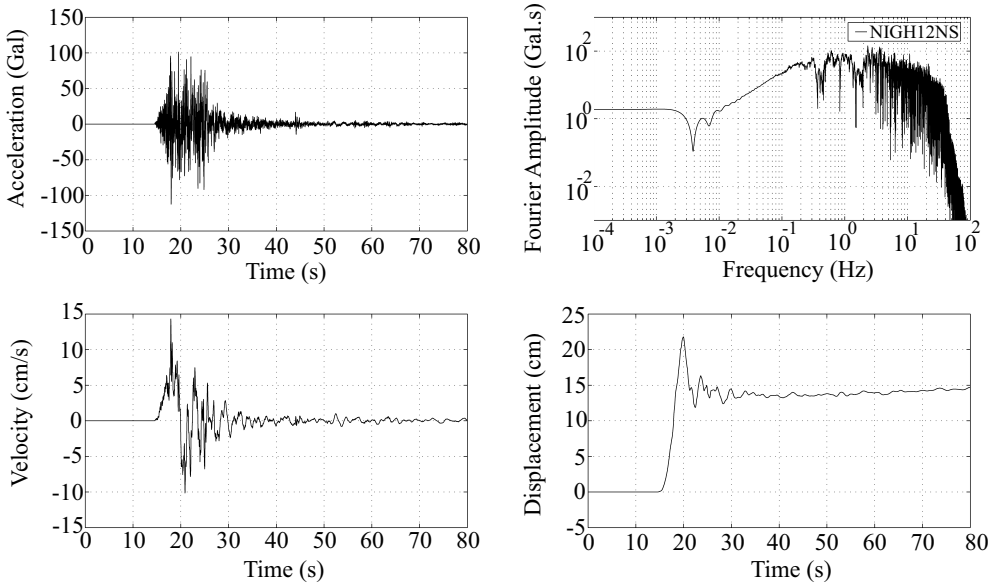

Figure 3.15: Acceleration, Fourier amplitude of the acceleration, acceleration derived velocity and displacement time histories of the 2004 Niigata-ken Chuetsu earthquake, NIGH12 downhole accelerometer, NS component.

note that A and T are not hand picked up at random, but really extracted from the Fourier transform.

In Figure 3.16, we compare the acceleration record and its Fourier transform (c, d), with a simple box-like function and its Fourier transform (a, b). It can be seen that in the frequency domain, the low frequency part of the record (d, in the box) is identical to a box-like function (b). We therefore observe that the acceleration record (c) is contaminated by a box-like function, whose amplitude and starting time can be determined uniquely from the Fourier spectra of the acceleration record. In this example, we obtain the following values from the Fourier transform of the acceleration record (Figure 3.16, d): A.T = 11.7177 Gal.s (Fourier amplitude at zero frequency) and 1/T= 0.0036467 s^{-1} (frequency when the Fourier amplitude is zero for the first time). Thus T = 1/(1/T) = 274.2186 s, A = A.T / T = 0.042731 Gal and the starting time of the step function (ts) = duration of the record - T = 300 s - T = 25.7814 s. In Figure 3.17b, the superposition in the frequency domain of the acceleration record and the

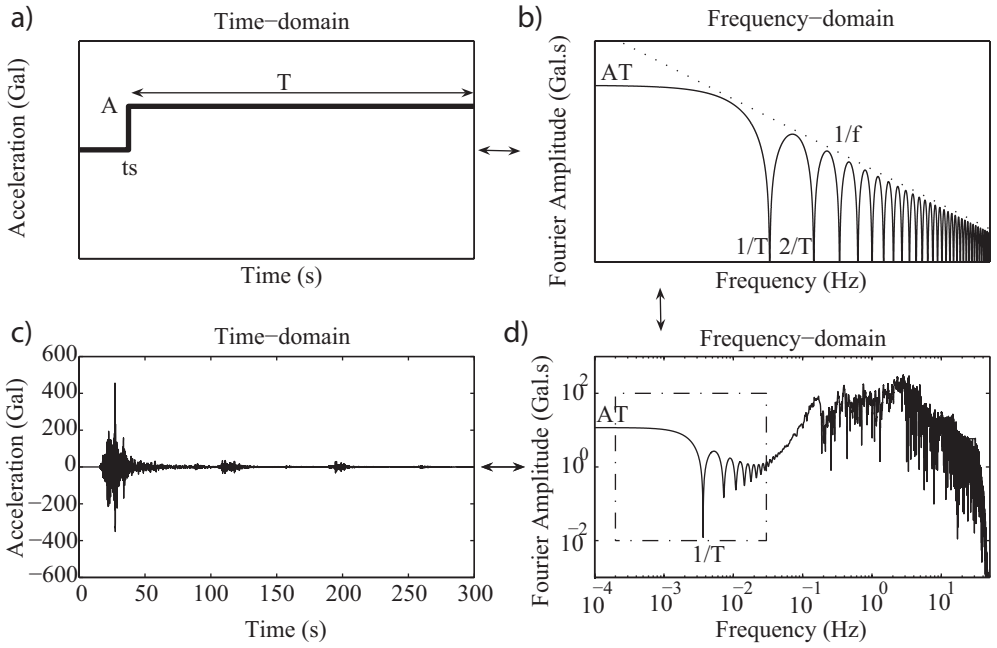

Figure 3.16: Comparison of (a, b) a step function and (c, d) an acceleration record in both time and Fourier domains. Example from the 2007 Niigata-ken Chuetsu-Oki earthquake, NIG019 station, EW component.

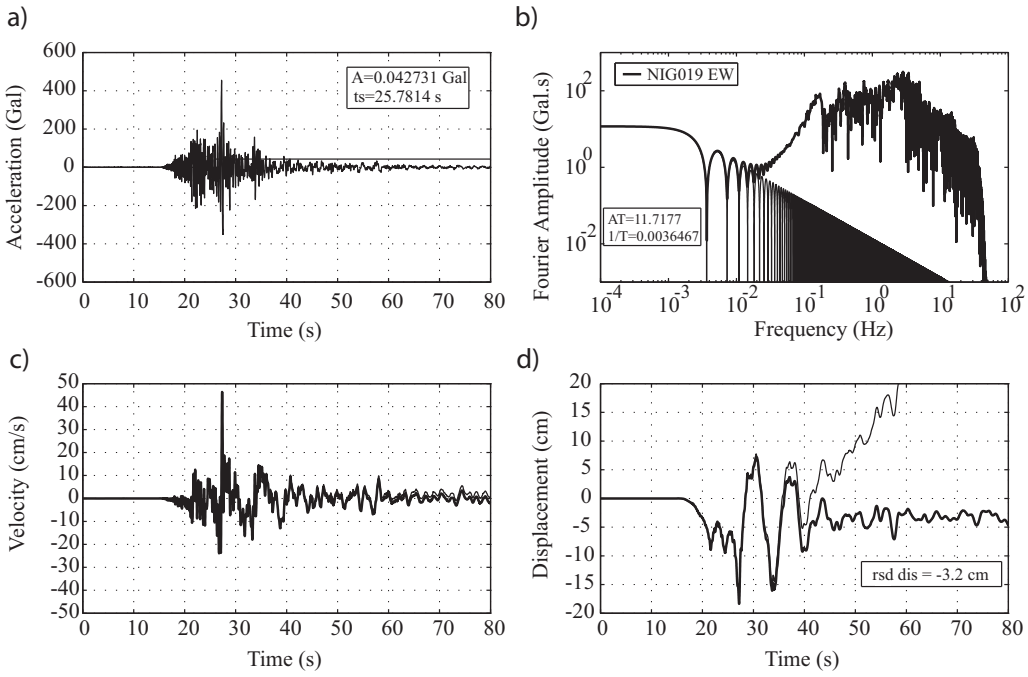

Figure 3.17: (a) Superposition of the acceleration record and a step function of amplitude A (not on scale) and starting time ts (determined above) used to correct the acceleration record. (b) Superposition in the frequency domain of the acceleration record and the step function of amplitude A and starting time ts shows extremely good match at low frequency. (c, d) Uncorrected and corrected velocity and displacement time histories. The corrected displacement history is obtained by subtracting the step function from the acceleration record, then double integrating the corrected acceleration time history. The displacement is stable after the earthquake.

step function of characteristics A and ts shows extremely good match at low frequencies.

Subsequent processing is applied in the time domain. A step function of amplitude A = 0.042731 Gal and of starting time ts = 25.7814 s is subtracted from the acceleration record (Figure 3.17, a and b). Note that we corrected the acceleration time series from a step function starting at ts (until the end of the record). While zero pads are added after the acceleration record, it is strictly speaking a rectangular box of amplitude A, starting at ts, until the end of the record (300 s in K-Net case).

Double integration of the corrected acceleration time history shows no more

drift: the displacement is perfectly stable after the shaking (Figure 3.17, d). The residual displacement is estimated at -3.2 cm.

Practical application: calculation of the double integration Numerical integrations must be accurate and their error small enough to be negligible. We evaluated the quality of three different integration methods of increasing complexity (Trapezoidal, Simpson and Newton-Cotes (s=5) rules), and found that the Simpson method is accurate enough for the purpose of this method. Practically, integrations are computed by using the Simpson's method.

Comments about the addition of zero pads to records Practically, adding zero pads to records is a common tool. The Fast Fourier Transform (F.F.T.) often uses it, because its execution if faster with power of two data long. For example, when using the F.F.T. to calculate the Fourier transform of a 30,000 data long record (e.g. a 300 s long record sampled at 100 Hz), computers add zeros up to the next power of two data long, i.e. $2^{15} = 32{,}768$ data.

Here, we compare an acceleration record that contains a step function (or a box-like function after the addition of zero pads) with a theoretical box-like function. Both have discontinuities at the end of the record and can therefore be compared. For this specific application, it is thus necessary not to smooth the box-like function at its end.

The figure 3.18 indeed shows the comparison of a box-like function and of a smoothed box-like function at its two ends in both time domain (a and b) and Fourier domain (c and d). The Fourier transform of the smoothed box-like function shows slight differences at low frequencies, especially a different 1/T frequency, but pronounced differences at higher frequencies, which make the comparison impossible with the acceleration records' low frequency content.

3.6 Conclusions of Chapter 3

The addition of long zero pads to records leads to better visualization of their Fourier amplitude spectra. This does not add information to records nor improve the instruments' capabilities: poor quality records remain poor quality records.

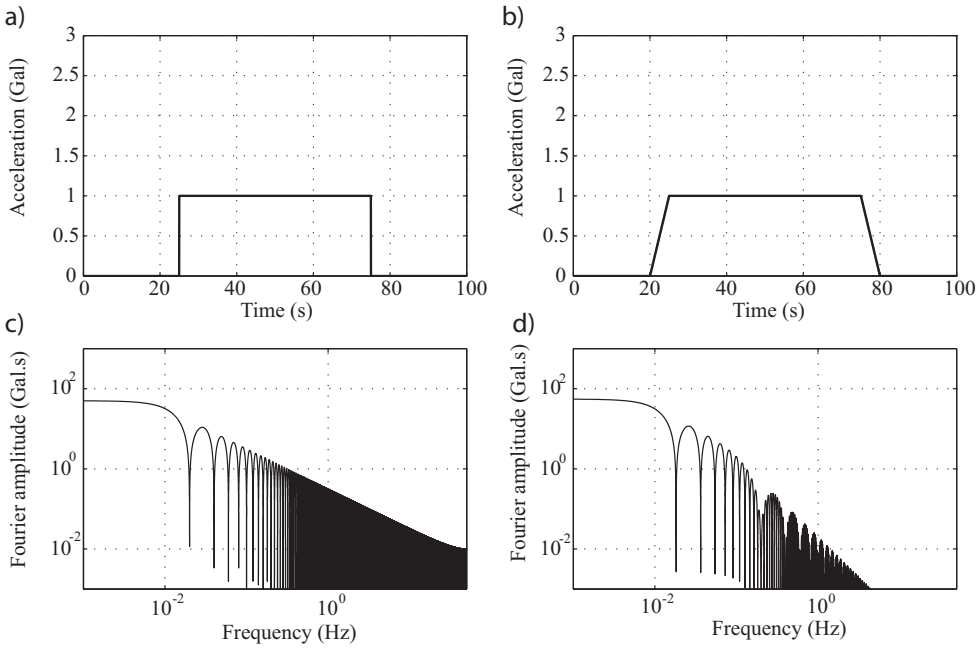

Figure 3.18: comparison of a box-like function and a box-like function smoothed at its two end (a and b), and also comparison of their Fourier transform (c and d). For this specific application, the discontinuities (a and c) in the time domain are needed to compare the box-like function with the low frequency content of the acceleration record.

Adding zero pads to records reduces the interval between frequencies at which computers calculate their Fourier amplitudes, until the records' Discrete-Time Fourier Transform (D.T.F.T.), best Fourier transform that one can expect to obtain from records, is visualized. Zeros padding records provides the possibility of retrieving the maximum frequency information from the available data, and so even at low frequencies.

Based on our knowledge of the instrument's response (chapter 2) and following the addition of long zero pads to records in order to improve the visualization of their low frequency, this chapter then proposes a simple method to remove the baseline offsets that contaminate strong-motion acceleration records. It is possible to obtain reliable estimates of the displacement time histories from acceleration records when the low frequency content of the acceleration record is dominated by 1/f electronic noise up to very small frequencies (processing scheme, case 1 in section 3.4) or by constant residual tilt (processing scheme, case 2 in section 3.5).

Chapter 4

Quantitative verification of the proposed method to estimate near-field displacement and permanent rotation, and its engineering application

4.1 General Remarks

We apply the methodological steps detailed in chapters 2 and 3 to strong-motion accelerations recorded in the near-field of large earthquakes. The accuracy of displacement time histories and permanent rotation retrieved from strong-motion seismometers is checked by comparing them with external measurements. As a practical application, we focus on the implications for the design of structures.

In section 4.2 are processed the strong-motion accelerations recorded in the near-field of the 2007 Niigata-ken Chuetsu-Oki Earthquake (Japan). Good agreements are found between the coseismic displacement estimated from strong-motion accelerograms and nearby 1-Hz GPS data.

In section 4.3, the origin of the simple step functions removed from the acceleration time series is confirmed to be the record of the instruments' coseismic

residual tilt. The accuracy of the permanent rotation angle estimated from acceleration time histories is validated by comparison with external rotation information. The data used come from Kasho Dam, a very well instrumented site that experienced a very strong shaking, including permanent rotation, during the 2000 Western Tottori earthquake (Japan).

Among the possible applications, this dissertation focuses in section 4.4 on the civil engineering one. The reliable translational acceleration time histories and permanent rotations now available should contribute to better design structures. They may be used as input motion for time domain analysis, either for numerical simulations or experimental modelisations, or to obtain improved displacement response spectra, especially at long periods, when the residual tilt is removed from the acceleration records.

4.2 Estimation of coseismic displacement from strong-motion accelerograms recorded during the 2007 Niigata-ken Chuetsu-Oki earthquake (Japan)

The K-Net and Kik-Net acceleration time histories recorded in the near-field during the 2007 Niigata-ken Chuetsu-Oki earthquake were processed according to the scheme described in the preceding chapter. The records of two Japanese Meteorological Agency (JMA) instruments are also added by extension of the method.

In the present section, we first detail the processing steps applied to accelerograms recorded near the epicenter of the earthquake (map in Figure 4.3), then compare the displacement time histories obtained from acceleration records with 1-Hz GPS data, when collocated. We finally draw a map of the residual displacements obtained by the two methods.

4.2.1 Summary of processing steps applied

The accelerograms recorded at the stations shown in Figure 4.3 have been processed. Each accelerogram, its Fourier transform, velocity and displacement time histories as well as the processing steps applied are given in Figures A2-A19 in appendix A. The processing details of the acceleration times series are summarized in Tables 4.1 and 4.2.

In the Tables 4.1 and 4.2, "no correction applied" does not mean that the residual tilt is equal to zero, but that it is so small that other sources of noise, especially the 1/f semiconductor noise, predominates at low frequencies.

Stable displacement time histories are obtained in processing case 1 (4 records) and case 2 (8 records). However, for intermediate situations (5 records), stable residual displacements are usually not obtained, and so an estimation of the displacement is given.

Note that at two stations, the processing scheme could not be applied. A retaining wall collapse had been reported at station NIG018 by NIED (2007), altering the acceleration record. Also, one record, JMA Kashiwasaki, NS component, shows more than one slope in the velocity time history. An additional pulse can be observed in the acceleration time series at the 40^{th} second.

Table 4.1: EW component.

	A (Gal)	Residual Displacement (cm)	Processing Type
NIG017	0.0048	≈ -2.0	Intermediate
NIG018	-	Problem of wall stability	-
NIG019	0.04273	-3.2	Case 2
NIG020	no correction applied	-2	Case 1
NIG021	0.00963	-2.3	Case 2
NIG023	no correction applied	-0.2	Case 1
NIG028	no correction applied	-2.1	Case 1
NIGH12	0.0048	≈ -1.5	Intermediate
JMA Takayanagi	0.2366	-1.8	Case 2
JMA Kashiwasaki	-1.0365	-13.8	Case 2

Table 4.2: NS component.

	A (Gal)	Residual Displacement (cm)	Processing Type
NIG017	0.0092	2.1	Case 2
NIG018	-	Problem of wall stability	-
NIG019	-0.0472	2.3	Case 2
NIG020	-0.0023	1.8	Case 2
NIG021	-0.0095	≈ 3.0	Intermediate
NIG023	0.00068	0.6	Intermediate
NIG028	no correction applied	0.8	Intermediate
NIGH12	no correction applied	1.2	Case 1
JMA Takayanagi	-0.1449	6.8	Case 2
JMA Kashiwasaki	2.7449	See text	Double slope

4.2.2 Comparison of displacements obtained from acceleration records with 1-Hz GPS data

The processing scheme's efficiency is tested: the displacement time series obtained by processing strong-motion records are compared with nearby 1-Hz GPS data as a check of the method.

During the earthquake, the K-Net NIG019 OJIYA station and the 1-Hz GPS OJIYA station recorded the event. Both stations are 600 m distant from each other. Displacement time histories calculated from processed acceleration records were compared with the 1-Hz GPS data (Figures 4.1 and 4.2). For the EW and the NS components, the seismic displacement and the 1-Hz GPS displacement time histories show extremely good similitude for both the residual and the oscillatory parts of the displacements.

In Kashiwasaki, two strong-motion accelerograms NIG018 and JMA Kashiwasaki, as well as two 1-Hz GPS stations K1 and K2 recorded the event. The area is in the very near-field of the earthquake and was subjected to very large displacements. It is known for having experienced soil related problems including liquefaction: at GPS station K2, tilt of the antenna pillar (Tabuchi *et al.*, 2008) had been reported; also, at NIG018 station, the collapse of a retaining wall around the station was reported (NIED, 2007). The data of these two instruments were removed from the set of records used. The records remaining at hands, i.e. the displacement time histories obtained from the JMA accelerometer and the K1

1-Hz GPS station (situated 3.5 km apart from each other) were compared. For the EW component, we found a good agreement for the residual displacement at about 14 cm. From the JMA seismometer, the amplitude of the oscillatory displacement reached almost 80 cm. There is a good agreement between the acceleration derived displacement and 1-Hz GPS displacement. The differences can be due to the quickly varying field of displacement in the area and to possible misorientation of the instruments during their installation. Regarding the NS component of the acceleration record, a pulse at 40 s made the processing scheme impossible to apply.

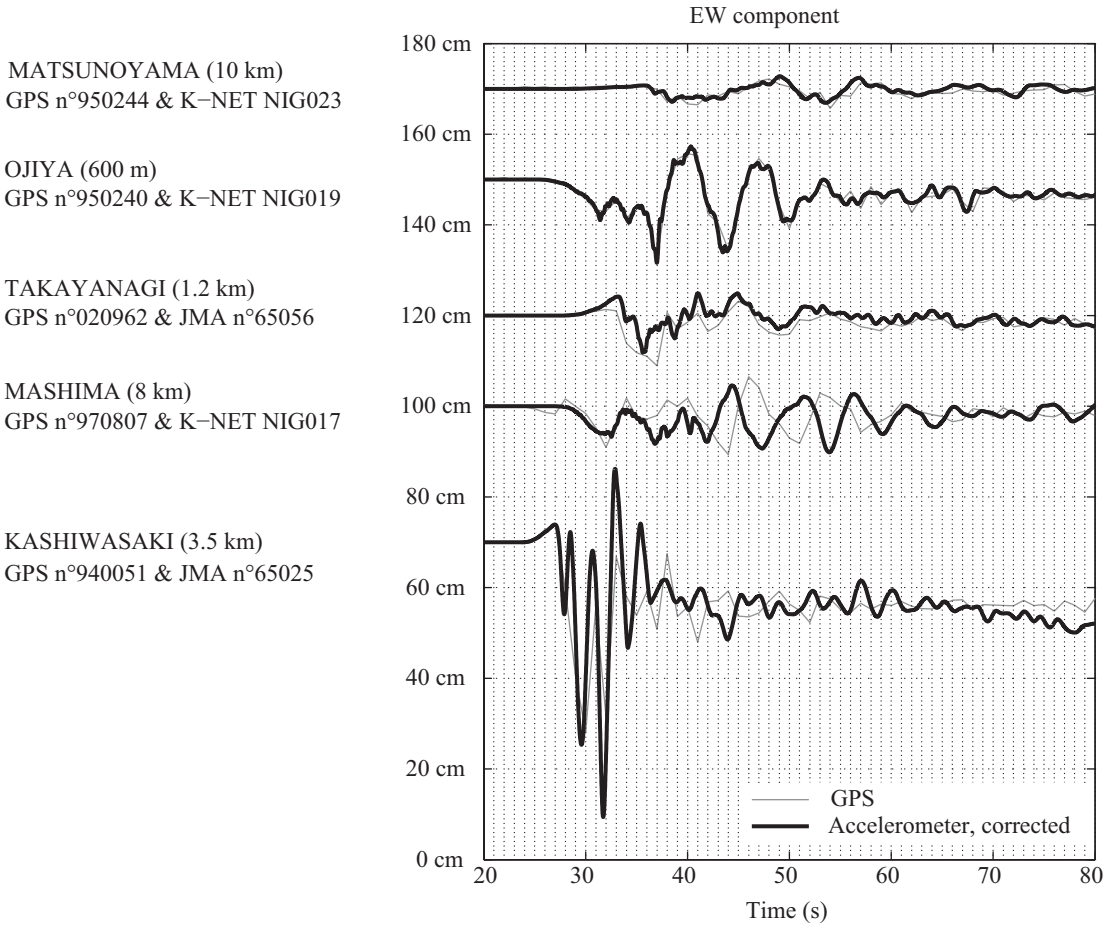

Figure 4.1: Accelerometer displacement time series (EW component) vs. nearby 1-Hz GPS data recorded during the 2007 Niigata-ken Chuetsu-Oki earthquake, Japan.

At Takayanagi, the JMA accelerometer and 1-Hz GPS station are 1.2 km apart from each other. They show similar residual displacement and good similitude during the oscillatory part of the displacement, considering the distance between the stations.

For the other two stations Mashima and Matsunoyama, the displacements obtained by the two methods show very good similitude considering that the distance between the two sensors is of several kilometers.

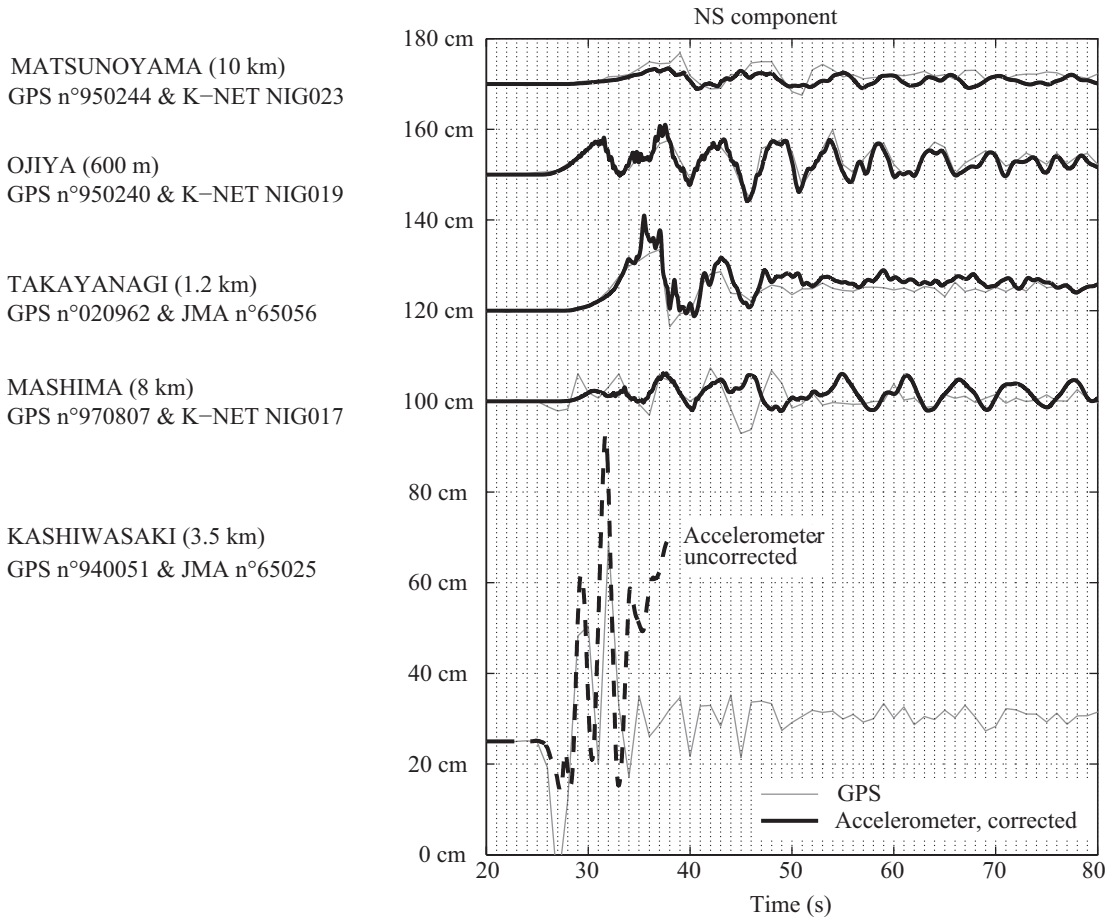

Figure 4.2: Accelerometer displacement time series (NS component) vs. nearby 1-Hz GPS data recorded during the 2007 Niigata-ken Chuetsu-Oki earthquake, Japan.

4.2.3 Comparison of coseismic residual displacement

In the near-field of the 2007 Niigata-ken Chuetsu-Oki earthquake, residual displacements calculated as suggested above were compared with displacements measured at surrounding GPS stations (Figure 4.3). When GPS and seismometer stations are collocated (a few hundred meters apart from each other), the residual displacements obtained by the two methods are almost identical. At other locations where accelerometers and GPS stations are a few kilometers distant from each other, residual displacements obtained by processing seismometer records are consistent with displacements measured by GPS stations.

4.2.4 Comparison of coseismic residual displacement obtained at three other earthquakes

The results obtained here were confirmed by applying this method to three other earthquakes, namely the 2004 Niigata-ken Chuetsu earthquake (Javelaud *et al*, 2005, 2006 and 2011b; Ohtake, 2006; Ohtake and Ohmachi, 2007), the 2007 Noto Hanto earthquake (Murakami, 2008; Inoue *et al.*, 2007) and the 2008 Iwate-Miyagi Nairuku earthquake (Furukawa *et al.*, 2010a and b, and 2011), Japan.

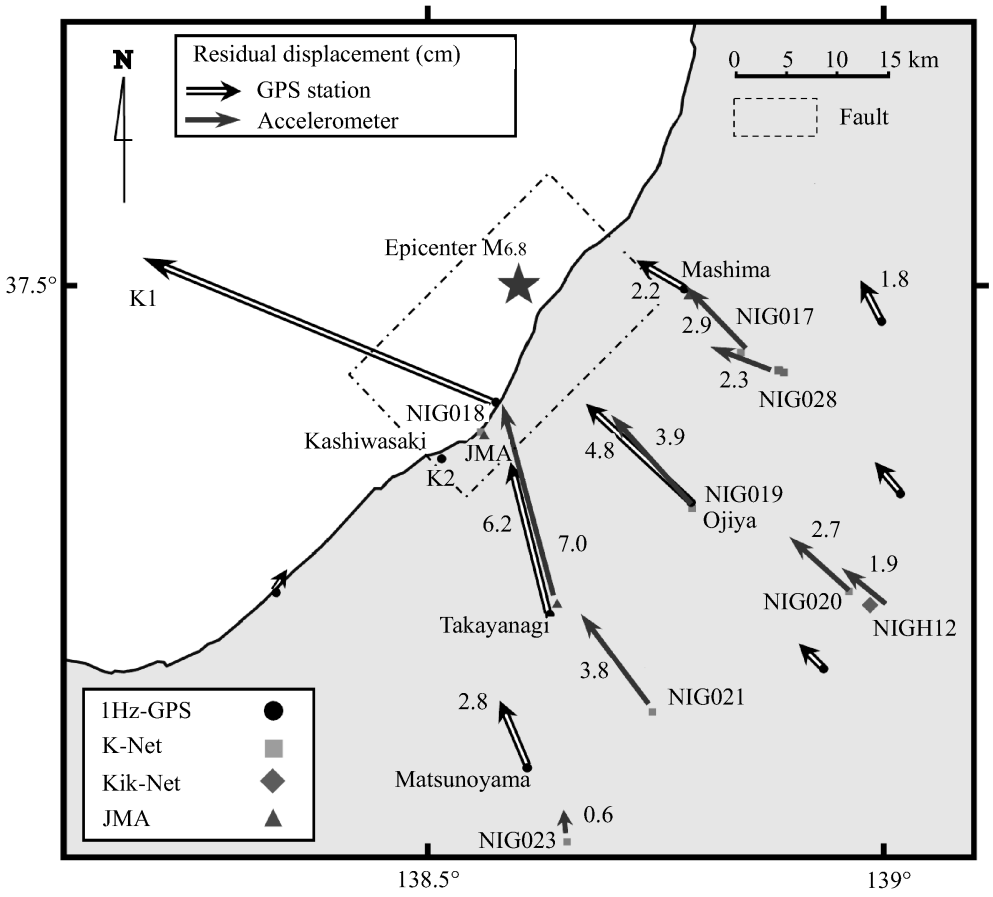

Figure 4.3: Comparison of coseismic residual displacement obtained from strong-motion seismometers and surrounding GPS stations during the 2007 Niigata-ken Chuetsu-Oki earthquake. Two JMA records were also processed by extension of the method.

4.3 Estimation of small permanent rotation from strong-motion recorded during the 2000 Western Tottori earthquake (Japan)

Modern strong-motion accelerometers record the instruments' translational accelerations as well as their rotation. The accuracy of permanent rotation angles derived from acceleration time histories can be checked by comparison with external rotation information. In practice, this can be done at exceptional sites that experience earthquake induced permanent rotation and where the permanent rotation is recorded by various instruments.

During large earthquakes, tectonic movements along faults generate in their near-field important deformations including transitory and permanent displacements, as well as surface tilting. Evidences of large scale deformation and significant tilting have been gathered for extremely large earthquakes such as the M 9.2 great Alaska Earthquake (1964) during which an area of at least 120,000 km^2 was tilted and resulted in relative vertical displacement of as much as 2.5 m (Kalkan and Graizer, 2007). Permanent tilting have also been estimated for smaller magnitude earthquakes, as for example during the M_w 6.7 Northridge Earthquake in 1994: a permanent rotation of a few degrees (5 x 10^{-2} rad) was measured at Pacoima dam's upper left abutment and rightly estimated by processing strong-motion records (Graizer, 2006a and 2006b).

Recovering tilt information from strong-motion records opens the possibility to retrieve tectonic permanent tilt when instruments are located at rock sites, including the bottom of boreholes and at the foundation of large structures founded on rock. In this section, we focus our study on Kasho dam. Built in 1989 above a hidden fault (Figure 4.4), this concrete gravity dam was hit by the powerful M_J7.3 2000 Western Tottori earthquake (Japan). The earthquake was caused by seismic rupturing of a left lateral N152° strike slip hidden fault underlying the dam site (Takasu *et al.*, 2001), and occurred at 13:30 (local time) on October 6.

Kasho dam, the nearest dam from the main shock's epicenter (epicentral distance of about 4 km) was subjected to strong earthquake shaking with peak accelerations of 531 Gal in its lower inspection gallery and 2051 Gal at its top (JCOLD,

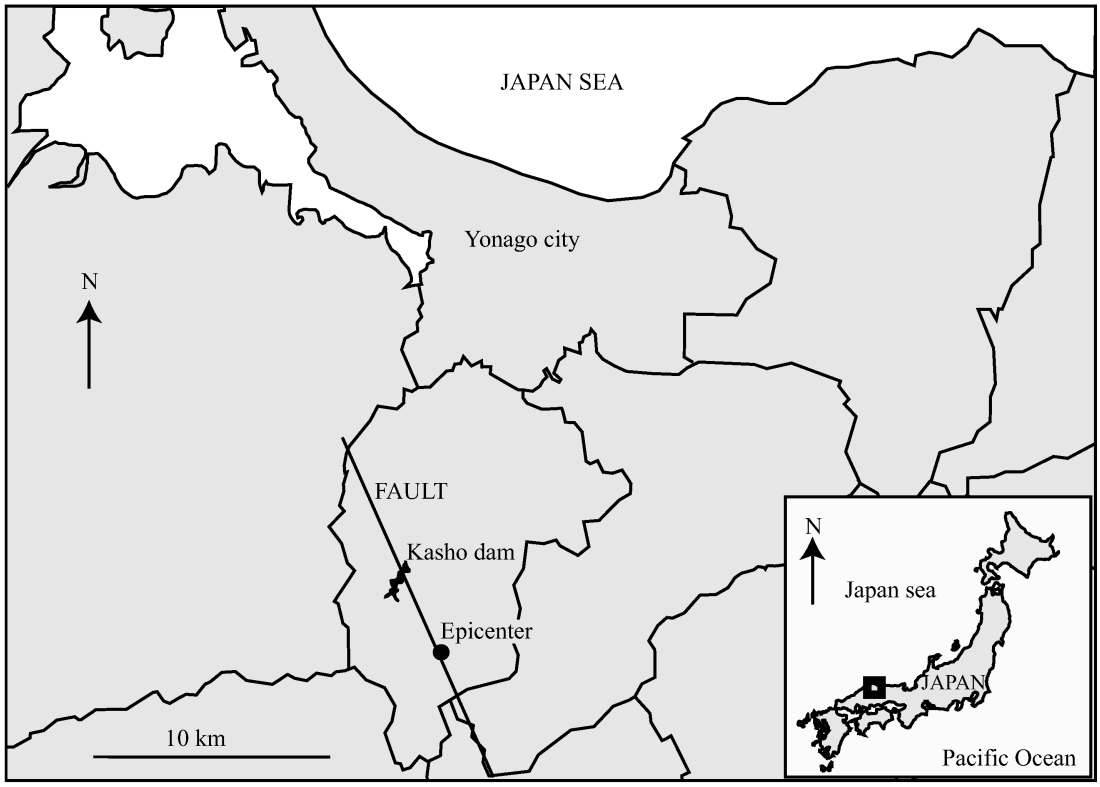

Figure 4.4: Simplified map showing Kasho dam, the main shock's epicenter, and the fault. Inset, situation of the enlarged map in western Honshu, Japan.

2002). Despite such acceleration levels, the dam did not suffer serious damage: no increase in water leakage and only minor cracking were reported on its sub-gate room's concrete floor. However, during the main shock, permanent rotation and permanent translational displacement of Kasho dam occurred. Immediate evidences were a sudden 6 cm drop of the reservoir's water level and a permanent shift of its plumb line. Overall dam and reservoir's permanent displacement and rotation were confirmed by the ground survey. Numerous aftershocks were recorded in the days and months following the earthquake, one of them having a magnitude of 5, and three of them having a magnitude greater than 4 (Ohmachi *et al.*, 2003).

The choice of Kasho dam for confirming the accuracy of rotation angles retrieved from strong-motion accelerograms is motivated (1) first, by the very large acceleration recorded at its foundation during the event, (2) second, the large

displacement evidences, including permanent displacement of the structure and a permanent tectonic tilting of about 10^{-4} rad, and (3) then, by the regular vertical field of deformation over the dam and reservoir areas (an area of a few square km as shown by the numerical simulation carried out by Ohmachi *et al.*, 2003), which validates that tilt, estimated by different methods within the area, can be compared.

Based on the analysis of the GTA-53 strong-motion seismometer deployed at Kasho dam, this section describes the dam's structure and the damages caused to it by the main shock (subsection 4.3.1). It also analyzes the dam's response to the earthquake in term of local tectonic rotation and displacement, based on the information available: strong-motion seismometer located in the low inspection gallery, plumb line readings, ground survey around the reservoir as well as numerical simulations. Strong-motion records are analyzed according to the method detailed in chapter 3. In the last subsection (subsection 4.3.2), we compare the tectonic rotation derived from acceleration records with those obtained from other methods.

4.3.1 Kasho dam's response to the earthquake

This subsection describes the dam's structure and the damage caused by the main shock. It analyses the dam's response to the earthquake in term of displacement and rotation, based on each kind of available information: strong-motion seismometers located within the low inspection gallery at the dam's foundation, plumb line readings, ground survey around the reservoir as well as numerical simulations.

Kasho dam is a concrete gravity dam with a height of 46.4 m and a crest length of 174 m. The dam body design was conducted by the seismic coefficient method using a horizontal coefficient of 0.12 (Ohmachi *et al.*, 2003). Earthquake actions in the vertical direction were not considered at the time of the construction for the design of attached structures. No damage concerning the dam safety was reported by the inspection following the earthquake (Yamaguchi *et al.*, 2002). Minor damage had however occurred to attached structures: after the main shock, cracks were observed in the sub-gate control room floor and sidewalls, a cantilever

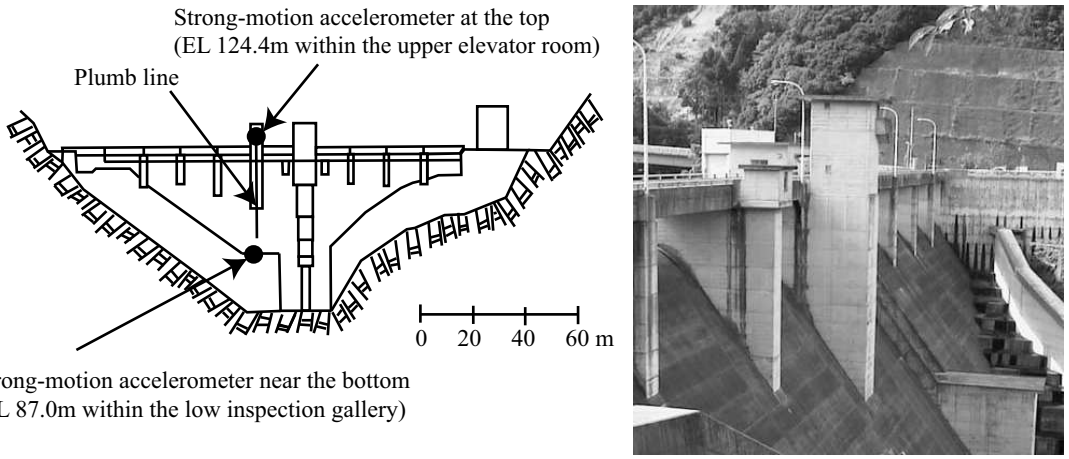

Figure 4.5: Schematic explanation of Kasho dam showing the location of the strong-motion seismometers and the plumb line. Right, Downstream view of Kasho Dam from the right bank.

structure projecting upstream from the dam (Yamaguchi *et al.*, 2002; Ohmachi *et al.*, 2003). Moreover, Yamaguchi *et al.* (2002), who attempted to model the dam response to the main shock, divided its structure into three parts of different thicknesses: the dam body itself, the elevator tower and its adjacent supporting structure, and the top of the elevator tower. These divisions were made so as to realistically take into account the differences in stiffness.

The reservoir water level lowered suddenly by about 6 cm at the time of the main shock. The sudden drop was followed by damped free vibration (seiching of the reservoir) that continued for several hours, characterized by a period of 6.5 min and a damping ratio of 2% (Ohmachi *et al.*, 2003). The water level was of 112 m at the time of the main shock whereas the reservoir's full water level is 118 m.

Ohmachi *et al.* (2003) simulated by 3D boundary element method the ground displacement generated by the main shock. In the simulation, the ground was simplified as a half-space of homogeneous elasticity with a shear wave velocity of 4 km/s. The fault was modeled with a N152° strike and a 86 degrees dip, and the rupturing by a uniform -7 degrees 1.4 m slip. Horizontal displacement time histories obtained around the dam are similar in shape, but of smaller amplitude, to those determined in the next paragraph from strong-motion records. The

sensor misorientation (detailed in the next paragraph) was taken into account by Ohmachi *et al.* (2003). The simulated vertical permanent displacement varies regularly over the dam and reservoir's area. This implies a constant tectonic rotation over the area, estimated at N242° 6 x 10^{-5} rad.

Kasho dam is equipped at its foundation by a modern three components digital strong-motion seismometer type GTA-53 (Meisei Electric Co. Ltd), firmly bolted to the concrete floor of the low inspection gallery at elevation 87.0 m (Figure 4.5). The instruments' response as well as the determination of their internal 1/f noise level have been detailed for each horizontal component in the subsection 2.3.5. The sensor misorientation was 10.5°W (Sato *et al.*, 2007): the North-South component's orientation was therefore N349.5°. The main shock acceleration time histories recorded by the horizontal components, after removing the pre-event mean, are shown in Figure 4.6a and b. We henceforth called them uncorrected accelerations. For each component, the displacement time histories, obtained by double integration of these uncorrected accelerations, show drift larger than expected for the true ground motions (Figure 4.6, g and h).

We processed the two uncorrected acceleration time histories according to the method proposed in chapter 3. After adding long zero pads to the two uncorrected acceleration records (so as to make the records 2^{23} data long), we found that in both cases their low frequency content (Figures 4.6, c and d) were well above the 1/f noise levels determined in the section 2.3.5 and were similar to the Fourier spectra of step functions. These situations correspond to the processing case number two in chapter 3. We therefore applied the case two's method and removed, in the time domain and from each record, a step function of characteristics derived from the records' Fourier spectra: respectively of amplitude A=-0.06952 Gal and A=-0.08162 Gal, and of starting time 20.84 s and 24.96 s from the EW and NS components. Double integration of these corrected acceleration time histories show no more drift (Figure 4.6, g and h). The residual displacements are of -4.0 cm for the EW component and +27.4 cm for the NS component. The overall residual displacement is 27.7 cm in the N341° direction. Permanent rotation angles are determined for each component from the step function amplitude. The results are summarized in Table 4.3 and shown in Figure 4.6, e and f). The overall permanent tilting (direction; angle) of the

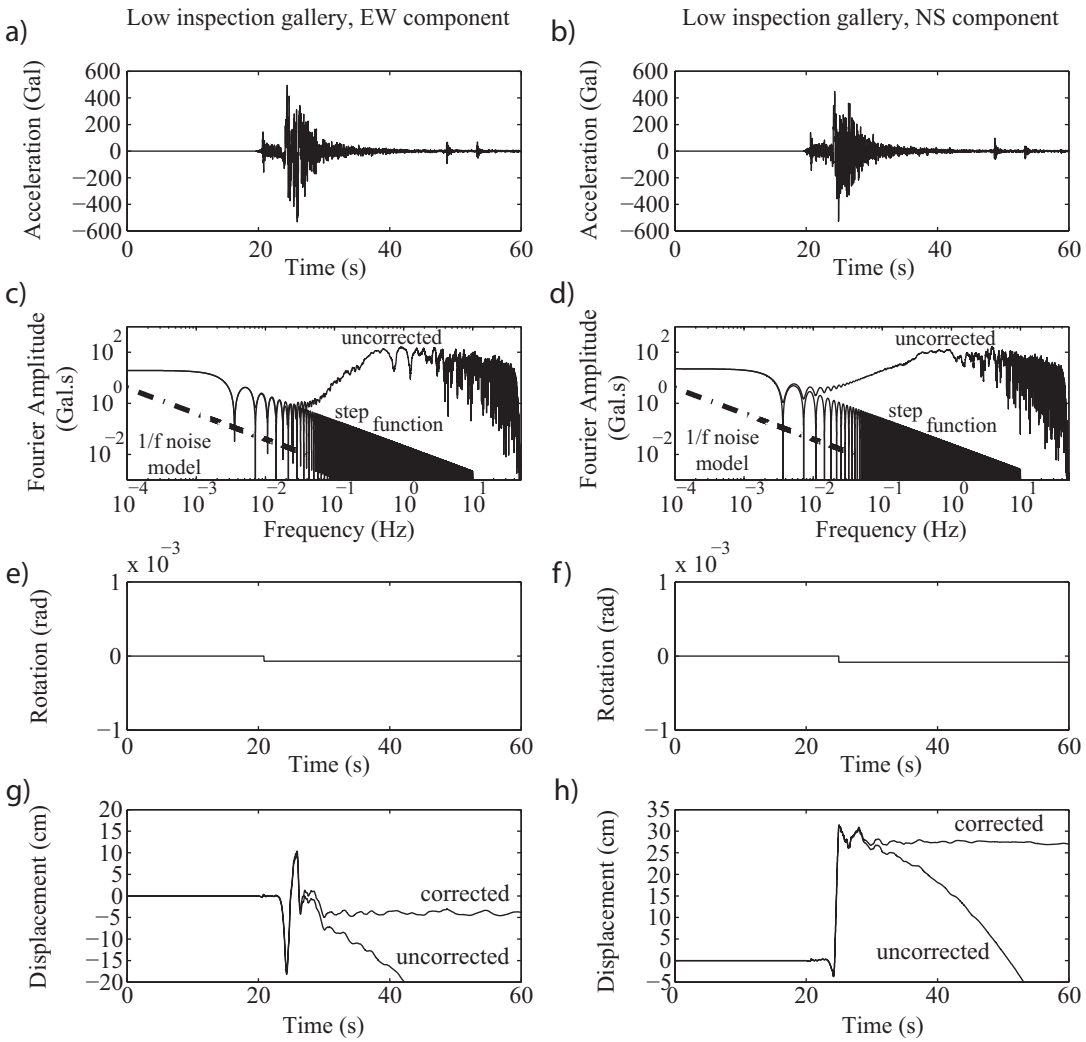

Figure 4.6: (a, b) Uncorrected acceleration time histories recorded within the low inspection gallery by the strong-motion seismometer's EW and NS components during the main shock. (c, d) Superposition in the frequency domain of the uncorrected acceleration records and step functions, of respective amplitudes A=-0.06952 Gal and A=-0.08162 Gal and starting time ts=20.84 s and ts=24.96 s for the EW and NS components, shows extremely good match at low frequencies. The 1/f noise models estimated in Figure 2.20 are well below the signals' Fourier amplitude: the low frequency contents of the main shock records are therefore controlled by the permanent tilt information. (e, f) Permanent rotation estimated for the EW and NS components from the step functions derived in c and d. (g, h) Uncorrected and corrected displacement time histories. The corrected displacement time histories are obtained by subtracting the step functions from the uncorrected acceleration records, then double integrating the corrected acceleration time histories. The displacements are stable after the earthquake.

instrument (therefore of the dam foundation) estimated from the strong-motion records, after correction of the sensor misorientation, is N209.9° 15.47 x 10^{-5} rad.

Kasho dam is also equipped with a plumb line installed in a vertical shaft (Figure 4.5), 30 cm in diameter, and fixed to the upper elevator room's floor next to the strong-motion accelerometer (Figure 4.7). The weight on the lower end is housed in a measurement device located at elevation 89.5 m in the dam's lower inspection gallery. The relative displacement between the dam's top and bottom is given by the readings of the plumb line.

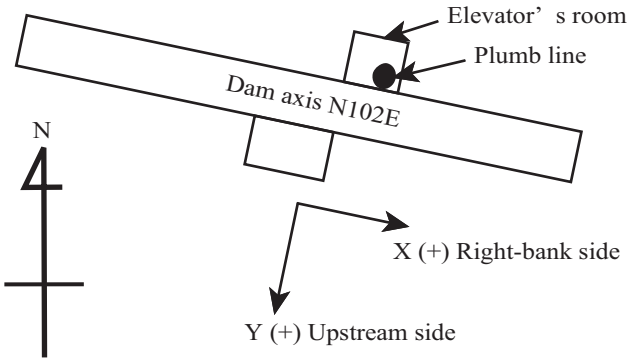

Figure 4.7: Kasho dam' s plan view showing the plumb lines position and axis orientation.

Plumb line readings from October 3 to October 14, 2000, are given in Figure 4.8. Last and first readings before and after the earthquake were done at 9:00 a.m. on the 6^{th} of October and at 1:54 a.m. on the 7^{th} of October, 2000. The coseismic plumb line deviation was -2.8 mm in the X (right-bank side) direction and +0.7 mm in the Y (Upstream) direction. The dam axis orientation, therefore the orientation of the X right-bank side direction, is N102°E.

The resultant coseismic displacement determined from the plumb line readings is therefore 2.9 mm and the azimuth of the deviation N268°. The coseismic

Table 4.3: Information retrieved from the low inspection gallery's main shock records.

Component	Amplitudes A of the step function	Equivalent tilt angle	Residual displacement
East-West	-0.06952 Gal	-7.09 x 10^{-5} rad	- 4.0 cm
North-South	-0.08162 Gal	-8.33 x 10^{-5} rad	+ 27.4 cm

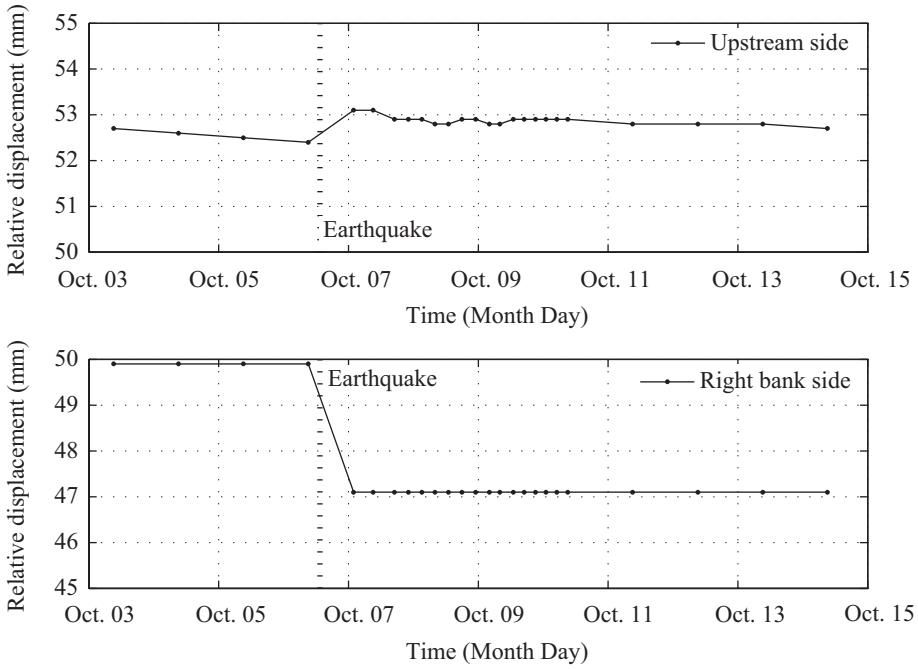

Figure 4.8: Kasho dam's plumb line readings at the begining of October, 2000.

rotation of the two points, plumb line's top and bottom, is given by the resultant displacement divided by the plumb line length, therefore 8.3 x 10^{-5}rad.

After the main shock, a ground survey was performed at 65 surveying points located around Kasho dam's reservoir. The positions of the surveying points around the reservoir and their vertical displacements are given in Figures 10 and 11 of Ohmachi *et al.* (2003). Although slightly positive around the dam, the surveying points' measured altitude variation is mainly negative as it regularly decreases with distance from the dam according to the N242° direction, up to around -20 cm at the upstream end of the reservoir. A few large negative vertical variations of up to -40 cm were measured at some surveying points but excluded from the analysis because they correspond to places where landslides had been reported (Yamaguchi *et al.*, 2002). An overall reservoir dipping direction and rotation angle can be estimated from the ground survey at N242° 17 x 10^{-5} rad, the rotation angle being provided by the regression slope in Figure 11 of Ohmachi *et al.* (2003). The horizontal displacements of surveying points were provided by Fusejima *et al.* (2003) who performed a geodetic survey around Kasho dam reser-

voir. Although the displacement field varies both in direction and in amplitude around the reservoir, the two nearest surveying points from the dam show quite consistent horizontal displacements, with an amplitude of about 30 cm in the N340° direction.

4.3.2 Comparison of permanent rotation and displacement obtained by the different methods

The permanent tectonic rotation and displacement information retrieved from strong-motion records are compared with those obtained from other methods, so as to check the accuracy of information derived from acceleration time histories.

Near-field permanent rotation. Permanent rotations obtained from the different methods are summarized in Table 4.4. At first glance, we can see a good homogeneity between all these permanent rotation estimations, with an overall direction of N240° ± 30° and an overall rotation angle of 11.5 x 10^{-5} ± 5.5 x 10^{-5}rad. This confirms that good estimates of permanent rotation can be obtained from strong-motion acceleration time histories.

Table 4.4: Summary of permanent rotations estimated by four different methods.

Method	Permanent rotation Direction	Permanent rotation Angle (rad)
Ground survey	N242°	17 x 10^{-5}
Simulation	N242°	6 x 10^{-5}
Plumb line readings	N268°	8.3 x 10^{-5}
Low inspection gallery's strong-motion seismometer	N210°	15.5 x 10^{-5}

The homogeneity would however probably have been even better if we were recording, measuring, simulating and comparing exactly the same things. Indeed, the ground survey was performed after the main shock but with a certain delay, which means that the effects of some aftershocks are included in the post-seismic survey. Regarding the simulation performed by Ohmachi *et al.* (2003), it is based on fault parameters and dynamic parameters, some of them being based on assumptions. Although the permanent rotation's orientation is consistent with

others, both the permanent rotation's amplitude and the residual displacement are about 2.5 times smaller than those obtained by processing strong-motion records or the ground survey. One of the reasons is the simplified ground model used. Concerning the plumb line measurements, some aftershocks are also included but more crucially the plumb line was fixed to the upper elevator room's floor. As described, the response of attached structures may not be identical to the response of the dam's main body, and therefore the plumb line record may include local effects due to the elevator tower.

Dam's permanent displacement. Permanent displacements obtained by the ground survey at reference points situated nearby the dam are compared with the displacements estimated from strong-motion time histories recorded at the dam foundation. Results are summarized in Table 4.5. The residual displacement obtained by the ground survey and by processing acceleration records show similar residual displacement and orientation.

Table 4.5: Summary of permanent displacements estimated by two different methods.

Method	Residual displacement Direction	Residual displacement Amplitude
Ground survey	N340°	≈ 30 cm
Low inspection gallery's strong-motion seismometer	N341°	27.7 cm

4.4 Practical implications for the design of structures

Among the potential applications that may benefit from reliable acceleration and displacement time histories, we focus in this section on civil engineering ones. In civil engineering, the seismic design of structures with long-period response such as chimneys, bridges or isolated structures, as well as the design of structures according to modern displacement based methods, requires the use of reliable ground motion and displacement response spectra up to long periods. The reliable

translational acceleration time histories and permanent rotations now available may be used as input motion for time domain analysis, either for numerical simulations or experimental modelisations. Alternatively, and investigated in this section, they may also be used to obtain improved displacement response spectra, especially at long periods, when the residual tilt is removed from the acceleration records.

The range of periods up to which accelerometers reliably record the translational ground motions is restricted. Both the long-period noise and the rotation of the instruments affect the displacement response spectra: for traditional analog acceleration records, the displacement response spectra are usually considered usable up to 2 or 3 seconds (Bommer and Elnashai, 1999; Boore and Bommer, 2005); historically, the installation of digital accelerographs provided higher quality records, less contaminated by noise, and subsequently reliable displacement response spectra up to longer periods (Tolis and Faccioli, 1999). Recent comparison with independent external measurements (broadband seismometers, GPS) showed that the displacement response spectra may be little or not affected by baseline offsets of modern instruments acceleration time histories up to periods of at least 10 seconds (Paolucci *et al.*, 2008; Wang *et al.*, 2007; Akkar and Boore, 2009). It should however be possible to obtain realistic displacement response spectra up to longer periods in the near-field of large earthquakes by processing translational accelerations recorded by modern (low-noise) strong-motion accelerometers, provided that the tilt information is removed from the acceleration records.

The objective of this section is to evaluate the improvement of the displacement response spectra at long periods when the permanent tilt is removed from strong-motion records. This can only be done at specific places where (1) high quality strong-motion acceleration instruments have recorded large events during which permanent rotation of the instruments occurred, and where (2) check of the results against external measurements is possible.

These requirements were met during the 2007 Niigata-ken Chuetsu-Oki Earthquake (section 4.2). We selected five sets of strong-motion acceleration time histories recorded in the near-field of that earthquake, together with their nearest 1-Hz GPS records. The instruments' locations are shown in Figure 4.9: K-Net station NIG019 Ojiya and GPS station n°950240 about 600 m distant from one

another, JMA station Takayanagi and GPS station n°020962 about 1.2 km distant from one another, JMA station Kashiwasaki (EW component) and GPS station n°940051 about 3.5 km distant from one another, K-Net station NIG017 Mashima and GPS station n°970807 about 8 km distant from one another, and K-Net station NIG023 Matsunoyama and GPS station n°950244 about 10 km distant from one another.

To compare the three displacement time histories (derived from uncorrected and corrected acceleration records and the 1-Hz GPS data) of each set of instruments, in both time and frequency domains, the earthquake shaking must start at

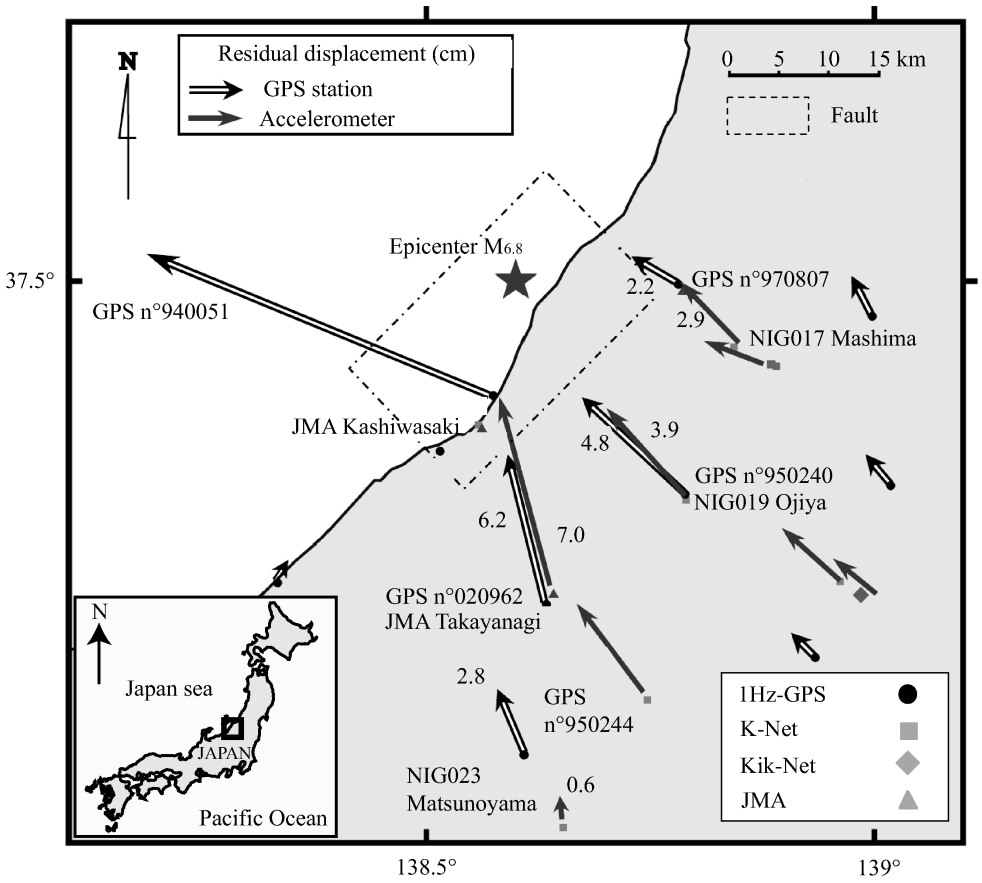

Figure 4.9: Simplified map showing the instrument's position and the coseismic residual displacements obtained from strong-motion seismometers and surrounding GPS stations during the 2007 Niigata-ken Chuetsu-Oki Earthquake. Inset, situation of the enlarged map in eastern Honshu, Japan.

the same instant, and the records must be of the same duration. Due to a longer pre-event portion for the GPS records, we increased the pre-event part of the acceleration records so that the earthquake shaking starts at the same instant for both acceleration and displacement records. We then removed from the acceleration records the post-event acceleration part in order to have 100 seconds long records. Finally, acceleration and displacement time histories were zero padded to obtain a detailed visualization of their Discrete Time Fourier Transform. 1-Hz GPS records' Fourier spectra are displayed (Figure 4.10, c and d) up to 0.5 Hz (Nyquiest frequency), whereas 100 Hz strong-motion records' spectra are plotted up to 50 Hz.

This detailed case study offers us the possibility of carrying out subsequent analysis, focusing here on the displacement response spectra, and of evaluating the evolution of the displacement response spectra's long-period content when the residual tilt is removed from acceleration records. Two different behaviors were observed in this specific case study, depending on the amplitude of the residual tilt: larger than 0.04 Gal (about 0.4 x 10^{-4} rad) or smaller than 0.01 Gal (about 0.1 x 10^{-4} rad).

4.4.1 Displacement response spectra when the accelerometers' residual tilt is larger than 0.04 Gal

The residual tilts recorded by the strong-motion seismometers have amplitudes larger than 0.04 Gal at Kashiwasaki (EW component), Ojiya NIG019 and Takayanagi (section 4.2).

At these three stations (five records: Kashiwasaki EW component, Ojiya EW and NS components, and Takayanagi EW and NS components), we first compared the long-period content of records in time and frequency domains. Similar behavior can be observed for the five records. To illustrate these observations, the Ojiya's EW component is displayed in Figure 4.10 (a, c). For the five records, the double integration of the uncorrected acceleration time histories show very large unrealistic drifts starting after the oscillatory part of the displacement, in-between the 40^{th} and the 50^{th} second. The corrected accelerations were obtained by removing residual tilts of amplitudes larger than 0.04 Gal from the uncor-

rected accelerations. The double integration of these corrected accelerations are very similar to the 1-Hz GPS displacement time histories for at least 65 seconds, and up to 100 seconds at Ojiya and for Takayanagi's EW component. Regarding the Fourier displacement spectra, the displacement spectra based on the uncorrected accelerations are dramatically different from the 1-Hz GPS displacement spectra: they have much higher Fourier amplitudes than the GPS spectra over the whole range of frequencies. However, the displacement spectra based on the corrected acceleration are almost identical to the GPS spectra over the whole range of frequencies, which shows that removing the permanent tilt from the ac-

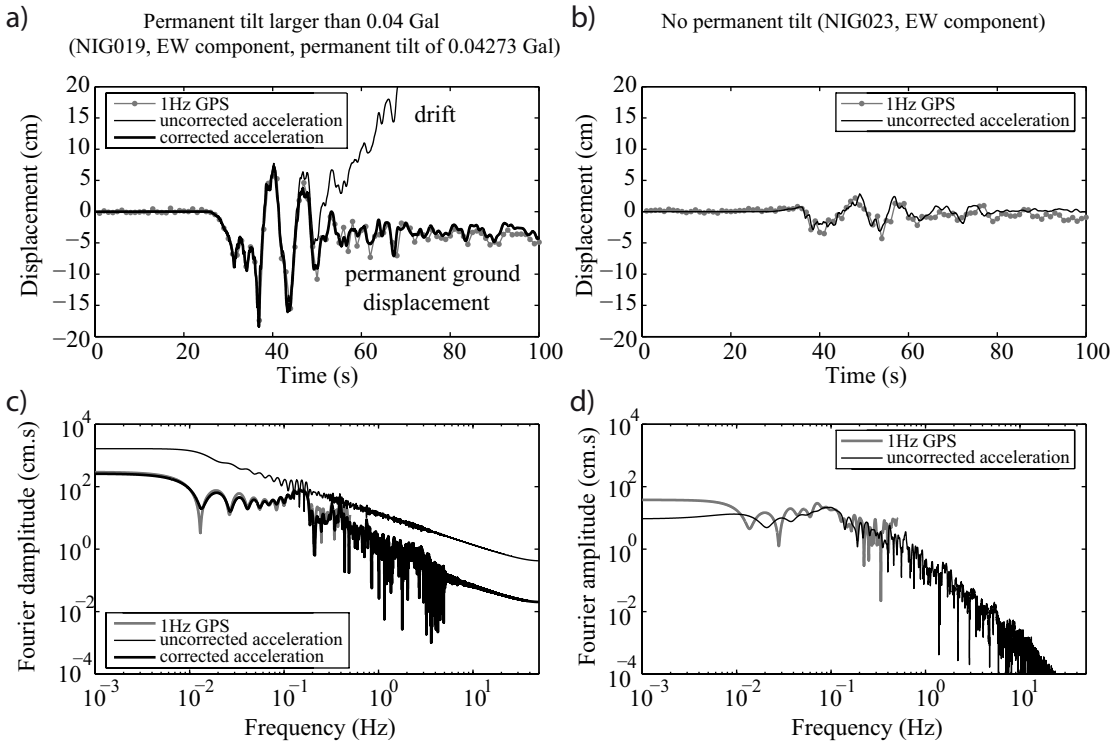

Figure 4.10: Typical displacement time histories in (a, b) time and (c, d) frequency domains when the permanent tilt is larger than 0.04 Gal (a, c: Ojiya NIG019 EW component) or smaller than 0.005 Gal (b, d: Matsunoyama NIG023 EW component). a, c) removing a permanent tilt larger than 0.04 Gal from the uncorrected acceleration leads to stable displacement after the oscillatory part of the record, and to a displacement series similar to the 1-Hz GPS one in (a) the time domain as well as in (b) the frequency domain up to 0.5 Hz (Nyquiest frequency of the 1-Hz GPS record).

celeration records provides accurate translational accelerations including at low frequencies.

Displacement response spectra calculated from uncorrected and corrected acceleration time histories are given in Figure 4.11 (a, b, and c). At long (infinite) periods, the displacement response spectra are by definition equal to the peak ground displacement. Their accuracy may therefore be checked by using the nearest GPS records. The peak ground displacement derived from the GPS records are also given in Figure 4.11.

At Kashiwasaki (EW component), Ojiya NIG019 and Takayanagi, removing the permanent tilt does not significantly change the response spectra up to periods ranging from 24 seconds (Ojiya NIG019, NS component's case) to 80 seconds (Ojiya NIG019, EW component's case), which is consistent with previous studies (Paolucci *et al.*, 2008; Wang *et al.*, 2007; Akkar and Boore, 2009). At longer periods, the displacement response spectra based on uncorrected accelerations diverge very quickly, while displacement response spectra computed from corrected accelerations do not diverge, and are close to their theoretical values obtained from their nearest 1-Hz GPS records (Figure 4.11 a, b and c).

The similarities between the very long period of the displacement response spectra and the GPS Peak Ground Displacement would however be even better if we were comparing accelerations and GPS data recorded at exactly the same places (avoiding any difference due to the ground motion's spatial variability) and if the GPS data were recorded at higher sampling frequencies. 1-Hz GPS measurements may indeed not capture the displacement maxima during the quickly varying oscillatory part of the displacement, and may therefore provide underestimations of the peak ground displacement.

In this specific case study, we observe that, among the sets of stations considered, the displacement response spectra at very long periods is the closest to the GPS Peak Ground Displacement at Ojiya. This is where the distance of the strong-motion sensor to its nearby GPS station is the smallest (600 m), and where the oscillatory part of the displacement was well captured by the GPS instrument. The combination of these two elements led to displacement response spectra reaching the GPS Peak Ground Displacement at very long periods.

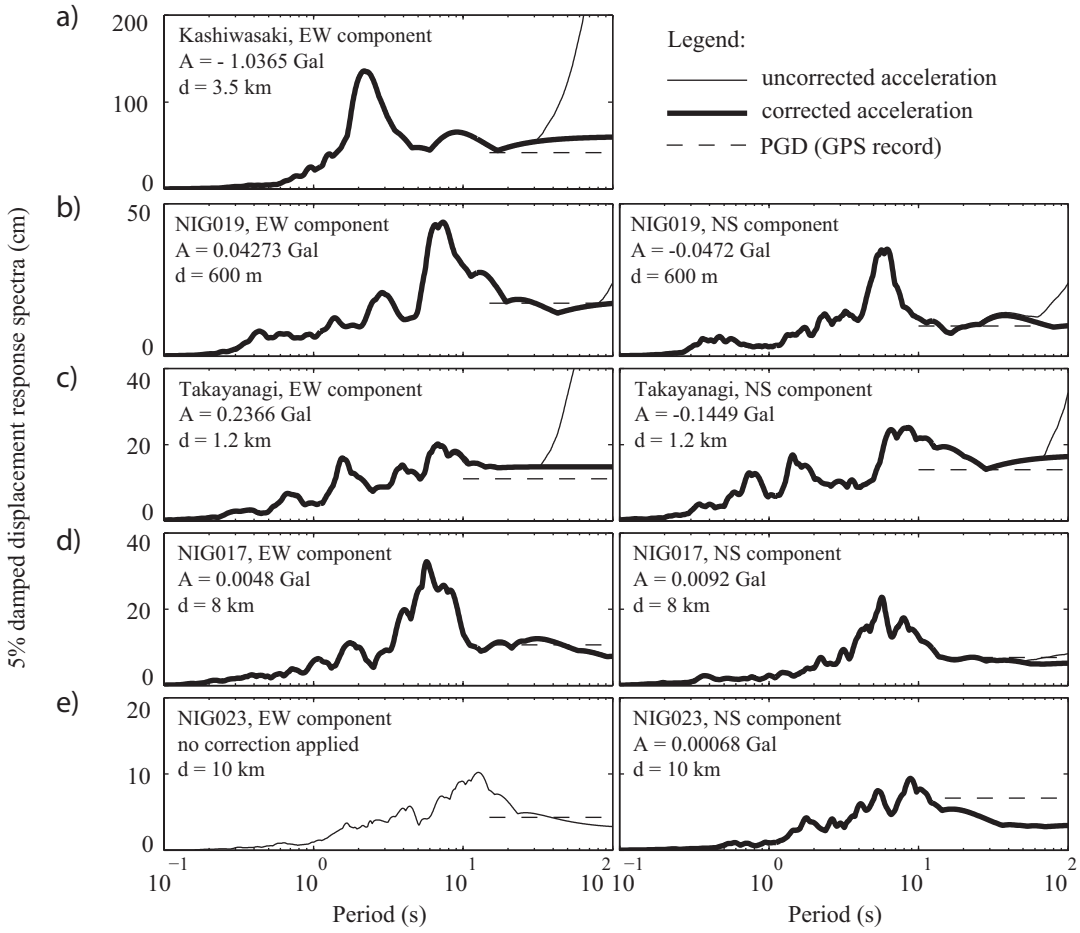

Figure 4.11: Displacement response spectra calculated from uncorrected and corrected acceleration time histories, together with the Peak Ground Displacement obtained from closely spaced 1-Hz GPS records at Kashiwasaki, Ojiya NIG019, Takayanagi, Mashima NIG017 and Matsunoyama NIG023. A is the amplitude of the residual tilt removed from each uncorrected acceleration record, and d the distance from each strong-motion seismometer to its nearest GPS station.

4.4.2 Displacement response spectra when the accelerometers' residual tilt is smaller than 0.01 Gal

Mashima and Matsunoyama stations were situated at places subjected to smaller shaking (translational acceleration & permanent rotation) and located further from their nearest 1-Hz GPS station (about 8 to 10 kms). The amplitudes of the residual tilt experienced by these stations are smaller than 0.01 Gal (section 4.2).

At Mashima, the double integration of the uncorrected acceleration time histories show unrealistic drifts but of smaller amplitude than in the subsection 4.4.1. At Matsunoyama station, the double integration of the uncorrected accelerations show no drift for the EW component (case 1 in section 3.1), whereas the NS component shows a slight one. To illustrate these observations, the Matsunoyama's EW component case is displayed in Figure 4.10 (b, d). For the four records, the amplitude of the observed drifts are related to the amplitude of the residual tilts, always smaller than 0.01 Gal (section 4.2), experienced by these stations. Regarding the Fourier displacement spectra, the displacement spectra, based on the uncorrected acceleration, are not dramatically different from the 1-Hz GPS displacement spectra when A $<$ 0.01 Gal, and are of the same order when A $<$ 0.005 Gal. Removing the permanent tilt from uncorrected accelerations usually provides improvements, and displacement spectra closer to the 1-Hz GPS ones.

For the two stations Mashima NIG017 and Matsunoyama NIG023, removing a permanent tilt of amplitude smaller than 0.01 Gal does not modify the displacement response spectra at periods shorter than 20 seconds (Mashima NIG017, NS component case), still consistent with the previous studies (Paolucci *et al.*, 2008; Wang *et al.*, 2007; Akkar and Boore, 2009). At longer periods, the two uncorrected and corrected acceleration derived spectra do not diverge significantly when A $<$ 0.005 Gal (Mashima NIG017 EW components, Matsunoyama NIG023 both components), but diverge at Mashima NIG017 NS component (A = 0.0092 Gal) to a lesser extent than seen in the previous subsection 4.4.1. Regarding the displacement response spectra at very long periods, they are close to the GPS's peak ground displacements except for Matsunoyama NIG023 NS component where it is much lower. Overall, they show in this case very good similitude considering that the stations are several kilometres away from each other.

4.5 Limitations of this method

Limitations of this method are reached in several circumstances, which include:

- **Instrumental limitations.** The presence of 1/f noise contaminating the translation acceleration makes it impossible to retrieve the displacement time histories accurately (processing scheme, intermediate situation in section 3.4) when its amplitude is larger than both the translational acceleration and the permanent rotation at low frequencies (Figure 4.12, a).

  This limitation does not exist when the Fourier amplitudes of the 1/f noise are smaller than those of both the translational acceleration and the permanent rotation (Figure 4.12, b). It happens (1) for an identical instrument with similar 1/f noise, when the translational acceleration and permanent rotation are larger than in Figure 4.12a, such as in Figure 4.12b or (2) if the earthquake were recorded by an instrument that had lower internal 1/f noise. This instrumental issue is currently being tackled by the development and deployment of instruments with as low as possible 1/f electronic noise. For example, the recent replacement of K-Net95 by K-Net02 seismometers (Aoi *et al.*, 2011), instruments with lower electronic noise, is providing great improvement in the determination of displacement time histories. Lower 1/f internal noise reduces the number of situations where it dominates the low frequency content of records. This consequently increases the number of situations where the translational acceleration and the permanent rotation are dominating the low frequency content of records (Figure 4.12, b). We expect that the development of instruments with always lower 1/f semiconductor noise will greatly ease the recovery of always smaller permanent rotation angles and of displacement time histories from strong-motion accelerograms.

- **A minimum original data length.** The method requires a minimum original data length. K-Net and Kik-Net usually release 300 s long signals recorded at a sampling frequency of 100 Hz or 200 Hz, which give good results when processed according to the proposed method.

- **Effect of the transient tilt.** In the near-field, removing the residual tilt is often all that is needed to obtain stable and reliable displacement time histories. The effect of the oscillatory part of the tilt is indeed assumed to have little effect on the displacement time histories. However, in the very near-field of the largest earthquakes, this assumption may not be valid (Furukawa, 2010a; Javelaud *et al.*, 2011).

- **Multiple baseline offsets.** The record, within a single accelerogram, of motions from more than one event, or from late pulses, cannot at the present time be processed successfully as this creates multiple baseline offsets that cannot be distinguished.

  This was observed for example within the JMA Kashiwasaki, NS component (Figure 4.13), where a late pulse occurs at about the 40^{th} second (a). The simple integration of the uncorrected acceleration time history shows (Figure 4.13, b) two constant slopes before and after the 40^{th} second.

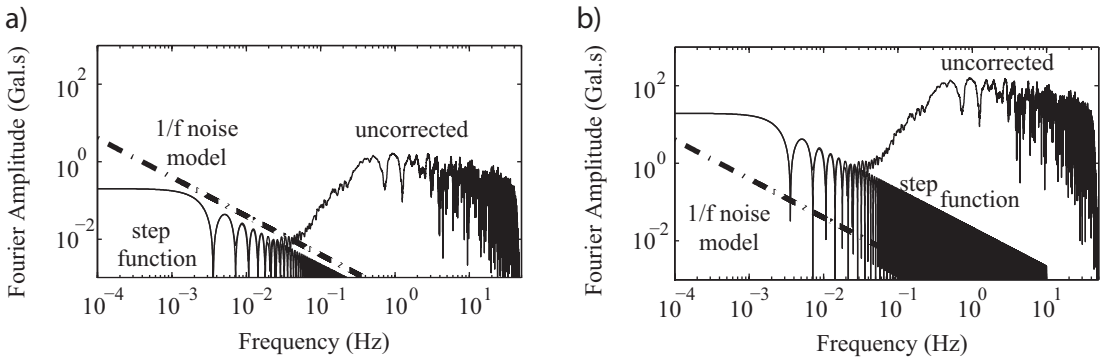

Figure 4.12: (a) The presence of large 1/f noise compared to the translational acceleration and the permanent rotation makes it impossible to retrieve the displacement time history. (b) It is possible to retrieve the permanent displacement time history when the translational acceleration and the permanent rotation are larger than the 1/f noise. This happens (1) when the translational acceleration and the permanent rotation have larger amplitudes than in (a), for an instrument with identical 1/f noise, or (2) when the translational acceleration and the permanent rotation have identical amplitudes than in (a), for an instrument with lower 1/f noise.

In the Fourier domain, the superposition of the Fourier spectra of the uncorrected acceleration record and a step function does not show a perfect fit at low frequencies. The corrected acceleration time history is obtained by removing the step function from the uncorrected acceleration record. Figure 4.13 (c), the corrected velocity time history is calculated by simple integration of the corrected acceleration. It is not equal to zero after the earthquakes. Then, the corrected displacement time history is not stable after the earthquake (Figure 4.13, d).

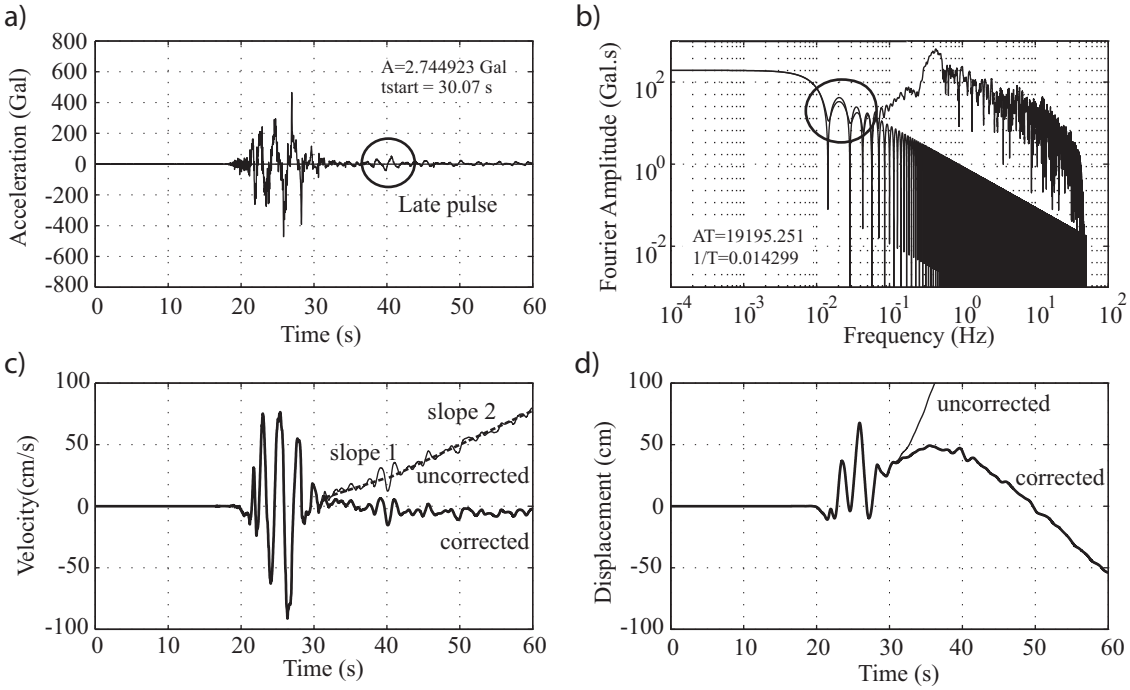

Figure 4.13: (a) Acceleration recorded by the JMA Kashiwasaki, NS component. It shows a late pulse at about the 40^{th} second. (b) The superposition of the Fourier spectra of the uncorrected acceleration record and a step function does not show a perfect fit at low frequencies. (c) The uncorrected velocity time history shows two constant slopes before and after the 40^{th} second. The corrected velocity time history is not equal to zero after the earthquakes. (d) The corrected displacement time history is not stable after the earthquake (d).

4.6 Conclusions of Chapter 4

In this chapter, we applied the methodological steps detailed in chapters 2 and 3 to strong-motion accelerations recorded in the near-field of large earthquakes, and checked the accuracy of displacement time histories (section 4.2) and permanent rotation (section 4.3) retrieved from strong-motion seismometers. As a practical application, the section 4.4 focused on implications for the design of structures. The conclusions drawn from this chapter are summarized as follows:

Estimation of coseismic displacement from strong-motion accelerograms.

- We analyzed strong-motion accelerograms and 1-Hz GPS data recorded in the near-field of the M_w 6.8 Japanese 2007 Niigata-ken Chuetsu-Oki earthquake (Japan). We found that it is possible to obtain reliable estimates of the displacement time histories from acceleration records when the low frequency content of the acceleration is dominated either by 1/f electronic noise up to very small frequencies or by constant residual tilt.

- Regarding the tilt, we observed that the transient tilt has usually no significant effect on the derivation of displacement time histories, whereas any residual tilt, of low amplitude but long duration, seriously alters the velocities and displacements.

Estimation of small permanent rotation from strong-motion records.

- We analyzed data recorded at Kasho dam during the 2000 Western Tottori earthquake (Japan), an exceptional site that experienced very strong shaking and a homogeneous tectonic rotation of the dam and its reservoir. We showed that simple step functions removed from the acceleration time series are records of the instruments coseismic residual tilt. In the example of Kasho dam, the tilt angle estimated here is 15.5 x 10^{-5} rad, to be related with the permanent tectonic tilting of the area.

Practical implications for the design of structures.

- We analyzed strong-motion accelerograms and 1-Hz GPS data recorded in the near-field of the M_w 6.8 Japanese 2007 Niigata-ken Chuetsu-Oki earthquake during which permanent rotations occurred. The comparison of displacement response spectra computed from uncorrected and corrected (by removing the permanent tilt of the instrument) strong-motion acceleration records shows that, when any, the permanent tilt is a fundamental factor that controls the long-period content of the displacement response spectra.

- From the analysis of this specific case study, we found that removing the permanent tilt from accelerations recorded by modern instruments does not modify significantly the displacement response spectra up to periods of about 20 seconds, which is consistent with previous studies.

- When the permanent tilt is larger than 0.04 Gal, it is necessary to remove it from the uncorrected accelerations to obtain realistic displacement response spectra up to longer periods. At Ojiya NIG019 indeed, where the distance to the nearest GPS station is the shortest one (600 m), the displacement response spectra computed from the corrected accelerations reach the peak ground displacements at periods of around 100 seconds. This shows that it is possible to obtain realistic displacement response spectra over a very wide range of periods by removing the residual tilting which contaminates the translational accelerations.

- When the permanent tilt is close to 0.01 Gal, it still affects the displacement response spectra, although to a lesser extent than previously, and should be removed from the uncorrected acceleration records to obtain more realistic displacement response spectra at long periods.

- Finally we found that, for the specific example detailed here, a permanent tilt of amplitude smaller than 0.005 Gal does not affect significantly the displacement response spectra.

Chapter 5

Conclusions

An original way of dealing with acceleration time histories recorded in the near-field of large earthquakes by modern strong-motion accelerometers had been presented. This contribution details how reliable ground displacement and permanent rotation may be retrieved in the near-field of large earthquakes from strong-motion accelerograms. The important conclusions of this dissertation are summarized below.

After a general introduction to this work in **Chapter 1**, we first performed in **Chapter 2** a comprehensive study of a modern strong-motion seismometer. We quantitatively evaluated the different sources of noise which collectively contribute to the noise in the digital acceleration data. We focused on the K-Net95, a modern high-quality instrument, and found that the instrument records translational acceleration and ground tilt. During the recording process, both are modified by the response of the seismometer, which is the sum of its theoretical response and of 1/f electronic noise at low frequencies. We also found that the residual rotation (residual tilt) and 1/f digital semiconductor noise are the two main sources of long-period noise that contaminate the translation acceleration records.

Original in this dissertation, the baseline offsets that contaminate the acceleration records are investigated, not in time domain, but in frequency domain. In that respect, it is essential to properly visualize the frequency content of records, especially at low frequencies.
In **Chapter 3**, we presented a method to visualize in details the records' Fourier

content. Long zero pads were added to the acceleration records before computing the Discrete Fourier Transform. This forces computers to calculate the records' Discrete Fourier Spectra at frequencies so close that very detailed visualizations of the records' Fourier Spectra are obtained, including at low frequencies. Long period baseline offsets that contaminate the acceleration records, if any, could at this point be visualized in details. We proposed a method to remove permanent residual rotation, when any, from the recorded acceleration time histories.

We applied the methodological steps detailed above to strong-motion accelerations recorded in the near-field of large earthquakes.
In **Chapter 4**, we observed that the low frequency content of accelerations recorded in the near-field of the 2007 Niigata-ken Chuetsu-Oki Earthquake (Japan) was often dominated by simple step functions, whose characteristics (starting time, amplitude) could be uniquely retrieved in the Fourier domain. Removing them from the acceleration records led to stable permanent displacements and reliable translational acceleration time histories. Good agreements were found between displacement time histories obtained using strong-motion records and nearby 1-Hz GPS data. Also, the origin of the simple step functions removed from the acceleration time series was confirmed to be record of the instruments coseismic residual tilt. The accuracy of the permanent rotation angle estimated from acceleration time histories were validated by comparison with external rotation information. The data used came from Kasho Dam, a very well instrumented site that experienced a very strong shaking, including permanent rotation, during the 2000 Western Tottori earthquake (Japan).
Among the possible applications, this dissertation focused on the civil engineering one, for which the method proved to give interesting results. The reliable translational acceleration time histories and permanent rotations now available should contribute to better design structures. Improved displacement response spectra, especially at long periods, are obtained when the residual tilt is removed from the acceleration records. Translational acceleration and permanent rotation may also be used as input motion for time domain analysis, either for numerical simulations or experimental modelisations.

While we developed the method, we focused on modern strong-motion accelerometers, having in mind future work, perspectives, and undertakings. We

suggest:

- an extensive comparison of displacement time histories and permanent rotation obtained from strong-motion accelerograms versus external displacement and rotation measurements. This would also contribute to better constrain the precision of the results obtained.

- the extension of the method to other instruments, networks and applications. Retrieving reliable acceleration time histories, displacement time histories and permanent rotation in the near-field of large earthquakes should be useful for several other fundamental purposes such as understanding seismic sources, tsunami prediction, estimation of ground strain, and design of lifelines.

- we close this dissertation certain that the method will gain in efficiency with the continuous development of unceasing higher quality strong-motion accelerometers that may especially have lower internal low frequency noise.

References

Aki, K., and P.G. Richards (2002). *Quantitative seismology.* University Science Books, Sausalito, California, 703pp.

Akkar S. and D.M. Boore (2009). On baseline corrections and uncertainty in response spectra for baseline variations commonly encountered in digital accelerograph records, *Bull. Seismol. Soc. Am.* **99**, 1671-1690.

Amini, A., and M.D. Trifunac (1983). Analysis of a feedback transducer, *Department of Civil Engineering, University of Southern California*, Report No. CE 83-03, 59pp.

Amini, A., and M.D. Trifunac (1985). Analysis of a force balance accelerometer, *Soil Dyn. Earthquake Eng.* **4**, 82-90.

Anderson, J.G. (2003). Strong-motion seismology. *in International Handbook of Earthquake and Engineering Seismology, Part B, W.H.K. Lee, H. Kanamori, P.C. Jennings, and C. Kisslinger (Editors)*, Academic Press, San Diego, 937-965.

Aoi S., T. Kunugi, H. Nakamura and H. Fujiwara (2011). Deployment of new strong-motion seismographs of K-Net and Kik-Net. *in Earthquake Data in Engineering Seismology, S. Akkar, P. Gülkan, T. Van Eck (Editors)*, Springer, 167-186.

Araki M., H. Morikawa, T. Ito, M. Tanigawa, and K. Matsumoto (2011). A

new data logger with large dynamic-range to observe from microtremors to strong motions, *8th International Conference on Urban Earthquake Engineering, Tokyo, Japan*, 109-113.

Asano K. and T. Iwata (2009). Source rupture process of the 2004 Chuetsu, Mid-Niigata Prefecture, Japan, Earthquake inferred from waveform inversion with dense strong-motion data, *Bull. Seismol. Soc. Am.* **99**, 123-140.

Bock Y., D. Agnew, P. Fang, J. Genrich, B. Hager, T. Herring, K. Hudnut, R. King, S. Larsen, J. Minster, K. Stark, S. Wdowinski and F. Wyatt (1993). Detection of crustal deformation from the Landers earthquake sequence using continuous geodetic measurements, *Nature* **361**, 337-340.

Bommer J.J. and A.S. Elnashai (1999). Displacement spectra for seismic design, *J. Earth. Eng.* **3**, 1-32.

Boore, D.M. (2001). Effect of Baseline Corrections on Displacements and Response Spectra for Several Recordings of the 1999 Chi-Chi, Taiwan, earthquake, *Bull. Seismol. Soc. Am.* **91**, 1199-1211.

Boore, D.M., C.D. Stephens, and W.B. Joyner (2002). Comments on baseline correction of digital strong-motion data: examples from the 1999 Hector Mine, California, earthquake. *Bull. Seismol. Soc. Am.* **92**, 1543-1560.

Boore, D.M. (2003). Analog-to-Digital conversion as a source of drifts in displacements derived from digital recordings of ground acceleration. *Bull. Seismol. Soc. Am.* **93**, 2017-2024.

Boore, D.M. and J. J. Bommer (2005). Processing of strong-motion accelerograms: needs, options and consequences. *Soil Dyn. Earthquake Eng.* **25**, 93-115.

Cavalié, O. (2007). Mesures InSAR et modélisation de faibles déformations d'origine anthropique (lac Mead, U.S.A.) ou tectonique (faille de Haiyuan, Chine),

Ph.D. thesis, Université de Paris XI.

Chanerley A.A. and N.A. Alexander (2010). Obtaining estimates of the low-frequency 'flying', instrument tilts and displacement time series using wavelet decomposition, *Bull. Earthq. Eng.* **8**, 231-255.

Chanerley A.A., N.A. Alexander, J. Berrill, H. Avery, B. Halldorsson, and R. Sigbjornsson (2013). Concerning baseline errors in the form of acceleration transients when recovering displacements from strong motion records using the undecimated wavelet transfrom, *Bull. Seismol. Soc. Am.* **103**, 283-295.

Clinton, J.F. (2004). Modern digital seismology - instrumentation, and small amplitude studies in the engineering world, *Ph.D. thesis*, California Institute of Technology.

Dotsenko S.F. and S.L. Soloviev (1995). On the role of residual shifts of ocean-bottom in tsunami generation underwater earthquakes, *Okeanologiya* **51**, 25-31.

Emore G.L., J.S. Haase, K. Choi, K.M. Larson and A. Yamagiwa (2007). Recovering seismic displacements through combined use of 1-Hz GPS and strong-motion accelerometers, *Bull. Seismol. Soc. Am.* **97**, 357-378.

Fujiwara, H., S. Aoi, T. Kunugi and S. Adachi (2004). Strong-motion observations networks of NIED: K-Net and KIK-Net, *in Proceedings of the Cosmos Workshop on Strong-Motion Record Processing*, Cosmos publication n° CP-2004/02.

Furukawa A., S. Inoue and T. Ohmachi (2010a). Verification of a quantitative method to estimate coseismic displacements in near-field from strong-motion accelerographs, *Japan Society of Civil Engineers, 2010 Annual Meeting*, I-326 (in Japanese).

Furukawa A., T. Ohmachi and S. Inoue (2010b). Need to improve the Seismic Deformation Method in application to near-field earthquakes, *Proceedings*

of the Second Symposium on Disaster Mitigation of Lifelines considering System Interactions, 64-69.

Furukawa A. (2011). Relation between observed ground displacement in the near-field and ground displacement based on Seismic Deformation Method. *Master thesis, Tokyo Institute of Technology.*

Fusejima Y., H. Sekiguchi, Y. Awata, and Y. Sugiyama (2003). Geodetic surveys of crustal deformation associated with the 2000 Tottori-ken Seibu earthquake. *Active Fault Research Center (AFRC), Geological Survey of Japan (GSJ), Annual Report on Active Fault and Paleoearthquake Researches* **3**, 157-162 (in Japanese).

Graizer, V.M. (1979). Determination of the true displacement by using strong-motion records. *Izv. USSR Acad. Sci., Phys. Solid Earth* **15**, 875-885.

Graizer, V.M. (1991). Inertial seismometry methods, *Izv. USSR Acad. Sci, Phys. Solid Earth* **27**, 51-61.

Graizer, V.M. (2005). Effect of tilt on strong motion data processing, *Soil Dynam. Earthquake Eng.* **25**, 197-204.

Graizer, V.M. (2006a). Theoretical basis for rotational effects in strong motion and some results. *In: Rotational Workshop, 16.02.2006, Menlo Park / Pasadena, CA.*

Graizer, V.M. (2006b). Tilts in strong ground motion, *Bull. Seismol. Soc. Am.* **96**, 2090-2102.

Graizer, V.M. and E. Kalkan (2008). Response of pendulums to complex input ground motion. *Soil Dyn. Earthquake Eng.* **28**, 621-631.

Graizer, V.M. (2010). Strong motion recordings and residual displacements: What are we actually recording in strong motion seismology? *Seism. Res. Lett.*

81, 635-639.

Hernandez, B., F. Cotton, M. Campillo and D. Massonnet (1997). A comparison between short term (co-seismic) and long term (one year) slip for the Landers earthquake: Measurements from strong-motion and SAR interferometry, *Geophys. Res. Lett.* **24**, 1579-1582.

Inoue S., Y. Murakami, and T. Ohmachi (2007). Evaluation of the near-field ground displacements based on numerical simulation, strong motion records and GPS records. *Proceedings of the 6^{th} Annual Meeting of Japan Association for Earthquake Engineering*, 218-219 (in Japanese).

Intergovernment Oceanographic Commission (2013). Tsunami glossary. *Technical series*, **85**.

Iwan W.D., M.A. Moser, and C.Y. Peng (1985). Some observations on strong motion earthquake measurement using a digital accelerograph, *Bull. Seismol. Soc. Am.* **75**, 1225-1246.

Javelaud, E.H., G. Kubo, T. Ohmachi, and S. Inoue (2005). Coseismic ground displacement due to the 2004 Niigata-ken Chuetsu earthquake, Japan. *Proceedings of the 4th Annual Meeting of Japan Association for Earthquake Engineering*, 312-313.

Javelaud, E.H., T. Ohmachi, and S. Inoue (2006). A quantitative method to estimate the coseismic residual tilt from strong-motion records, *Proceedings of the 30th Annual Meeting of San-daigakuin*, 5-6.

Javelaud, E.H., T. Ohmachi, Y. Murakami and S. Inoue (2010). A quantitative approach to estimate coseismic displacements in the near-field from strong-motion accelerographs: example of the 2007 Niigata-ken Chuetsu-Oki earthquake, Japan. *Joint Conference Proceedings of the 7th International Conference on Urban Earthquake Engineering (7CUEE) & 5th International Conference on Earth-*

quake Engineering (5ICEE), Tokyo, Japan, 299-303.

Javelaud E.H., T. Ohmachi, and S. Inoue (2011). A quantitative approach for estimating coseismic displacements in the near field from strong-motion accelerographs. *Bull. Seismol. Soc. Am.* **101**, 1182-1198.

Javelaud, E.H., S. Inoue, A. Furukawa and T. Ohmachi (2011b). Evaluation of coseismic displacements in the near-field from strong-motion seismometers. Analysis of four recent large earthquakes. *8th International Conference on Urban Earthquake Engineering (8CUEE), Tokyo, Japan*, 189-192.

Javelaud E.H., T. Ohmachi, and S. Inoue (2012). Estimating small permanent rotation from strong-motion records: what is comparison with external measurements telling us? *Bull. Seismol. Soc. Am.* **102**, 2257-2263.

Javelaud E.H. and H. Morikawa (2013). Reliable displacement response spectra at long periods in the near-field of large earthquakes. *Bull. Seismol. Soc. Am.* **103**, 2534-2539

JCOLD (Japan Commission on Large Dams) (2002). Acceleration records on dams and foundations n°2 (CD-ROM version)

Kalkan E. and V. Graizer (2007). Coupled tilt and translational ground motion response spectra, *J. Struct. Eng.* **133**, 609-619.

Kinemetrics Inc. K2 and Makalu User's Manual, Document 302200.
www.kinemetrics.com, date of access: 2010/05/17.

Kinoshita, S., M. Uehara, T. Tozawa, Y. Wada, and Y. Ogue (1997). Recording characteristics of the K-Net95 strong-motion seismograph, *Jishin 2* **49**, 467-481 (in Japanese).

Kinoshita, S. (1998). Kyoshin-Net (K-Net), *Seism. Res. Lett.* **69**, 309-332.

Kobayashi, T., M. Tobita, M. Koarai, T. Okatani, A. Suzuki, Y. Noguchi, M. Yamanaka, and B. Miyahara (2012). InSAR-derived crustal deformation and fault models of normal faulting earthquake (M_j 7.0) in the Fukushima-Hamadori area. *Earth Planets Space* **64**, 1209-1221.

Larson K.M., P. Bodin and J. Gomberg (2003). Using 1-Hz GPS data to measure deformations caused by the Denali Fault Earthquake, *Science* **300**, 1421-1424.

Larson K.M. (2009). GPS seismology, *J. Geod.* **83**, 227-233.

Lee V.W. and M.D. Trifunac (2009). Empirical scaling of rotational spectra of strong earthquake ground motion, *Bull. Seismol. Soc. Am.* **99**, 1378-1390.

Levin B.W. and M.A. Nosov (2008). *Physics of tsunamis*, Springer, 327pp.

Massonnet D., M. Rossi, C. Carmona, F. Adragna, G. Peltzer, K. Feigl and T. Rabaute (1993). The displacement field of the Landers earthquake mapped by radar interferometry, *Nature* **364**, 138-142.

McComb, H.E., A.C. Ruge, and F. Neumann (1943). The determination of true ground motion by integration of strong-motion records: A symposium, *Bull. Seismol. Soc. Am.* **33**, 1-63.

Meisei Electric Co. Ltd. GTA-53 Users Manual (in Japanese).

Mitra, S.K. and J.F. Kaiser (1993). *Handbook for digital signal processing*, John Wiley & Sons, 1268pp.

Miyake, H., K. Koketsu, K. Hikima, M. Shinohara, and T. Kanazawa (2010). Source fault of the 2007 Chuetsu-oki, Japan, Earthquake, *Bull. Seismol. Soc. Am.* **100**, 384-391.

Miyazaki, S., K. M. Larson, K. Choi, K. Hikima, K. Koketsu, P. Bodin, J. Haase, G. Emore, and A. Yamagiwa (2004). Modeling the rupture process of the 2003 September 25 Tokachi-Oki (Hokkaido) earthquake using 1-Hz GPS data, *Geophys. Res. Lett.* **31**, L21603.

Murakami Y. (2008). Evaluation of near field displacements. *Master thesis, Tokyo Institute of Technology.*

Nakamura Y., and A. Saito (1983). P/S phase recognition of seismic waves and epicentral azimuth using single station data. *Proceeding of 17th meeting for earthquake engineering research* (in Japanese).

Nakumura Y. (1988). On the urgent earthquake detection and alarm system (UrEDAS). *Proceeding of 9th World Conference on Earthquake Engineering, Tokyo-Kyoto, Japan*, **VII**, 673-678.

NIED (National Research Institute for Earth Science and Disaster Prevention, Japan). Strong-motion seismograph networks (K-Net and Kik-Net). http://www.kyoshin.bosai.go.jp/, date of access: 2013/04/28.

NIED (2000). Fundamentals of Strong Motion, *CD version.*

NIED (2007). Topic of seismic activity: the 2007 Niigata-ken Chuestu-Oki earthquake - about the NIG018 Kashiwazaka station. http://www.kyoshin.bosai.go.jp//kyoshin/topics/chuetsuoki20070716/K-NET_Kashiwazaki.pdf, latest accessed: 2013/04/28 (in japanese).

Nosov M.A. (2011). Residual horizontal displacement of water particles in the vicinity of tsunami source. *8th International Conference on Urban Earthquake Engineering (8CUEE), Tokyo, Japan*, 1541-1546.

Ohmachi T., H. Tsukiyama, and H. Matsumoto (2001). Simulation of tsunami induced by dynamic displacement of seabed due to seismic faulting, *Bull. Seis-*

mol. Soc. Am. **91**, 1898-1909.

Ohmachi T., N. Kojima., A. Murakami., and N. Komaba (2003). Near field effects of hidden seismic faulting on a concrete dam. *Journal of Natural Disaster Science* **25**, 7-15.

Ohtake, K. (2006). Near-field earthquake displacements of the non-liquefiable ground relevant to damage to buried pipelines. *Doctor thesis. Tokyo Institute of Technology.*

Ohtake K. and T. Ohmachi (2007). Near-field earthquake displacements of the non-liquefiable ground relevant to damage to buried pipelines. *5^{th} AWWARF/JWWA Water System Seismic Conference.*

Okada Y., K. Kasahara, S. Hori, K. Obara, S. Sekiguchi, H. Fujiwara, and A. Yamamoto (2004). Recent progress of seismic observation networks in Japan - Hi-Net, F-Net, K-Net and Kik-NEt -. *Earth. Planets Space* **56**, xv-xxviii.

Oppenheim A.V. and R.W. Schafer (2010). *Discrete-Time Signal Processing*, Pearson, Third edition, 1132pp.

Paolucci R., A. Rovelli, E. Faccioli, C. Cauzzi, D. Finazzi, M. Vanini, C. Di Alessandro, and G. Calderoni (2008). On the reliability of long-period response spectral ordinates from digital accelerograms. *Earthquake Eng. Struct. Dyn.* **37**, 697-710.

Park S.W., H. Ghasemi, J. Shen, P.G. Somerville, W.P. Yen and M. Yashinsky (2004). Simulation of the seismic performance of the Bolu Viaduct subjected to near-field ground motions. *Earthquake Eng. Struct. Dyn.* **33**, 1249-1270.

Sato N., H. Kawasaki, and T. Ohmachi (2007). Revision of strong motion records at Kasho dam during the 2000 Western Tottori-Prefecture earthquake. *Journal of Japan Society of Dam Engineers* **17**, 295-304 (in Japanese).

Scherbaum, F. (2001). *Of Poles and Zeros: Fundamentals of Digital Seismology*, Kluwer Academic Publishers, Dordrecht, The Netherlands, 268pp.

Shakal, A.F. and C.D. Petersen (2001). Acceleration offsets in some FBA's during earthquake shaking. *Abstracts of the 96th annual meeting of the Seismological Society of America, in Seism. Res. Lett.* **72**, 233.

Smith, S. (1999). *The Scientist and Engineer's Guide to Digital Signal Processing*, Snd edn, California Technical Publishing.

Tabuchi, H., T. Harada, and K. Ishibashi (2008). A southeasterly-dipping static fault model of the 2007 Niigata-ken Chuetsu-oki, Japan, earthquake based on crustal movements, tsunamis, aftershock distribution and neotectonics, *Report of Research Center for Urban Safety and Security, Kobe University* **3** 1-10.

Takasu S., H. Yoshida, Y. Yamaguchi, T. Sasaki, and T. Iwashita (2001). Behavior of dams due to the Western Tottori Prefecture Earthquake in 2000. *U.S.-Japan Cooperative Program in Natural Resources (UJNR) Panel on Wind and Seismic Effects, 33rd joint meeting, Tsukuba.*

Todorovska, M.I., M.D. Trifunac, E.I. Novikova, and S.S. Ivanovic (1995). Correction for misalignment and cross axis sensitivity of strong earthquake motion recorded by SMA-1 accelerographs. *Department of Civil Engineering, University of Southern California*, Report No. CE 95-06.

Todorovska, M.I. (1998). Cross-axis sensitivity of accelerographs with pendulum like transducers-mathematical model and inverse problem, *Earthquake Eng Struct Dyn* **27**, 1031-1051.

Tolis S.V. and E. Faccioli (1999). Displacement design spectra. *J. Earth. Eng.* **3**, 107-125.

Trifunac, M.D. (1971). Zero baseline correction of strong-motion accelerograms, *Bull. Seismol. Soc. Am.* **61**, 1201-1211.

Trifunac, M.D. (1972). A note on correction of strong-motion accelerograms for instrument response, *Bull. Seismol. Soc. Am.* **62**, 401-409.

Trifunac, M.D., F.E. Udwadia, and A.G. Brady (1973). Analysis of errors in digitized strong-motion accelerograms, *Bull. Seismol. Soc. Am.* **63**, 157-187.

Trifunac, M.D., V.W. Lee and M.I. Todorovska (1999). Common problems in automatic digitization of strong-motion accelerograms, *Soil Dyn. Earthq. Eng.* **18**, 519-530.

Trifunac, M.D. and M.I. Todorovska (2001). A note on the useable dynamic range of accelerographs recording translation, *Soil Dyn. Earthq. Eng.* **21**, 275-286.

Wang G.Q., D.M. Boore, H. Igel, and X.Y. Zhou (2003). Some observations on colocated and closely spaced strong ground-motion records of the 1999 Chi-Chi, Taiwan, earthquake, *Bull. Seismol. Soc. Am.* **93**, 674-693.

Wang G.Q., D.M. Boore, G. Tang, and X. Zhou (2007). Comparisons of ground motions from colocated and closely spaced one-sample-per-second global positioning system and accelerograph recordings of the 2003 M 6.5 San Simeon, California, Earthquake in the Parkfield region, *Bull. Seismol. Soc. Am.* **97**, 76-90.

Wielandt E. (2002). Seismometry, *in International Handbook of Earthquake and Engineering Seismology, Part A, W.H.K. Lee, H. Kanamori, P.C. Jennings, and C. Kisslinger (Editors)*, Academic Press, San Diego, 283-304.

Wong H.L. and M.D. Trifunac (1977). Effects of cross-axis sensitivity and misalignment on response of mechanical optical accelerographs, *Bull. Seismol. Soc. Am.* **67**, 929-956.

Yamaguchi Y., T. Sasaki, and K. Kanenawa (2002). Damages of dams caused by the Western Tottori-prefecture Earthquake in 2000 and stability evaluation analysis about Kasho dam. *The 22nd U.S. Society on Dams Annual Meeting and Conference Pre-Conference Workshop 3rd U.S.-JAPAN Workshop on Advanced Research on Earthquake Engineering for Dams.*

Appendix A

This appendix contains the details of the processing, according to the section 4.2, of the strong-motion accelerations recorded in the near field of the 2007 Niigata-ken Chuetsu-Oki earthquake (Japan).

The accelerograms recorded at the stations shown in Figure A1 have been processed. Each accelerogram, its Fourier transform, velocity and displacement time histories as well as the processing steps applied are given below in Figures A2 to A19. The parameters described in the processing scheme section 4.2 are given in each figure, when relevant: the residual displacement (rsd. dis), the amplitude of the residual acceleration (A) and the starting time of the step function (tstart), as well as the Fourier amplitude at zero frequency AT and the frequency when the Fourier amplitude of the signal decreases to zero for the first time 1/T.

The processing details of the acceleration time histories are summarized in Tables 4.1 and 4.2.

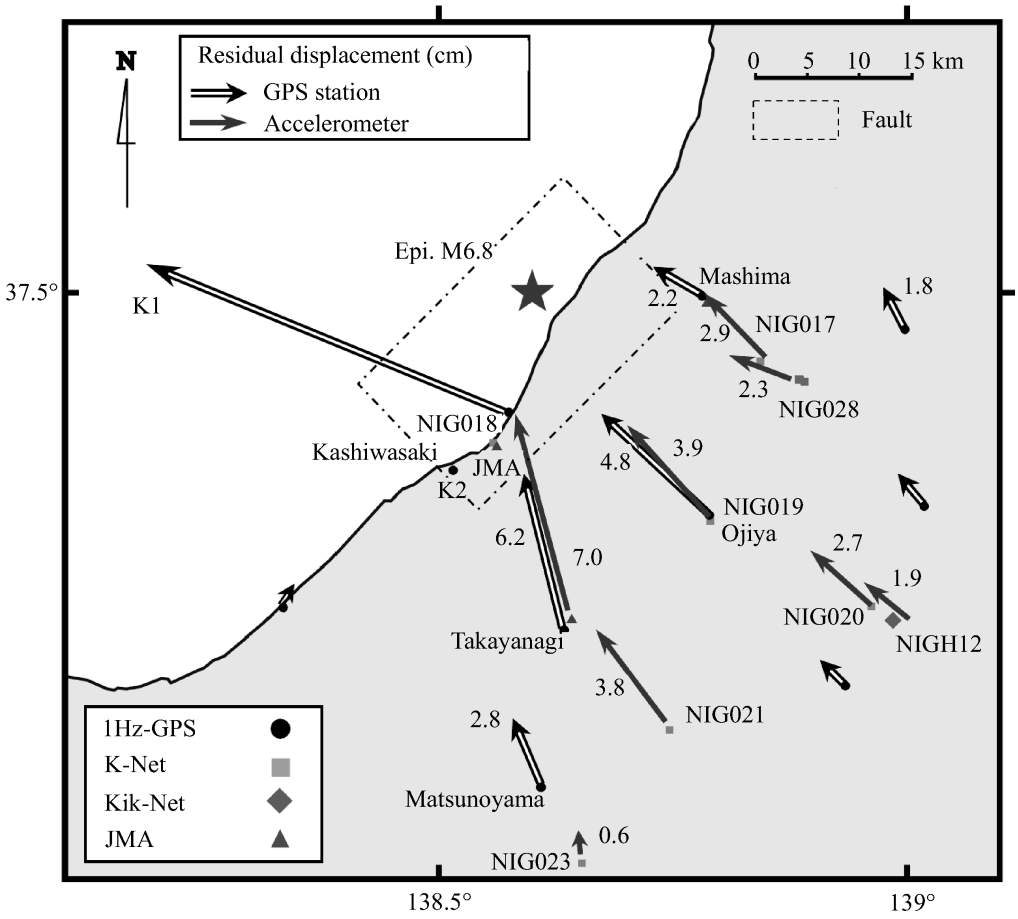

Figure A1: Map showing the position of the strong-motion seismometers and GPS stations, whose records of the 2007 Niigata-ken Chuetsu-Oki earthquake, Japan, are used in this study.

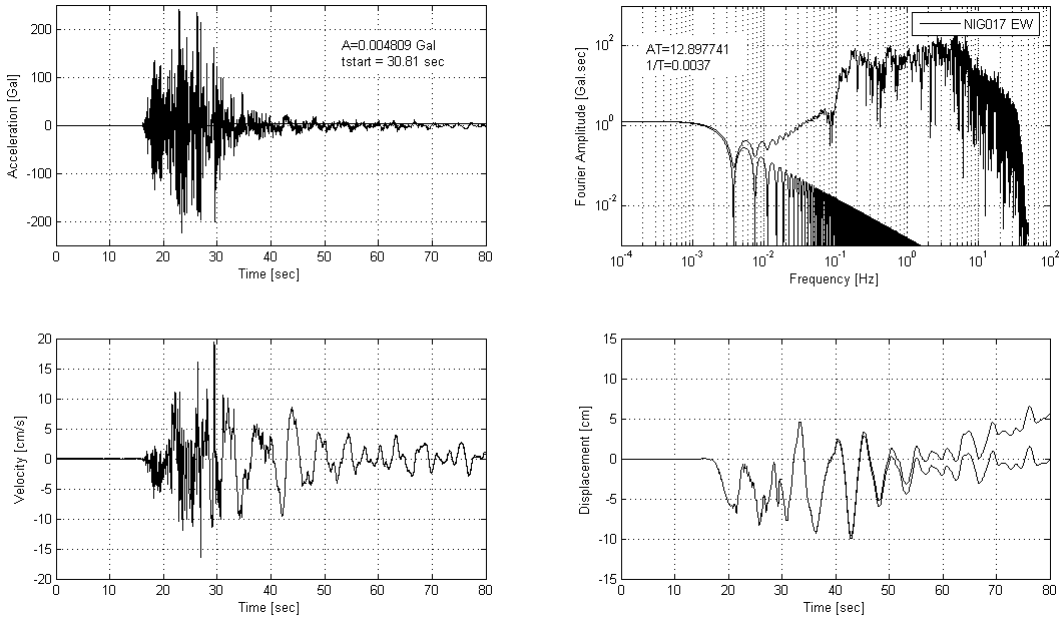

Figure A2: K-Net NIG017 station, EW component.

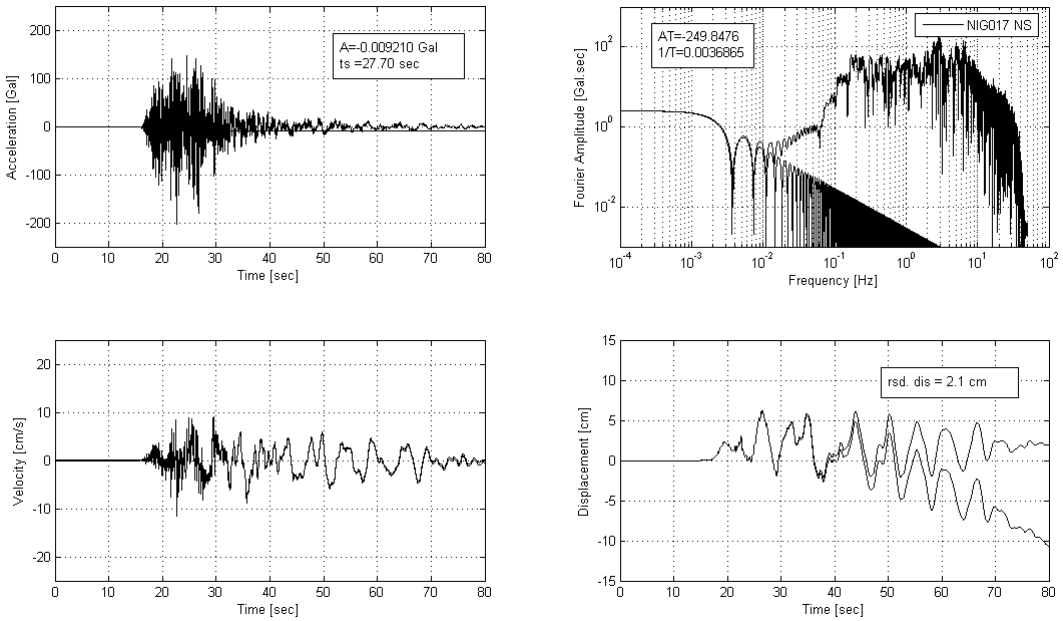

Figure A3: K-Net NIG017 station, NS component.

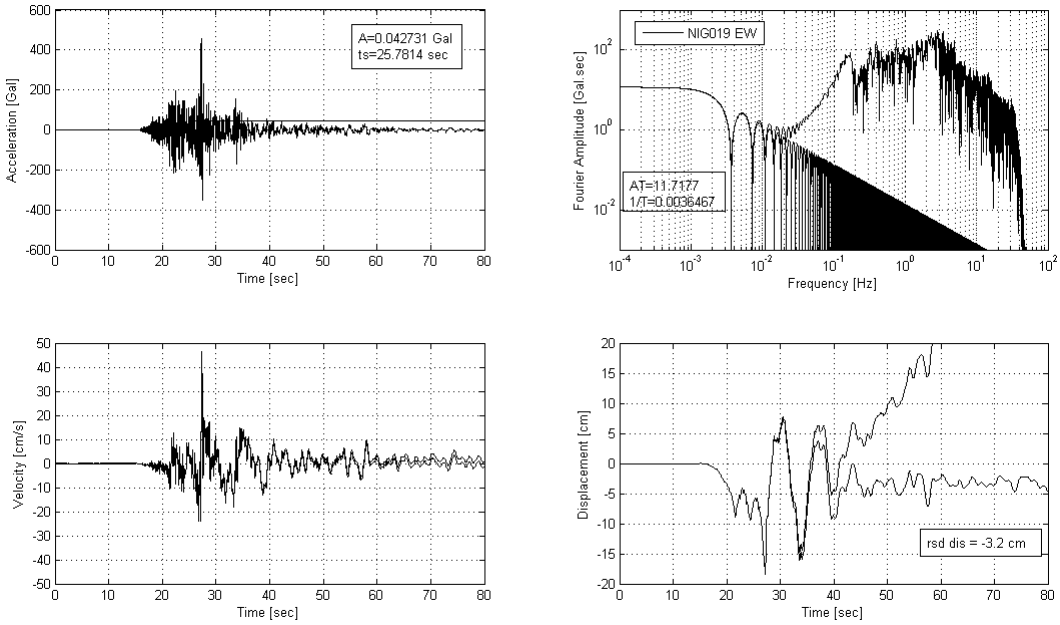

Figure A4: K-Net NIG019 station, EW component.

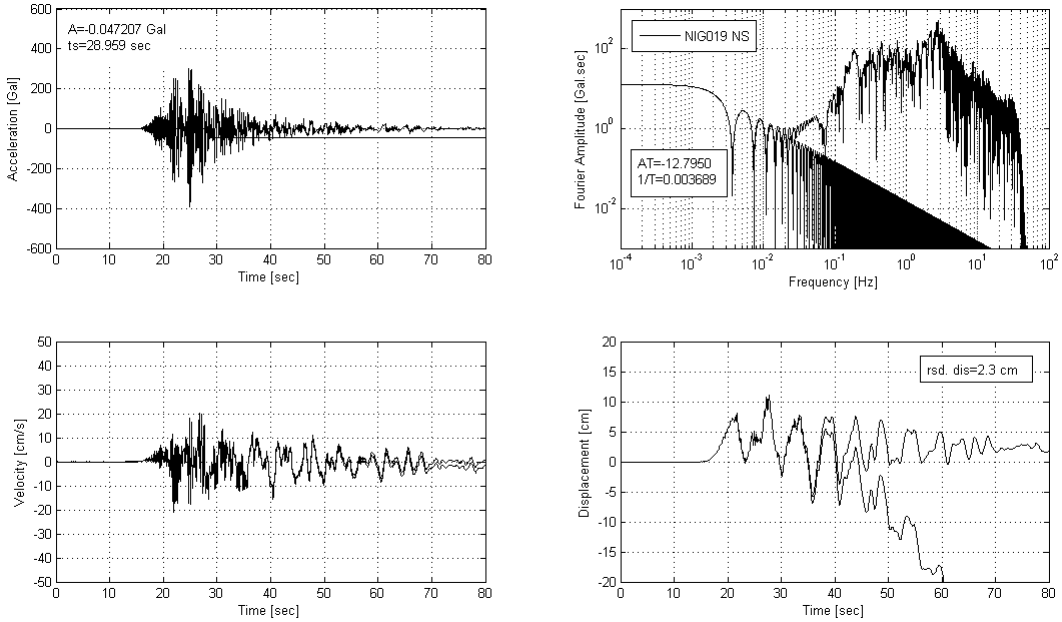

Figure A5: K-Net NIG019 station, NS component.

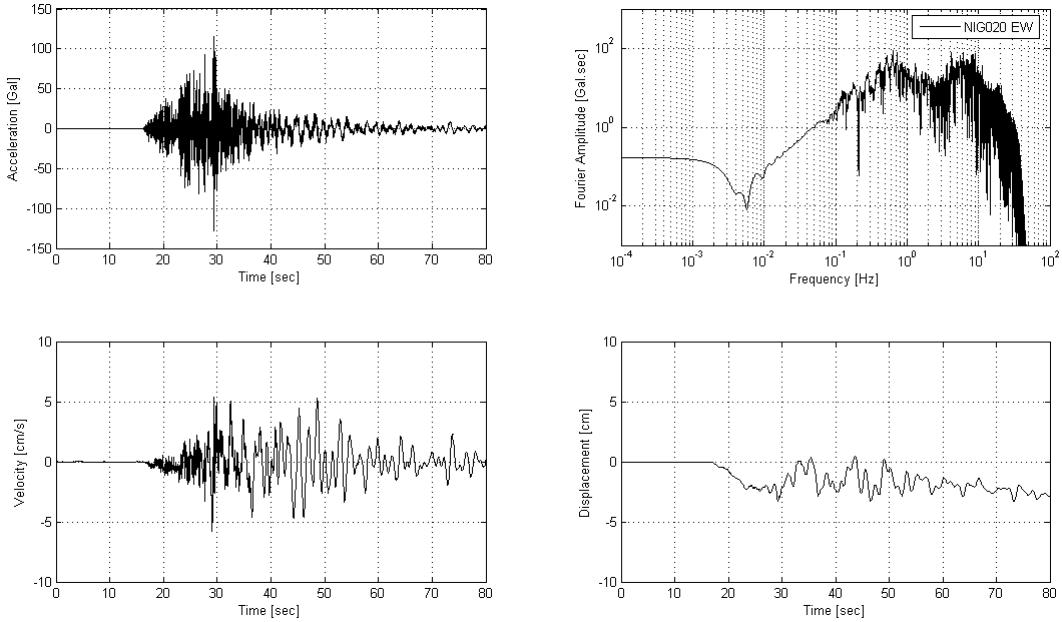

Figure A6: K-Net NIG020 station, EW component.

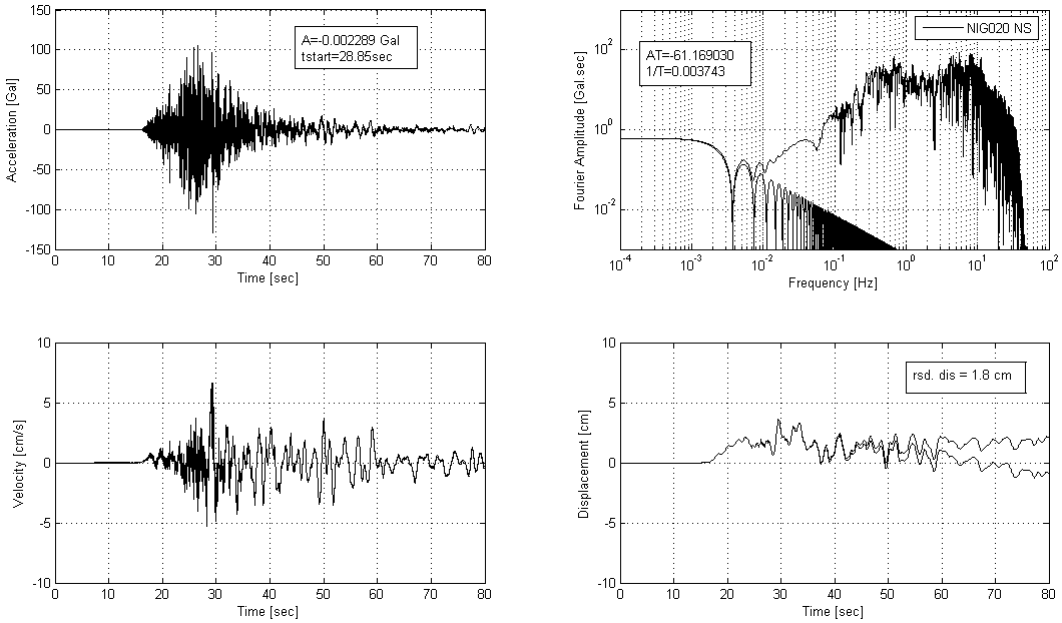

Figure A7: K-Net NIG020 station, NS component.

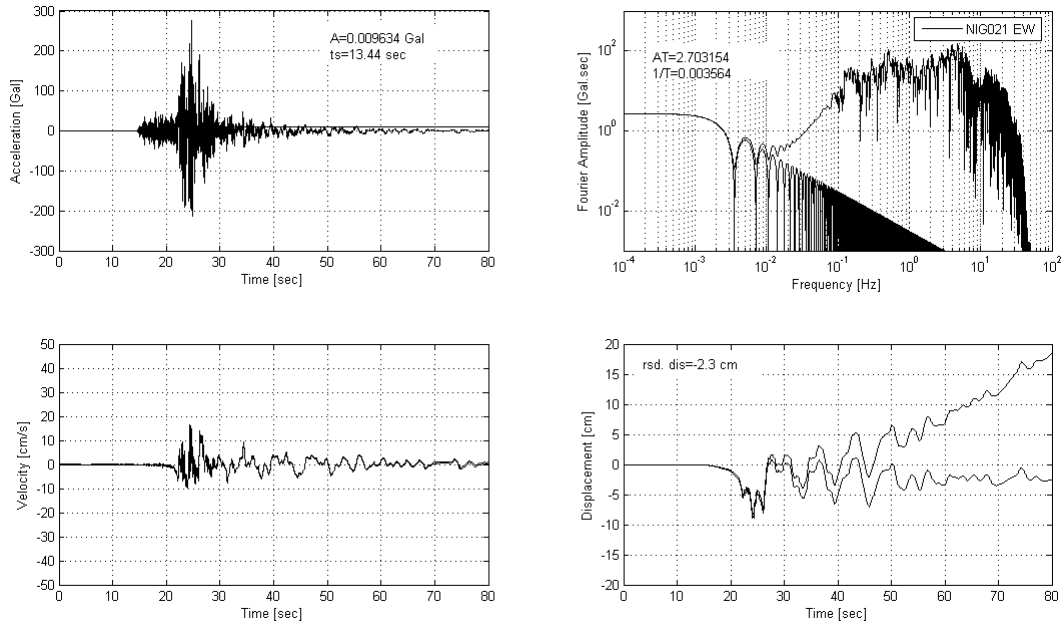

Figure A8: K-Net NIG021 station, EW component.

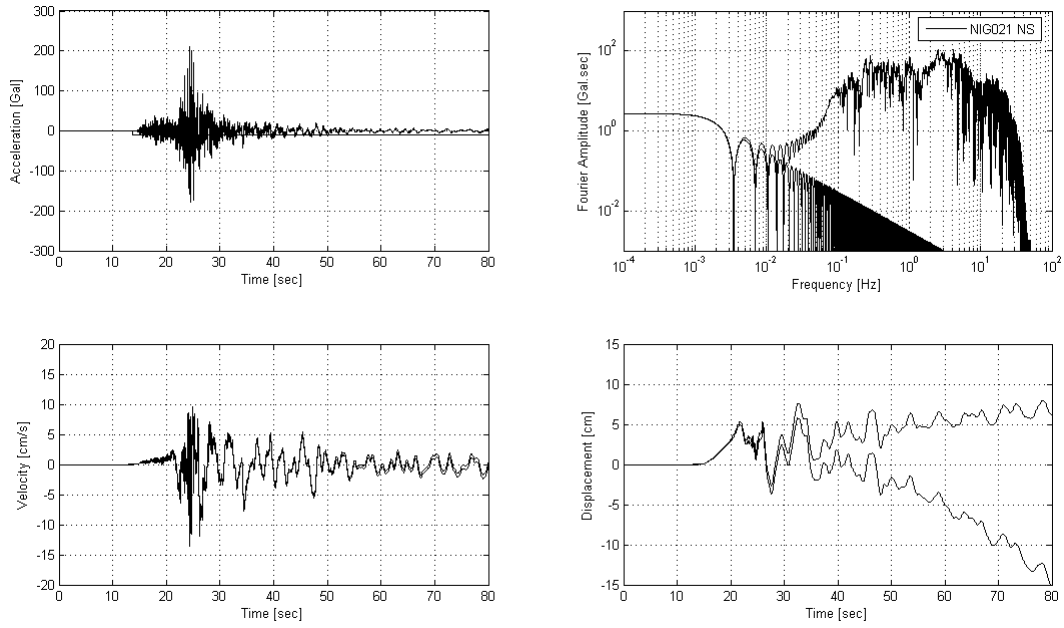

Figure A9: K-Net NIG021 station, NS component.

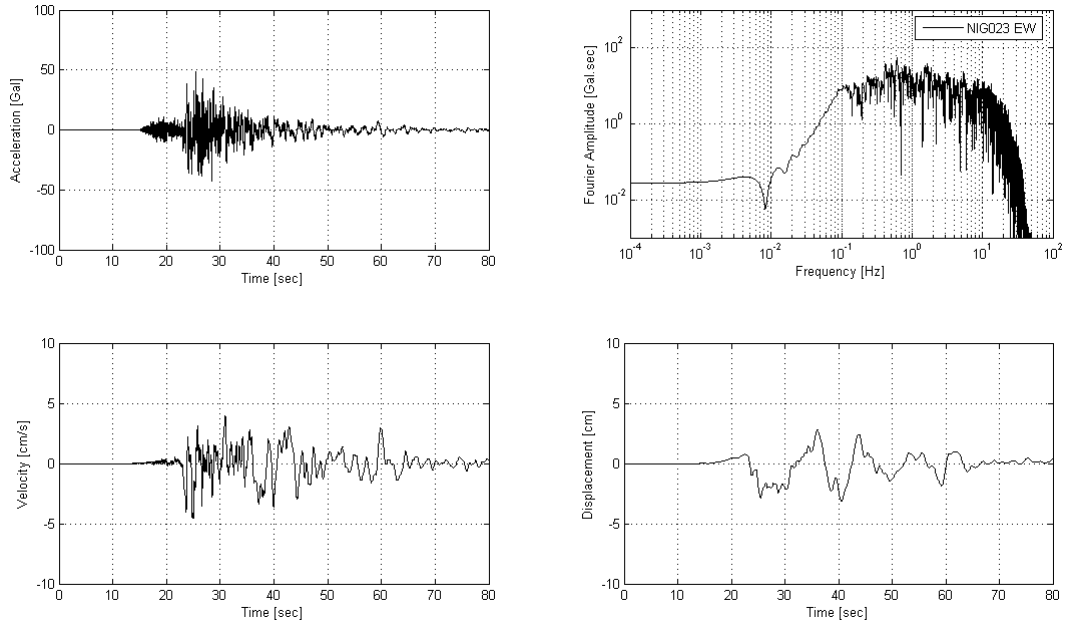

Figure A10: K-Net NIG023 station, EW component.

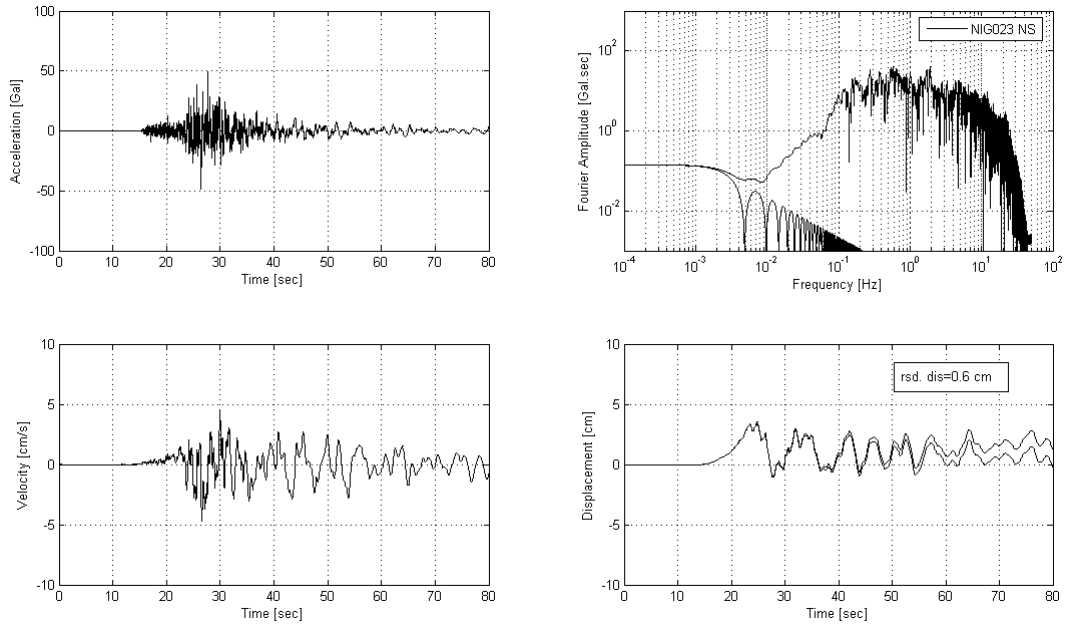

Figure A11: K-Net NIG023 station, NS component.

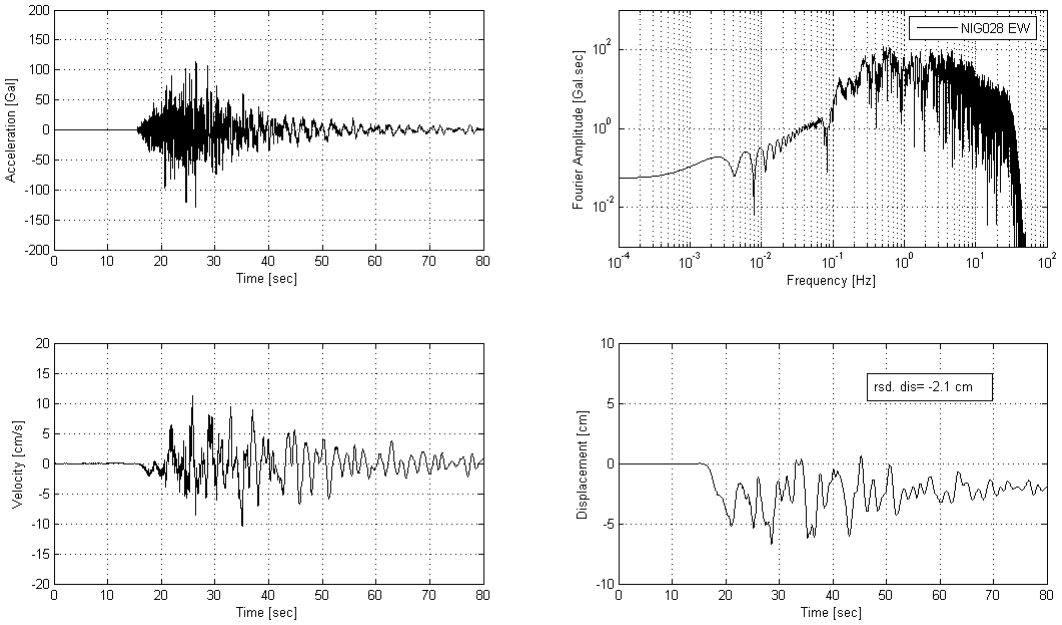

Figure A12: K-Net NIG028 station, EW component.

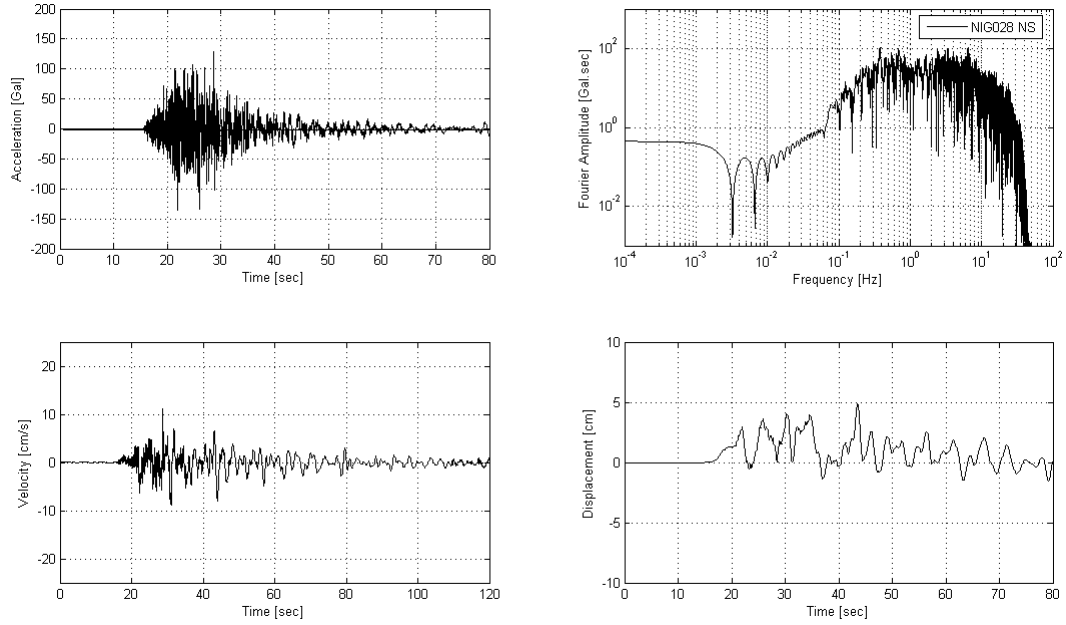

Figure A13: K-Net NIG028 station, NS component.

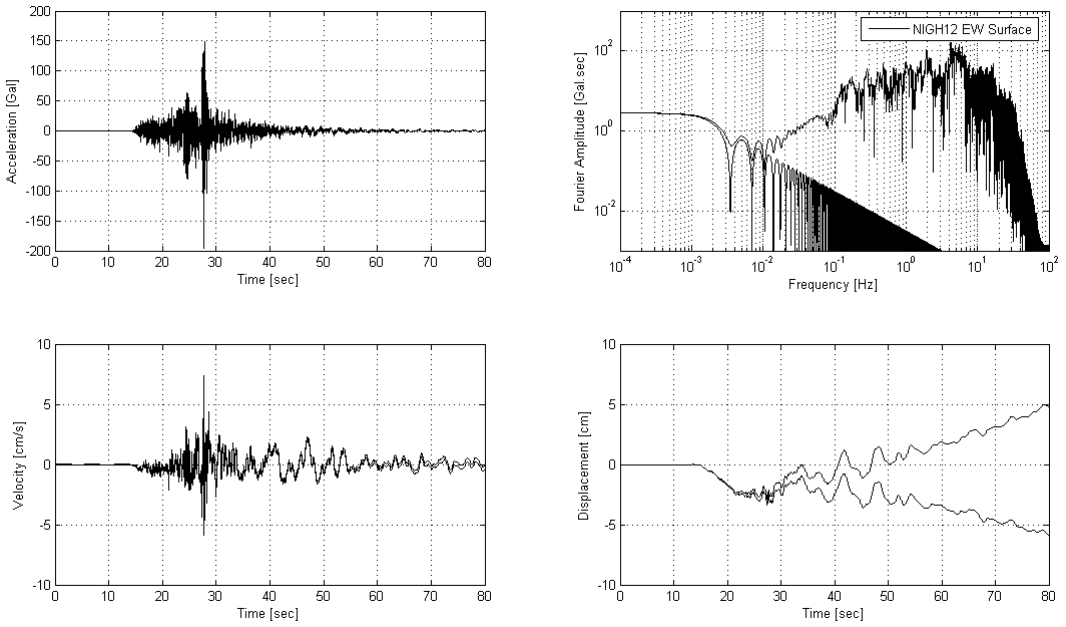

Figure A14: Kik-Net NIGH12 station, surface instrument, EW component.

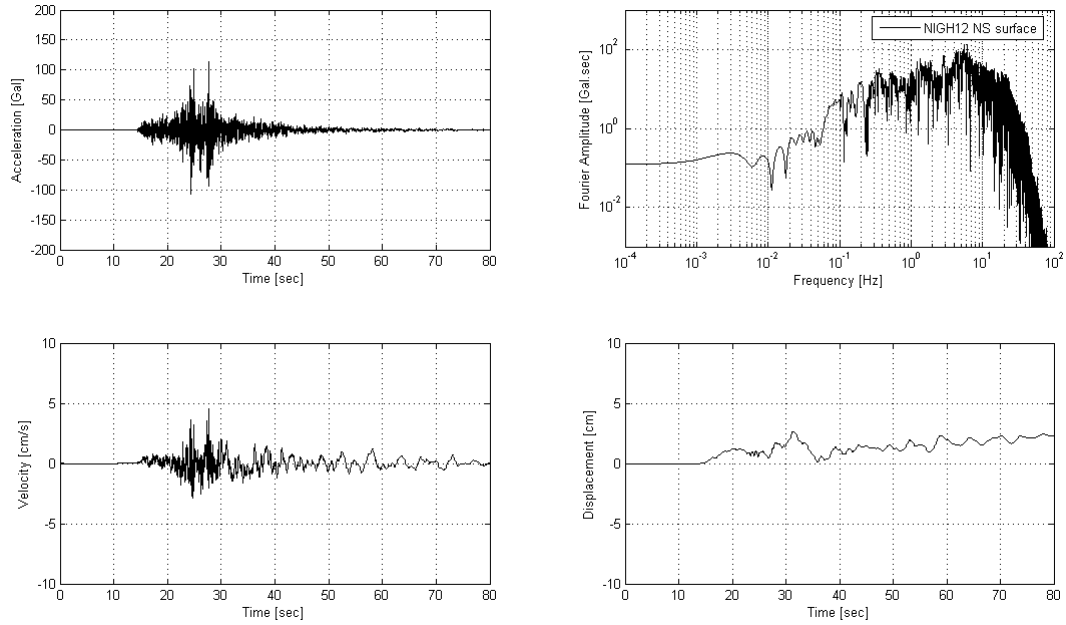

Figure A15: Kik-Net NIGH12 station, surface instrument, NS component.

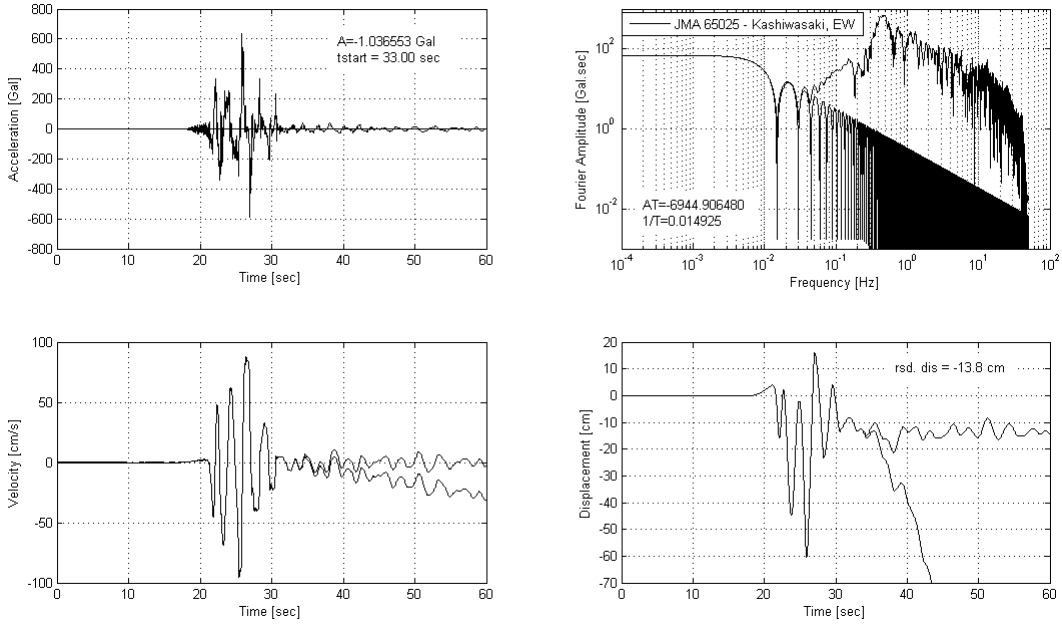

Figure A16: JMA, KASHIWASAKI station, EW component.

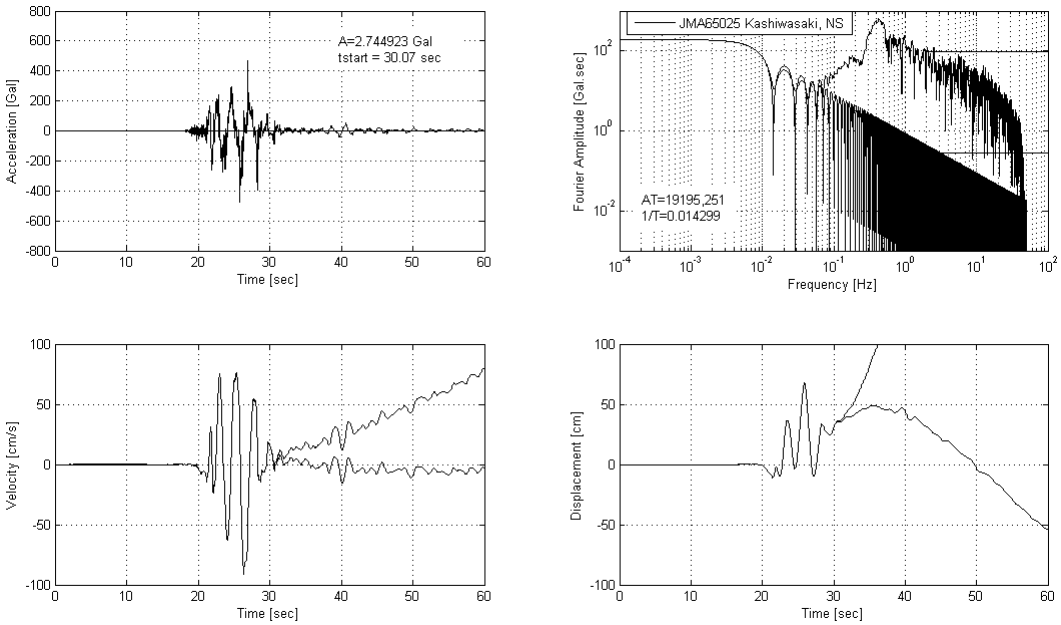

Figure A17: JMA, KASHIWASAKI station, NS component.

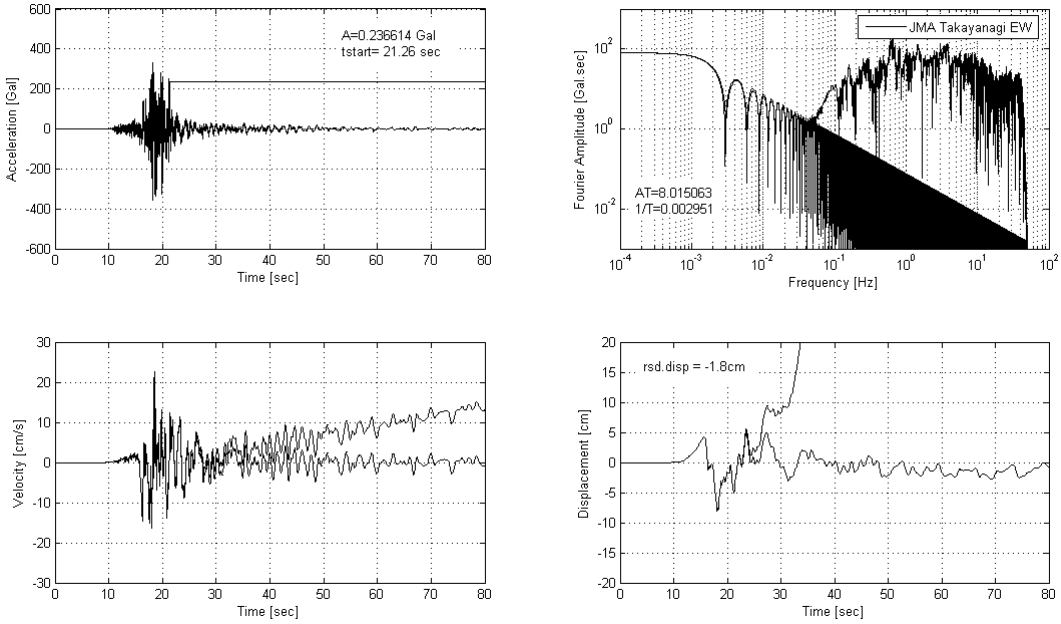

Figure A18: JMA, TAKAYANAGI station, EW component.

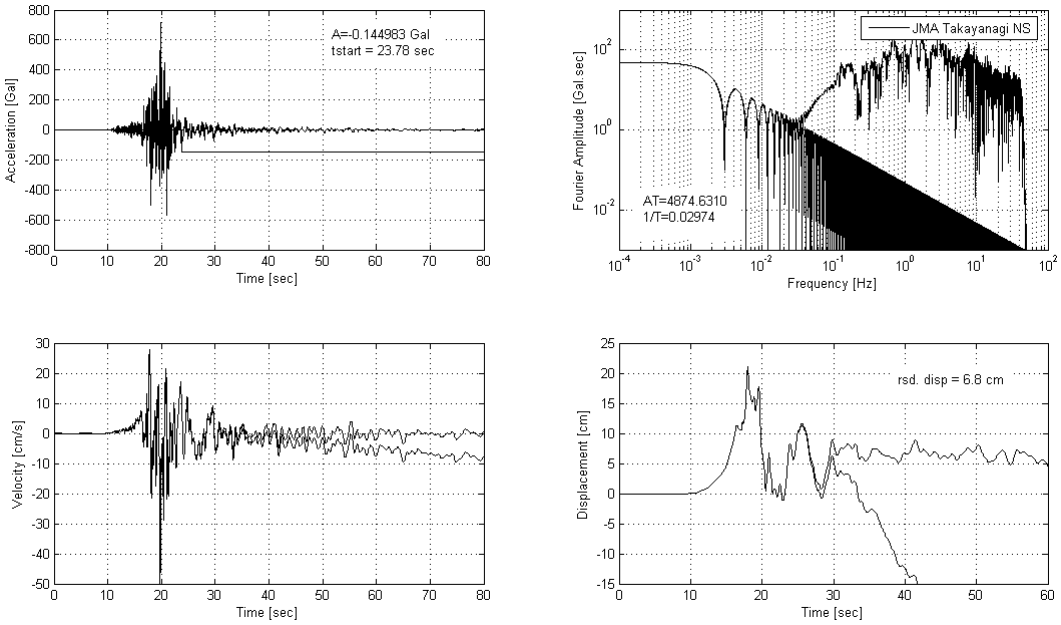

Figure A19: JMA, TAKAYANAGI station, NS component.

Appendix B: List of publications

Reviewed papers

Javelaud E., Ohmachi T. and S. Inoue (2011). A quantitative approach for estimating coseismic displacements in the near-field from strong-motion accelerographs. Bulletin of the Seismological Society of America, 101-3, 1182-1198.

Javelaud E., Ohmachi T. and S. Inoue (2012). Estimating small permanent rotation from strong-motion records: what is comparison with external measurements telling us? Bulletin of the Seismological Society of America, 102-5, 2257-2263.

Javelaud E. and H. Morikawa (2013). Reliable displacement response spectra at long periods in the near-field of large earthquakes. Bulletin of the Seismological Society of America, 103-4, 2534-2539.

Awards

2004 - 2006	Monbukagakusho scholarship program (18 months) at Tokyo Institute of Technology.
2010	Young Researcher Award for Best Presentation. 7^{th} International Conference on Urban Earthquake Engineering and 5^{th} International Conference on Earthquake Engineering, Tokyo Institute of Technology, March 2010.
2011	Betbeder-Matibet Award French Association For Earthquake Engineering (A.F.P.S.).

Conference / meeting papers

Javelaud E., Kubo G., Ohmachi T. and S. Inoue (2005). Coseismic ground displacement due to the 2004 Niigata-ken Chuetsu Earthquake, Japan. Proceedings of the Annual Meeting of Japan Association for Earthquake Engineering, Kyoto (Japan), 312-313.

Javelaud E.H., T. Ohmachi, and S. Inoue (2006). A quantitative method to estimate the coseismic residual tilt from strong-motion records, Proceedings of the 30^{th} Annual Meeting of San-daigakuin, 5-6.

Javelaud E., Ohmachi T., Murakami Y. and S. Inoue (2010). A quantitative approach to estimate coseismic displacement in the near-field from strong-motion accelerographs: example of the 2007 Niigata-ken Chuetsu earthquake, Japan. 7^{th} International Conference on Urban Earthquake Engineering and 5^{th} International Conference on Earthquake Engineering (Japan), 299-303.

Javelaud E., Inoue S., Furukawa A. and Ohmachi T. (2011). Evaluation of coseismic displacements in the near-field from strong-motion seismometers. Analysis of four recent large earthquakes. 8^{th} International Conference on Urban Earthquake Engineering, Tokyo (Japan), 189-192.